



14th Annual Meeting of the Bulgarian Section of SIAM
December 17-19, 2019
Sofia

BGSIAM'19

EXTENDED ABSTRACTS

HOSTED BY THE JOINT INNOVATION CENTRE
BULGARIAN ACADEMY OF SCIENCES

14th Annual Meeting of the Bulgarian Section of SIAM
December 17-19, 2019, Sofia

BGSIAM'19 Extended abstracts

©2019 by Fastumprint

ISSN: 1313-3357 (print)
ISSN: 1314-7145 (electronic)

Printed in Sofia, Bulgaria

PREFACE

The Bulgarian Section of SIAM (BGSIAM) was formed in 2007 with the purpose to promote and support the application of mathematics to science, engineering and technology in Republic of Bulgaria. The goals of BGSIAM follow the general goals of SIAM:

- To advance the application of mathematics and computational science to engineering, industry, science, and society;
- To promote research that will lead to effective new mathematical and computational methods and techniques for science, engineering, industry, and society;
- To provide media for the exchange of information and ideas among mathematicians, engineers, and scientists.

During BGSIAM'19 conference a wide range of problems concerning recent achievements in the field of industrial and applied mathematics will be presented and discussed. The meeting provides a forum for exchange of ideas between scientists, who develop and study mathematical methods and algorithms, and researchers, who apply them for solving real life problems. The conference support provided by SIAM is highly appreciated.

The strongest research groups in Bulgaria in the field of industrial and applied mathematics, advanced computing, mathematical modelling and applications will be presented at the meeting according to the accepted extended abstracts. Many of the participants are young scientists and PhD students.

LIST OF INVITED SPEAKERS:

- Peter Dragnev (Purdue University Fort Wayne, Indiana, USA)
“On the universal optimality of the 600-cell: the Levenshtein framework lifted”
- Ivan Ivanov (Texas A&M University, USA)
“Quantifying Important Genes in a Gene Regulatory Network with Applications to Network Compression”
- Marcin Paprzycki (Systems Research Institute, Polish Academy of Sciences)
“Semantic Technologies in a Decision Support System”
- Tony Spassov (Sofia University, “St. Kliment Ohridski”, Bulgaria)
“Nanomaterials for hydrogen production and storage”

The present volume contains extended abstracts of the presentations (Part A) and list of participants (Part B).

Ivan Georgiev
Chair of BGSIAM Section

Hristo Kostadinov
Vice-Chair of BGSIAM Section

Elena Lilkova
Secretary of BGSIAM Section

Sofia, December 2019

Table of Contents

Part A: Extended abstracts	1
<i>A. Alexandrov, V. Monov</i> Method for remote continuous Pulse Oximetry for Critical Congenital Heart Disease screening	3
<i>T. Aleksandrova, H. Kostadinov, N. Manev</i> Watermarking Audio Signals: Analysis of Noise Effect and Error Characteristics	5
<i>Vera Angelova</i> Perturbation analysis of the matrix equation $X - A^* \sqrt[2^m]{X^{-1}} A = I$	6
<i>K. Angelov, N. Kolkovska</i> Numerical Study of Soliton Solutions to the Two Dimensional Boussinesq Equation	8
<i>Atanas Atanasov, Ivan Georgiev, Milen Petrov</i> Application of the mixed integer programming in determining the optimal honeybee colony's location based on the productive potential of the bee forage species	10
<i>B. Batgerel, I.V. Puzynin, T.P. Puzynina, I.G. Hristov, R.D. Hristova, Z.K. Tukhliev, Z.A. Sharipov</i> Modeling the Long-Range Effect of Copper Nanoclusters Irradiating a Copper Target	12
<i>Y. Boneva, V. Ivanov</i> Improvement of air pollution caused by traffic through different signal timing policies — case study of Sofia	14
<i>Milen Borisov, Svetoslav Markov</i> A Study of Self-catalyzed Exponential Decay Chains with a Fast Rate Parameter	16
<i>S. Boumova, T. Ramaj, M. Stoyanova</i> Computing distance distributions of ternary orthogonal arrays	17
<i>St. Bushev</i> Some results on 3D printing technology	19
<i>Hristo Chervenkov and Kiril Slavov</i> ETCCDI Thermal Climate Indices in the CMIP5 Future Climate Projections over Southeast Europe	21
<i>Hristo Chervenkov and Kiril Slavov</i> Solar Radiation Modelling for Bulgaria Based on Assimilated Surface	

Data	22
<i>Danilchenko A.S., Nasedkin A.V., Nasedkina A.A.</i>	
Finite Element Modeling of Effective Properties of Nanostructured Poroelastic Composites with Surface Effects	23
<i>Peter Dragnev</i>	
On the universal optimality of the 600-cell: the Levenshtein framework lifted	25
<i>Stefka Fidanova, Krassimir Atanassov</i>	
New Ant Colony Optimization Including Weights	26
<i>Ivan Georgiev, Roumen Iankov, Maria Datcheva</i>	
Numerical determination of elastic material properties of closed cell aluminum foam	27
<i>K. Georgiev, S. Margenov</i>	
Numerical methods for fractional diffusion-reaction problems based on operator splitting and BURA	29
<i>Slavi G. Georgiev, Lubin G. Vulkov</i>	
Reconstruction of Time-Dependent Implied Volatility by Market Observations for European Options in Jump–Diffusion Models	31
<i>Gerdjikov V. S.</i>	
On mKdV equations and 2-dimensional Toda field theories: algebraic structures and Hamiltonian properties	33
<i>Stanislav Harizanov, Svetozar Margenov, Nedyu Popivanov</i>	
Analysis of a Space-Fractional Diffusion Problem with a Piecewise Constant Diffusion Coefficient	35
<i>Raoul Hölder, Elham Mahmoudi, Markus König, Chenyang Zhao, Maria Datcheva</i>	
System and Parameter Identification Methods for Ground Models in Mechanized Tunneling	36
<i>Radoslava Hristova, Ivan Hristov</i>	
Computing reliable solutions of chaotic dynamical systems using multiple-precision arithmetic	38
<i>J. Jeliazkov, H. Kostadinov</i>	
Incentivizing Research Using DLT-based Smart Contract Platforms	40
<i>I. Jordanov, N. Vitanov, E. Nikolova</i>	
Nonlinear waves in a generalized model of interacting high density populations	41
<i>D. Kamenov, S. Harizanov, S. Nikolova, D. Toneva</i>	
Increasing the Resolution and Readability of Digital Images	43

<i>Juri D. Kandilarov, Lubin G. Vulkov</i> Numerical Study of an Initial Concentration Identification Problem in Porous Media	45
<i>Kristina G. Kapanova, Velislava Stoykova</i> Studying the Social Impact of #NAPLeaks Networks Discussions: Responsive Fusion(s), Diffusion(s), Confusion(s)	47
<i>Ivaylo Katsarov, Nevena Ilieva, Ludmil Drenchev</i> Quantum effects on dislocation motion in pure and hydrogen charged Fe from ring-polymer molecular dynamics	48
<i>Eunji Kim, Ivan Ivanov, Edward R. Dougherty</i> Quantifying Important Genes in a Gene Regulatory Network with Applications to Network Compression	50
<i>Miglena N. Koleva, Sergey V. Polyakov, Lubin G. Vulkov</i> Exponential difference scheme approximations for Richards' equation with piecewise constant and degenerate absolute permeability	52
<i>Petia Koprinkova-Hristova, Ivan Georgiev</i> Image segmentation via Echo state network	54
<i>N. Kutev, M. Dimova, N. Kolkovska</i> Finite time blow up of the solutions to nonlinear dispersive equations with critical initial energy	56
<i>Nilolay Kutev, Sonia Tabakova, Stefan Radev</i> Axisymmetric oscillatory flow of Carreau fluid in tube	58
<i>T. Lazarova, P. Petkov, N. Ilieva, E. Lilkova, L. Litov</i> In silico study of the self-organisation process in mono-component solutions of antimicrobial peptides	59
<i>Konstantinos Liolios, Georgios Skodras, Krassimir Georgiev, Ivan Georgiev</i> Analysis of contaminant removal in constructed wetlands under step-feeding: A Monte Carlo based stochastic treatment accounting for uncertainty	61
<i>Rositsa Maksimova, Krassimir Kolev</i> Live-graphing with LoRaWAN and Python	63
<i>Lubomir Markov</i> Two series which generalize certain sums expressed in terms of zeta values	65
<i>Vladimir Myasnichenko, Rossen Mikhov, Leoneed Kirilov, Nikolay Sdobnyakov, Denis Sokolov, Stefka Fidanova</i> Simulation of Diffusion Process in Bimetallic Nanofilms	67

<i>Elena V. Nikolova, Denislav Z. Serbezov</i>	
Chaotic behaviour in a generalized model of three interacting economic sectors	69
<i>Tzvetan Ostromsky, Venelin Todorov, Ivan Dimov, Stoyan Apostolov, Yuri Dimitrov, Zahari Zlatev</i>	
Sensitivity Study of a Large-Scale Air Pollution Model by Using Latin Hypercube Sampling	70
<i>Marcin Paprzycki</i>	
Semantic Technologies in a Decision Support System	72
<i>Ludmila Parashkevova</i>	
Characterization of porous materials by homogenization models based on a generalized mixture rule	73
<i>Marek Pecha, Stanislav Harizanov</i>	
Comparison analysis of graph-Laplacian-based methods for image segmentation	75
<i>Iliyan Petrov</i>	
Information theory with new vision on hierachy and evolution in dynamic systems	77
<i>Svilen I. Popov, Vassil M. Vassilev</i>	
Some sufficient conditions for the well-posedness of a clamped Timoshenko beam type system	79
<i>Evgenija D. Popova</i>	
Parameterized Solutions to a Class of Interval Parametric Linear Systems	80
<i>Peter Rashkov</i>	
Dimension reduction in epidemiological models for vector-borne diseases	82
<i>N. Shegunov, O. Iliev, P. Armyanov</i>	
Comparison Between Different Permeability Field Approximations in MLMC Applications	84
<i>D. Slavchev, S. Margenov</i>	
Performance analysis of a Parallel Hierarchical Semi-Separable compression solver in shared and distributed memory environment for BEM discretization of Flow around Airfoils	86
<i>Tony Spassov</i>	
Nanomaterials for hydrogen production and storage	88
<i>Dimiter Syrakov, Emilia Georgieva, Maria Prodanova, Maria Dimitrova, Damyan Barantiev</i>	

Effects of satellite data assimilation on air quality parameters simulated by the Bulgarian Chemical Weather Forecast System (BgCWFS)	89
<i>M. Terziyska, Zh. Terziyski, Y. Todorov, K. Kolev</i>	
Extreme Learning Distributed Adaptive Neuro-Fuzzy Architecture for Chaotic Time Series Prediction	91
<i>Venelin Todorov, Ivan Dimov, Tzvetan Ostromsky, Stoyan Apostolov, Yuri Dimitrov, Zahari Zlatev</i>	
Quasi-Monte Carlo methods based on low discrepancy sequences for sensitivity analysis in air pollution modeling	92
<i>Petar Tomov, Iliyan Zankinski, Todor Balabanov</i>	
Genetic Algorithm Selection Operator Based on Recursion and Brute-Force	93
<i>Velichka Traneva, Stoyan Tranev</i>	
Inuitionistic Fuzzy Anova Approach to the Management of Movie Sales Revenue	94
<i>Krassimira Vlachkova, Krum Radev</i>	
Interpolation of data in \mathbb{R}^3 using quartic triangular Bézier surfaces	96
<i>Roumen Borisov, Nikolay K. Vitanov, Zlatinka I. Dimitrova</i>	
Probability distributions connected to the flows of substance in a channel of a network	98
Part B: List of participants	101

Part A
Extended abstracts¹

¹Arranged alphabetically according to the family name of the first author.

Method for remote continuous Pulse Oximetry for Critical Congenital Heart Disease screening

A. Alexandrov, V. Monov

Cardiovascular diseases are the most common cause of death worldwide over the last few decades in the world. Early detection of heart defects can reduce the mortality rate especially by the screening of newborn babes. The early detection of babies with critical congenital heart defects (CCHDs) is critical because it is needed an extremely fast reaction [1]. In most cases, the main screening tests used to identify CCHD include prenatal ultrasonography and postnatal clinical examination. However, even though both of these methods are available, a significant proportion of babies are still missed. Routine pulse oximetry has been reported as an additional screening test that can potentially improve the detection of CCHD [2],[3] (NCBI Cochrane Database sources).

Oxygen is integral to countless biological processes. The transport of oxygen throughout the human body is performed by the circulatory system, and more specifically, hemoglobin *Hb* in red blood cells. Critical medical information can be obtained by measuring the amount of oxygen in the blood, as a percentage of the maximum capacity.

The pulse oximeter is a medical instrument that is used to measure the amount of oxygen in the blood. Pulse oximetry shortens the time passed before the detection of hypoxemia i.e. deficiency of oxygen.

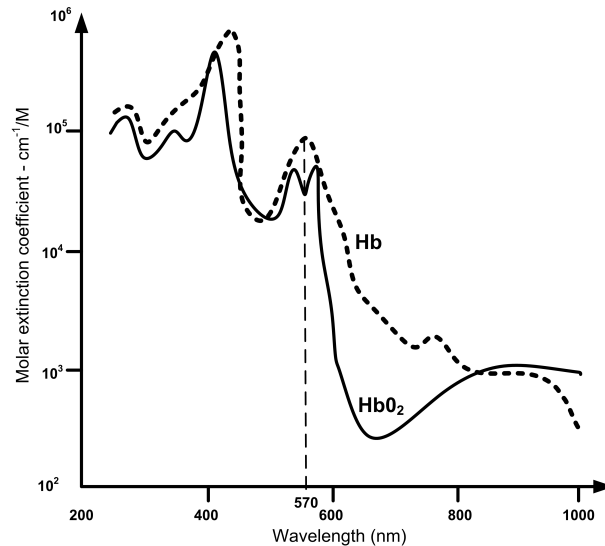


Fig.1 Light absorption in function of blood oxygen concentration
In reflection pulse oximetry LEDs transmit light that is reflected back to a photo detector on the same side of the human skin as the LEDs. Transmission pulse oximetry

is the most common form of pulse oximetry used in the operating room, although reflective pulse oximetry is becoming more popular because of the improved accuracy and ease of placement.

When the heart contracts there is a surge of arterial blood, which momentarily increases arterial blood volume across the measuring site. This results in more light absorption during the surge. If light signals received at the photo detector are looked at as a waveform, there should be peaks with each heartbeat and troughs between heartbeats.

The proposed k-Nearest Neighbors (kNN) algorithm for blood oxygen level analysis is a type of instance-based learning algorithm machine learning. It is a classifier type algorithm where the learning is based on the similarity of the data vectors. The rationality of kNN is that similar samples belonging to the same class have a high probability.

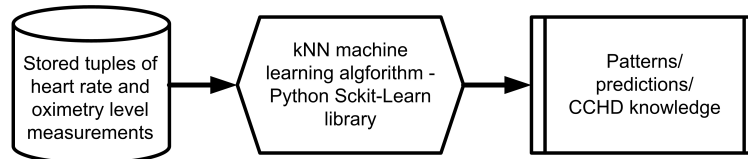


Fig.2 Method of kNN based machine learning Pulse oximetry for CCHD detection The current research considers a new design and method for real-time patient monitoring system architecture using a custom design 570 nm green light based reflection oximetry method. This can ensure sensitively better accuracy, compared to the wide used red and infrared light oximetry methods. A new, improved pulse oximetry algorithm, using a machine learning technique based on a kNN algorithm is proposed for an automated CCHD screening of newborn babes. Additionally, the proposed method and system architecture allow intelligent and reliable continuous remote monitoring of all ages heart disease patients round-the-clock by his/her caretaker.

References

- [1] Friedberg, M., Silverman, N., Moon-Grady, A., Tong, E., Nourse, J., Sorenson, B., Lee, J., Hornberger, L., Prenatal detection of congenital heart disease. *J Pediatr.* 2009, 155(1): 26–31.
- [2] Koppel, R., Druschel, C., Carter, T., Goldberg, B., Mehta, P., Talwar, R., Bierman, F., Effectiveness of pulse oximetry screening for congenital heart disease in asymptomatic newborns. *Pediatrics.* 2003, 111(3): 451–455.
- [3] Liske, M., Greeley, C., Law, D., Reich, J., Morrow, W., Baldwin, H., Graham, T., Strauss, A., Kavanaugh-McHugh, A., Walsh, W., Tennessee Task Force on Screening Newborn Infants for Critical Congenital Heart Disease Report of the Tennessee task force on screening newborn infants for critical congenital heart disease. *Pediatrics.* 2006, 118(4), e1250–e1256.

Watermarking Audio Signals: Analysis of Noise Effect and Error Characteristics

T. Aleksandrova, H. Kostadinov, N. Manev

The possibility of embedding watermarks robust against compression in musical audio files is investigated in this paper. The compression itself can be considered as a communication channel whose statistical characteristics are sensitive to the compressed musical genre. We study the compression format Advance Audio Coding (AAC) and collect statistical data for different musical genres. AAC is designed to be the successor of the MP3 format and it generally achieves better sound quality than MP3 format at the same bit rate. AAC is the default audio format for the most modern devices and platforms that dominates in recent years.

The process of embedding and retrieving a watermark can be regarded as a binary communication channel. In this paper, we propose a method of embedding watermarks based on a combination of key-dependable dither modulation and Haar wavelet transform. We investigate its statistics to give recommendation how to choose the most proper embedding parameters such as quantization step, the level of the Haar reconstruction and in which sub-bands to embed.

We aim after a comprehensive analysis of the embedding technique to propose a method of choosing the parameters so that to achieve acceptable probability of errors (according to characteristics of the watermark) without perceptible loss of the quality of the audio file.

References

- [1] B. Chen and G.W. Wornell, Quantization index modulation: A class of provably good methods for digital watermarking and information embedding, *IEEE Trans. on Information Theory*, vol. 47 no.4, pp. 1423–1443, 2001.
- [2] R. Martinez-Noriega, M. Nakano, B. Kurkoski, and K. Yamaguchi, High Payload Audio Watermarking: toward Channel Characterization of MP3 Compression, *Journal of Information Hiding and Multimedia Signal Processing*, vol. 2, no. 2, 91-107, (2011).

Perturbation analysis of the matrix equation

$$X - A^* \sqrt[m]{X^{-1}} A = I$$

Vera Angelova

In finite difference approximation to an elliptic differential equation, when applying LU decomposition for solving the appeared system of linear equations, the non-linear matrix equation

$$F(X, A) := X - A^* \sqrt[m]{X^{-1}} A - I = 0 \tag{1}$$

can arise. Here, the matrix A is a parameter matrix, X is the unknown matrix, I is the identity matrix, m is a positive integer and A^* denotes the complex conjugate transpose of the matrix A .

Both the necessary and sufficient conditions for existence of positive definite solution of (30) are proved in [5]. Some properties of the positive definite solutions to $X - A^* \sqrt[m]{X^{-1}} A = I$ are discussed in [3]. Efficient and numerically stable iterative methods for computing a positive definite solution are proposed in [1, 5]. Due to the floating point computing environment, the numerical solution of (30) is contaminated with rounding and parameter errors. The error in a computed solution depends on the sensitivity of the solution to perturbations in the data. Thus, the perturbation estimates of the error in the computed solution are an obligatory element of the numerical solution to an equation. Perturbation estimates for the maximal solution and an error bound for the approximate solution to the real equation $X + A^T \sqrt{X^{-1}} A = P$ are derived in [2]. A perturbation bound and the backward error of the solution to the more general equation $X - A^* X^{-p} A = Q$, with $p \in (0, 1]$ are evaluated in [4].

In this paper we study the sensitivity of equation (30) to perturbation in the data A . We suppose that the matrix coefficient A is subject to perturbation $A \rightarrow A + \delta A$, so as the positive definite solution X of equation (30) and the solution $X + \delta X$ of the perturbed equation

$$F(X + \delta X, A + \delta A) = 0 \tag{2}$$

exist. The perturbation δA represents the rounding errors and the errors of approximation in the solution, computed by a numerically stable algorithm. The error δX in the solution $X + \delta X$ to the perturbed equation (31) is a continuous function of the elements of the data perturbation δA . For the aim of a norm-wise forward perturbation analysis, we rewrite the perturbed equation (31) in equivalent operator form in terms of the Fréchet derivatives of $F(X, A)$ in X at the point (X, A) . Then, we assume the invertibility of the partial Fréchet derivative $F_X(X, A)$ of $F(X, A)$ in X at the point (X, A) , so as to express the perturbation δX to the solution of equation (31) in operator form

$$\delta X = \Theta(\delta X, \delta A). \tag{3}$$

Applying the techniques of the Lyapunov majorants to the vector representation of (3) and the fixed-point principles, computable bounds for the Frobenius norm $\delta_X := \|\delta X\|_F$ of the perturbation in the solution as a function of the perturbation $\delta_A := \|\delta A\|_2$ in the data, are formulated. The effectiveness of the bounds is illustrated by a numerical example.

References

- [1] S. El-Sayed and M.A. Ramadan. On the existence of a positive definite solution of the matrix equation $X + A^* \sqrt[2^m]{X^{-1}} A = I$. *Intern. J. Computer Math.*, 76:331–338, 2001.
- [2] N. El-Shazly. On the perturbation estimates of the maximal solution for the matrix equation $X + A^T \sqrt{X^{-1}} A = P$. *Journal of the Egyptian Mathematical Society*, 24:644–649, 2016.
- [3] I. Ivanov, B. Minchev, and V. Hasanov. Positive definite solutions of the equation $X - A^* \sqrt{X^{-1}} A = I$. In B. Cheshankov and M. Todorov, editors, *Applications of Mathematics in Engineering'24*, pages 113–116. Heron Press, Sofia, 1999.
- [4] Jing Li and Yuhai Zhang. Perturbation analysis of the matrix equation $X - A^* X^{-p} A = Q$. *Linear Algebra Appl.*, 431(9):1489–1501, 2009.
- [5] M.A. Ramadan and N.M. El-Shazly. On the matrix equation $X + A^\top \sqrt[2^m]{X^{-1}} A = I$. *Appl. Math. Comput.*, 173:992–1013, 2006.

Numerical Study of Soliton Solutions to the Two Dimensional Boussinesq Equation

K. Angelow, N. Kolkovska

In this paper we evaluate propagating wave solutions to the two dimensional Boussinesq Equation (BE)

$$u_{tt} - \Delta u - \beta_1 \Delta u_{tt} + \beta_2 \Delta^2 u + \Delta f(u) = 0 \quad \text{for } (x, y) \in \mathbb{R}^2, t \in \mathbb{R}^+, \quad (4)$$

$$u(x, y, 0) = u_0(x, y), u_t(x, y, 0) = u_1(x, y) \quad \text{for } (x, y) \in \mathbb{R}^2, \quad (5)$$

where $f(u) = \alpha u^2$, $\alpha > 0$, $\beta_1 > 0$, $\beta_2 > 0$ are dispersion parameters, and Δ is the two-dimensional Laplace operator. We suppose that the solution of (4)-(5) is a sufficiently smooth function.

The BE is famous with the approximation of shallow water waves or also weakly non-linear long waves. It is often used for simulation of various physical processes e.g. turbulence in fluid mechanics, vibrations in acoustics, geotechnical engineering, atmosphere dynamics, etc.

Boussinesq equation (4) admits localized stationary propagating solutions of type $u(x, y, t) = U(x, y - ct)$. They are obtained by different approximation techniques in [4, 5, 6]. The time behavior and structural stability of the solutions to (4)-(5) with initial data from [4, 5, 6] are presented in [3, 7, 8] using numerical methods with second order of approximation in space and time.

In [2] the stationary propagating solutions to (4) are evaluated with high accuracy of fourth and sixth order of approximation. The resulting solutions differ from the solution developed in [4, 5, 6] especially for velocities c close to $\min(1, \frac{\beta_2}{\beta_1})$.

The aim of this paper is to present and apply a high accuracy numerical method for solving (4)-(5) with initial data obtained in [2].

To construct the numerical method, we first introduce a uniform mesh Ω_h on a computational domain Ω and apply finite differences of second, fourth and sixth order for the approximation Δ_h to the Laplace operator Δ . In this way we obtain the following system of second order ODE's with respect to unknowns $u_{i,j}(t) = u(x_i, y_j, t)$

$$(u_{i,j})_{tt} = (E - \beta_1 \Delta_h)^{-1} (\Delta_h u_{i,j} - \beta_2 \Delta_h^2 u_{i,j} - \Delta_h f(u_{i,j})), \quad (6)$$

where E is the identity operator.

Then the values of the solutions on the next time $u_{i,j}(t + \tau)$ are evaluated using Taylor series expansion of $u_{i,j}$ at time t with degrees corresponding to the order of space approximation. All time derivatives in the Taylor series expansion are evaluated iteratively by differentiating (6) with respect to the time variable. This is possible since the highest time derivative in (6) is isolated on the one side of equation (6).

An explicit formula for the numerical solution is applied on the computational boundary $\partial\Omega$. The formula is taken from [1] and adjusted for the hyperbolic equation (4)

$$u_B(x, y, t) = \mu_u \frac{(1 - c^2)x^2 - (y - ct)^2}{((1 - c^2)x^2 + (y - ct)^2)^2}. \quad (7)$$

Near the computational boundary $\partial\Omega_h$ we do not change any of the cross stencils used in the approximation of the discrete Laplacian - we use the values (7) at points outside the computational domain. In the implementation of the numerical method Fast Poisson Solver (FPS) technique is used at each time step. The band matrices produced at each time level are inverted by Thomas or similar technique.

In this way the numerical solution to (4)-(5) is computed by Taylor series method with high accuracy of second, fourth and sixth order both in space and time on relatively coarse grid.

The performed numerical tests validate the numerical method for solving BE. The results show that the Taylor series method achieves the prescribed high accuracy.

We solve BE with two sets of initial parameters and initial data obtained in [2]. The resulting two numerical solutions are stable in form and their maxima are changed for long period of time $T = 40$ with small errors. Thus the obtained solutions show soliton behavior.

References

- [1] K. Angelow, *New Boundary Condition for the Two Dimensional Stationary Boussinesq Paradigm Equation*, International Journal of Applied Mathematics, **32**, **1** (2019), 141–154.
- [2] K. Angelow and N. Kolkovska, *Numerical Study of Traveling Wave Solutions to 2D Boussinesq Equation*, Serdica J. Computing, Accepted for publication.
- [3] A. Chertock, C. Christov and A. Kurganov, *Central-upwind schemes for the Boussinesq paradigm equation*, Comp. Sci. High Performance Comp. IV, NNFM, **113** (2011), 267–281.
- [4] M. Christou and C. Christov, *Fourier-Galerkin method for 2D solitons of Boussinesq equation*, Mathematics and Computers in Simulation, **74** (2007), 82–92.
- [5] C. Christov, *Numerical implementation of the asymptotic boundary conditions for steadily propagating 2D solitons of Boussinesq type equation*, Math. Computers Simul., **82** (2012), 1079–1092.
- [6] C. Christov and J. Choudhury, *Perturbation solution for the 2D Boussinesq equation*, Mech. Res. Commun., **38** (2011), 274–281.
- [7] C. Christov, N. Kolkovska and D. Vasileva, *On the numerical simulation of unsteady solutions for the 2D Boussinesq paradigm equation*, LNCS, **6046** (2011), 386–394.
- [8] M. Dimova, D. Vasileva, *Comparison of two numerical approaches to Boussinesq paradigm equation*, LNCS, **8236** (2013), 255–262.

Application of the mixed integer programming in determining the optimal honeybee colony's location based on the productive potential of the bee forage species

Atanas Atanasov, Ivan Georgiev, Milen Petrov

This study aims to apply multi-objective mixed integer programming for the determination of the optimal honeybee colony's location based on the productive potential of the bee forage species in selected areas in Northeast part of Bulgaria. The study was conducted in 2019 based on the assessment existing bee forage resources as Lime (*Tilia cordata*), Acacia (*Robinia pseudoacacia*), Oilseed rape (*Brassica napus*), Sunflower (*Helianthus annuus L*) and the number of bee colonies kept in the Northeast part of Bulgaria in village Brestovica. Geographical location of experimental apiaries in Brestovica is 43°32'4.02" N, 25°45'14.10" E and at an altitudinal range of 222 m above sea level. If all the factors remain constant, the productivity of the bee colonies is in correlation with nectar secretion potential of bee forage species and the existing honeybee colony density. Bees play an important role in nature. As pollinators, bees help in the production of flowering crops and in the maintenance of plant biodiversity. Like any animals, bees are threatened by overpopulation. It is very important for the proper development of bee colonies to find the best location of a bee hive in a certain area in such a way that each colony will have enough food resources and at the same time to minimize the apiary share that will be underfed (due to overpopulation).

Multi-objective Mixed Integer Programming, which is already an established tool in optimization, is used to achieve the posed goal. This paper proposes a practical technological solution for 13 apiaries ($A_1 - A_{13}$) spaced at a certain distance from each other with different numbers of bee hives as follows: $A_1 = 200$; $A_2 = 40$; $A_3 = 80$; $A_4 = 350$; $A_5 = 350$; $A_6 = 45$; $A_7 = 250$; $A_8 = 35$; $A_9 = 26$; $A_{10} = 30$; $A_{11} = 250$; $A_{12} = 120$; $A_{13} = 40$ with 1816 total number of bee colonies located in study region with 13 fields with flowering vegetation's with Y_j caring capacity of plant cluster- j . The number of fields with Sunflower is 6 with $Y_1 = 1372,2$ kg/da; $Y_2 = 558,3$ kg/da; $Y_3 = 755,4$ kg/da; $Y_4 = 362,4$ kg/da; $Y_5 = 344,4$ kg/da; $Y_6 = 4620,60$ kg/da; the number of fields with Oilseed rape with $Y_7 = 945,48$ kg/da; $Y_8 = 3542,71$ kg/da; $Y_9 = 386,01$ kg/da; the number of fields with Lime with $Y_{10} = 2775,85$ kg/da; $Y_{11} = 3651,61$ kg/da; the number of fields with Acacia $Y_{12} = 12754,65$ kg/da; $Y_{13} = 607,05$ kg/da.

The result of this paper is a general model that determines the optimal distribution of honeybee colonies for any size and orientation of a field with diverse kinds of plants. As an example, the best relocation of the local breed of bee *Apis mellifera macedonica* colonies is determined. The used mathematical program assumes that bee colonies are non-migratory, a beehive contains one colony only, the input and output values are deterministic, the resources have constant carrying capacity, and the strength of each bee colony does not change for a certain period of time. Multi-objective mixed-integer

problem is solved via Matlab software operations research capabilities.

Two fundamental criteria are imposed: to maximize $f_1(\mathbf{X}) = \sum_{i=1}^m \mathbf{X}_i$ and to minimize $f_2(\mathbf{E}) = \sum_{i=1}^m \mathbf{E}_i$. The aim is to find the **Pareto-optimal** solutions. The vector objective $\max F = [f_1(X); -f_2(E)]^T$ is linear and the constraints in the optimization model are linear so the feasible set is convex. Imposing part of the variables to be integer makes the solving process harder. These problems belong to the so called NP complexity class (nondeterministic polynomial time). Some of the coordinates of the Pareto-optimal solutions in this case are a discrete set and it is not necessary for them to coincide with the coordinates of the Pareto-optimal solutions lacking the integer constraints. Since the feasible set is convex, to find the Pareto-optimal solutions in presence of mixed-integer constraints. A generalized objective is built as a linear combination of the singular objectives $\max Z = \lambda^1 f_1 + \lambda^2 (-f_2)$ with weights λ^r , $r = 1, 2$ and constraints $\sum_{r=1}^2 \lambda^r = 1$, $\lambda^r \geq 0$, $r = 1, 2$. In this way the multi-objective problem is transformed into a global optimization problem with a scalar criterion and for its solving different methods could be applied. Since the feasible set is convex, this approach could not generate pseudooptimal solutions. Weights λ^r are initialized with uniformly distributed random values (exploring the domain of the generalized objective vector) and for every pair of random weights a single-objective integer problem is solved. The domain exploration is done via quasirandom Sobol sequence, which is a low-discrepancy sequence.

Defining a single unambiguous solution in case of a multiple and self-contradictory objectives always requires additional information and to a some extent projects a subjective intuition for a compromise. The choice of a compromise solution instead of a scientifically justified definition of the Pareto-optimal solution set requires from the decision-taker (sometimes a team of experts) experience, intuition and informal knowledge of the optimization problem. As a result of a calculation corresponding to one point on Pareto frontier, it was found that the fraction of X_i relocated at site (i) can be accommodated by plant cluster (j), or as follows: 194 bee hives of A_1 ; 40 bee hives of A_2 ; 80 bee hives of A_3 ; 350 bee hives of A_5 ; 45 bee hives of A_6 ; 250 bee hives of A_7 ; 35 bee hives of A_8 ; 26 bee hives of A_9 ; 250 bee hives of A_{11} ; 40 bee hives of A_{13} can be relocated at site 6 with $Y_6 = 4620, 60$ kg/da. 350 bee hives of A_4 and 30 bee hives of A_{10} can be relocated at site 12 with $Y_{12} = 12754, 65$ kg/da. 120 bee hives of A_{12} can be relocated at site 4 with $Y_4 = 362, 4$ kg/da. The amount of overpopulation at site (i) in term of colony strength $E_4 = 224, 4$; $E_6 = 62, 21$; $E_9 = 30574, 05$. The solution has an indication of overpopulation. This is the optimal solution for the given carrying capacities of plant clusters. If we want to reduce the overpopulation we have to change carrying capacities of the plant clusters.

ACKNOWLEDGMENTS. The study was supported by contract of University of Ruse "Angel Kanchev", No. BG05M2OP001-2.009-0011-C01, Support for the development of human resources for research and innovation at the University of Ruse "Angel Kanchev". The project is funded with support from the Operational Program "Science and Education for Smart Growth 2014 - 2020" financed by the European Social Fund of the European Union.

Modeling the Long-Range Effect of Copper Nanoclusters Irradiating a Copper Target

B. Batgerel, I.V. Puzynin, T.P. Puzynina, I.G. Hristov, R.D. Hristova, Z.K. Tukhliev, Z.A. Sharipov

The molecular dynamics method [1] simulated the interaction of copper nanoclusters [2, 3] with energies from the range 100 eV – 2 keV with copper targets of various sizes. The conditions for the formation of shock waves in the targets depending on the energy of the nanoclusters and the size of the targets are established. Classification of the arising structural changes in target depth depending on energy of a nanocluster and the size of a target is carried out. The effect of shock waves is used to explain the long-range effect [4], in which structural changes in the target are observed at a depth exceeding the penetration depth of the nanocluster. The results obtained confirm that the action of shock waves is one of the possible mechanisms for the formation of the long-range effect.

Figures 1 show the results when the target is irradiated by a single nanocluster with an energy of 50 eV/atom. Figures demonstrate the dynamics of the propagation of a thermal wave at the target depths, as well as the formation of a crater on the surface of the irradiated target.

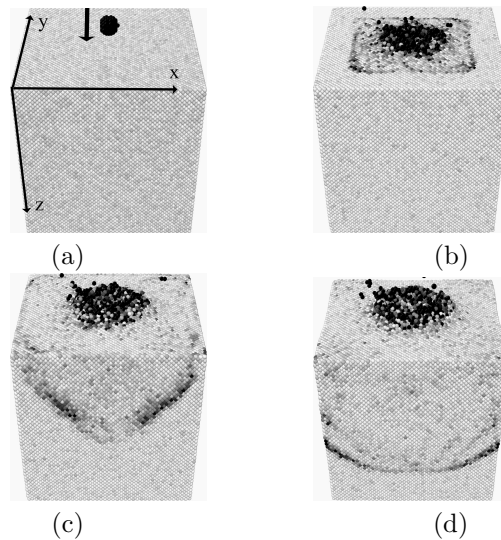


Figure 1: Dynamics of the propagation of a thermal wave and the formation of a crater on the surface of a target when irradiated with one nanoclusters with an energy of 100 eV/atom at instants 1 ps (a), 4 ps (b), 7 ps (c), and 10 ps (d). The calculated region was a parallelepiped with sides $11 \times 11 \times 18$ nm, the number of particles in the target was 183,000.

The work was financially supported by RFBR grant No. 17-01-00661-a and by a grant of the Plenipotentiary Representative of the Republic of Bulgaria at the JINR.

References

- [1] Holmurodov, H.T., Puzynin, I.V., et al.: Methods of molecular dynamics for modeling physical and biological processes. *PEPAN* **2**(34), 472–515 (2010) (Russian)
- [2] Batgerel, B., Dimova, S., Puzynin, I., et al.: Modeling Thermal Effects in Metals Irradiated by Copper Nanoclusters. *EPJ Web Conf.* **173**, 06001 (2018)
- [3] Batgerel, B., Puzynin, I., et al.: Molecular Dynamic Modeling of Long-Range Effect in Metals Exposed to Nanoclusters. Springer Nature Switzerland AG, LNCS 11189, 318–325 (2019)
- [4] Aparina, N.P., Gusev, M.I., et al.: Some aspects of the long-range effect. *Problems of Atomic Science and Engineering (PASE), Ser. Thermonuclear Fusion.* **3**, 18–27 (2007) (Russian)

Improvement of air pollution caused by traffic through different signal timing policies — case study of Sofia

Y. Boneva, V. Ivanov

Different approaches exist related to mitigation of traffic pollution e.g. pedestrian zones, catalytic converters, policies to reduce traffic congestions, signal timing policies etc. This research focuses on the signal timing traffic management policies and their impact on air pollution.

The traffic can be managed either on the basis of historical data and the result is fixed-time signal plans or on the basis of real-time data for the traffic and then an adaptive traffic control is applied. Each approach has its particularity. The fixed-time signal plans are better in terms of set up and maintenance. Whereas, adaptive time control is more expensive but is more adequate to the needs of the traffic and it was shown in this study that it improves the air pollution indicators. This can be considered as a direct result from the improvement of traffic indicators such as density, queues, speed etc.[1-5] A software simulation with the traffic software simulators AIMSUN and TRANSYT was performed. AIMSUN uses the environmental model of Panis et al. 2006 and QUARTET to estimate the air pollution in the modeled network. For the purposes of this study the Panis et al. 2006 model was used. A microscopic traffic simulation model to evaluate the environmental effects of the application of different signal timing policies was used. A network of four connected junctions along Shipchenski Prohod Blvd. in Sofia was simulated.

Parameters - Car	Current signal timing plan	Green wave fixed-time plan	Actuated control	Units
Fuel Consumption	355.53	307.52	289.86	
IEM Emission - CO2	874077.52	788275.5	762346.78	g
IEM Emission - NOx	1835.5	1680.73	1614.73	g
IEM Emission - PM	340.52	288.71	271.36	g
IEM Emission - VOC	1131.69	963.57	876.51	g

Table 1: Fuel consumption and vehicle emission for different signal timing policies

Optimizing fixed time plans for green waves give better results in terms of air pollution indicators in contrast to the actually observed signal time plans for the network. Further, the change from fixed-time signal plans to actuated control gives even better results for the air pollution indicators. These experiments lead to the conclusion that traffic pollution can be influenced by signal timing policies. The experimental results from the application of different signal timing policies are presented in Fig. 1 (in absolute values) and Fig.2 (change in percentage).[6,7] As it is obvious from the data the most favorable outcome is achieved by using actuated control of junctions. The improvement is visible by all indicators of air pollution more precisely CO2, NOx,

Parameters - Car	Current signal timing plan	Green wave fixed-time plan (change in percent)	Actuated control
Fuel Consumption	355.53	-13.50	-18.47
IEM Emission - CO2	874077.52	-9.82	-12.78
IEM Emission - NOx	1835.5	-8.43	-12.03
IEM Emission - PM	340.52	-15.21	-20.31
IEM Emission - VOC	1131.69	-14.86	-22.55

Table 2: Fuel consumption and vehicle emission for different signal timing policies

PM (Particulate matter) and VOC (Volatile organic compounds) emissions. These four air pollution indicators along with the fuel consumption are investigated by this research.[8]

References

- [1] Panis L, Broekx S, Liu R. Modelling instantaneous traffic emission and the influence of traffic speed limits. *Science of the Total Environment* **2006**; 371: 270–285
- [2] Aimsun Microscopic 8 Macroscopic Modelling Manual, , TSS Transport Simulation Systems **October 2013**
- [3] Boneva Y., Fixed-Time Signal Timing Versus Actuated Control of Traffic Lights — Case Study of Shipchenski Prohod Blvd. in Sofia, Bulgaria, Proceedings for International Conference AUTOMATICS AND INFORMATICS, 2019, 03-05 October 2019, ISSN 1313-1850, CD: ISSN 1313-1869, John Atanasoff Society of Automatics and Informatics, Sofia, Bulgaria , 2019, pp. 53–56
- [4] Transyt -Aimsun Link (Version 2), User Guide, Issue B by James C Binning, Copyright Copyright TRL Limited 2010 All rights reserved (2013)
- [5] T. Stoilov, K. Stoilova, V. Stoilova, Bi-level Formalization of Urban Area Traffic Lights Control. *Studies in Computational Intelligence*. Book: Innovative Approaches and Solutions in Advanced Intelligent Systems, Margenov S. et al. Editors, Vol. 648, Springer, ISBN:978-3-319-32206-3, ISSN:1860-949X, DOI:10.1007/978-3-319-32207-0 20, 303-318. SJR:0.19 (2016)
- [6] Garvanov, I., C. Kabakchiev, V. Behar, M. Garvanova, Target detection using a GPS Forward-Scattering Radar, International Conference Engineering Telecommunications, 2015, Moscow-Dolgoprudny, Russia, pp. 29-33, 2015 (2015)

A Study of Self-catalyzed Exponential Decay Chains with a Fast Rate Parameter

Milen Borisov, Svetoslav Markov

The study is dedicated to the 150-th jubilee of the Bulgarian Academy of Sciences

We consider a two-step exponential decay reaction chain (Bateman equations involving three species and two reactions, resp. two rate parameters). We study the time evolution of the concentrations of the species under the assumptions of homogeneity and mass action kinetics. We focus on the situation when one of the chain-links is very fast, that is its rate parameter is very large relatively to the other one, and analyse the behavior of the solutions. We prove that a two-step exponential decay chain with a very fast chain-link can be “approximated” by a one-step decay reaction. We then generalize the problem by considering a self-catalyzed exponential decay chain and study the relevant kinetic equations. We show that the type of evolution of the growing third species varies between saturation and logistic type depending on the values of the parameter’s rates. Thus, the growth model obtained generalizes the saturation and the logistic growth models and is suitable for fitting of real-world biological data.

Acknowledgments. This work is supported by the National Scientific Program “Information and Communication Technologies for a Single Digital Market in Science, Education and Security (ICTinSES)”, contract No DO1–205/23.11.2018, financed by the Ministry of Education and Science in Bulgaria.

References

- [1] Anguelov R, Borisov M, Iliev A, Kyurkchiev N, S. Markov, On the chemical meaning of some growth models possessing Gompertzian-type property. *Math. Meth. Appl. Sci.* 2017;1–2.
- [2] Bateman H, The solution of a system of differential equations occurring in the theory of radio-active transformations, *Proc. Cambridge Phil. Soc.*, 15 1910, 423–427.
- [3] Markov S, Reaction networks reveal new links between Gompertz and Verhulst growth functions, *Biomath* 8 (2019), 1904167.
- [4] Markov S, On a class of generalized Gompertz–Bateman growth–decay models, *Biomath Communications* 6 (1) (2019) 52–59.

Computing distance distributions of ternary orthogonal arrays

S. Boumova, T. Ramaj, M. Stoyanova

In 1940 Rao introduced certain combinatorial arrangements named orthogonal arrays (OAs). They play important roles in statistics (used in designing experiments), computer science and cryptography. OAs are related to Latin squares, Hadamard matrices, finite geometry and error-correcting codes. Although much has been done in this area, there are still many unsolved problems ([7]).

Polynomial and combinatorial techniques ([4, 6, 5]) are used to compute all feasible distance distributions of ternary orthogonal arrays of relatively small lengths and strengths. We use properties of orthogonal arrays (with given parameters) and some relations with their derived OAs to reduce the possible distance distributions. If after applying all constraints there is no distance distribution, the ternary OA with the given parameters does not exist.

An OA of strength τ is an $M \times n$ matrix with entries from a set of q distinct symbols arranged so that every $M \times \tau$ submatrix contains each of the q^τ possible τ -tuples equally often as a row (say λ times).

The number of rows M (which represents the number of runs in the experiment and may require too many resources) should be reduced. This brings us to the following important problems:

- ★ **Existence:** for which values of the number of rows, columns, strength and levels does an OA exist?
- ★ **Construction:** how can we construct an array, if one exists.
- ★ **Non-isomorphic classes:** find the numbers of non-isomorphic orthogonal arrays for given parameters.

We improve the known methods ([1, 3, 2]) for computing and reducing the possibilities for distance distributions of OAs. This is the key for investigating the structure of OAs. The next step is applying the new conditions so that OAs must be satisfied. If not then we get nonexistence results, i.e. there is no $OA(108, 16, 3, 3)$ and confirm the nonexistence result for $OA(108, 17, 3, 3)$ from our previous work ([2]).

References

- [1] P. Boyvalenkov, H. Kulina, Investigation of binary orthogonal arrays via their distance distributions, Problems of Information Transmission, 49, 2013, No. 4, 320-330.
- [2] S. Boumova, Tanya Marinova, Tedis, Ramaj, Maya Stoyanova, Nonexistence of $OA(108, 17, 3, 3)$ orthogonal array, 2019, submitted.

- [3] P. Boyvalenkov, Tanya Marinova, Maya Stoyanova, Nonexistence of a few binary orthogonal arrays, *Discrete Applied Mathematics*, 217(2), 2017, pp. 144-150.
- [4] P. Delsarte, An Algebraic Approach to the Association Schemes in Coding Theory, *Philips Res. Rep. Suppl.* 10, 1973.
- [5] A. Hedayat, N.J.A. Sloane, J. Stufken, *Orthogonal Arrays: Theory and Applications*, Springer-Verlag, New York, 1999.
- [6] V.I. Levenshtein, Universal bounds for codes and designs, in: V.S. Pless, W.C. Huffman (Eds.), *Handbook of Coding Theory*, Elsevier, Amsterdam, 1998, pp. 499–648. Ch. 6.
- [7] <http://neilsloane.com/oadir/index.html>

Some results on 3D printing technology

St. Bushev

Here we look at Stefan-Schwartz tasks for 3D Printer - solidified in core bodies. The following experiments are used.

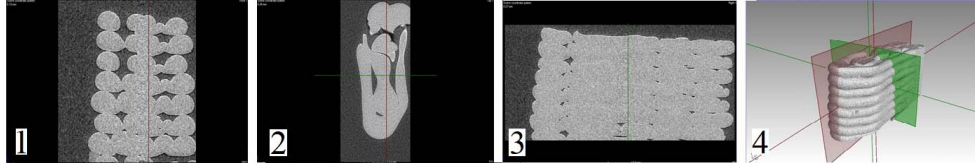


Figure 1. Material deposition on a substrate with 3D Printer Technology: 1 - initial deposition; 2 - development of postponement; 3 - final stage of the deposition; 4 - general view of the deposited layers.

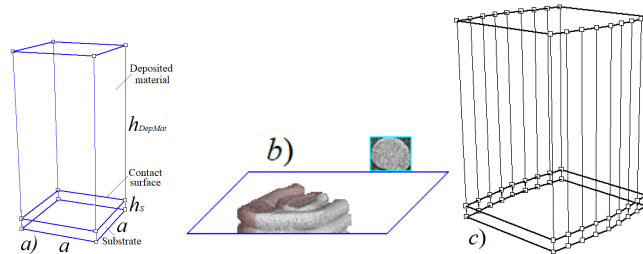


Figure 2. Basic geometry subject to mathematical modeling by finite elements method: contact between two materials in a contact spot a) system dimensions $a = 1 \mu\text{m}$, $h_s = 1 \mu\text{m}$ and $h = 17 \mu\text{m}$; b) contact surface with pre-fabricated material and its cross-section (from Figure 1); c) Other body of dimensions $X = 8 \mu\text{m}$, Y having a maximum projection in the middle of $9 \mu\text{m}$ and $H = 17 \mu\text{m}$.

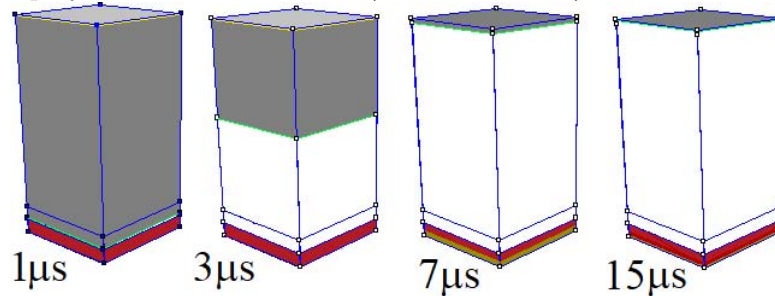
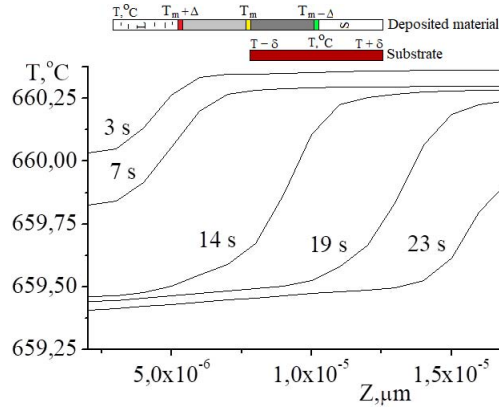


Figure 3. Solidification process in the main body (Figure 2 a) by solidification zone (see Fig. 4). The figure shows the contact volume of the deposited material with the dimensions of the substrate.



In Figure 4, we present temperature scales for the considered solidification processes in deposited material on the substrate and time-temperature curves for that process of the geometry (Fig. 2 c):

Solidification: by temperature scales - representation of a zone of first-order phase transition by isothermal lines, $T_m = 660.1^\circ C$, $\Delta = 0.2^\circ C$; $T_m - \Delta = 660.1 - 0.2 = 659.9^\circ C$ and $T_m + \Delta = 660.1 + 0.2 = 660.3^\circ C$; time-temperature curves - the temperature field of phase conversion is represented by the temperature field at specific moment of the time.

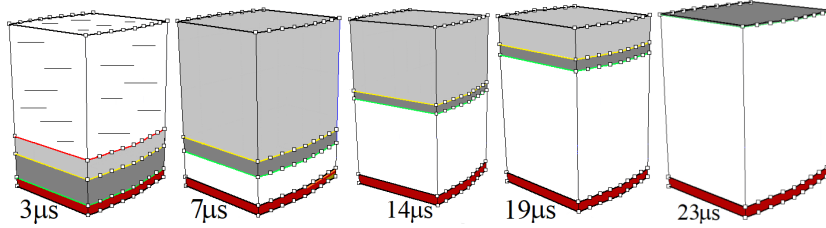


Figure 5. Solidification in geometry of Fig.2 c. The fundamental engineering process is a first-order phase transition that must be organized so that there are no macro- and micro-level defects. For this, we understand by organization an accurate fundamental knowledge based on mathematics and mathematical physics and experiment.

Stefan-Schwartz's tasks are an important foundation because: 1. They are the mathematical basis of the first- and second-order phase transitions at the macro-level; 2. The use of geometries similar to those presented here is an important research experiment; 3. These tasks can be repeated pen and ink literally.

ETCCDI Thermal Climate Indices in the CMIP5 Future Climate Projections over Southeast Europe

Hristo Chervenkov and Kiril Slavov

An important task in the modern climatology is to assess extreme climate and weather events alongside various aspects of the mean climate. The climate indices find multiple applications in climate research and related fields due to their robustness and fairly straightforward calculation with standardized methodology and interpretation. The Expert Team on Climate Change Detection and Indices (ETCCDI) facilitated the analysis of such extremes over the last decades by defining a set of climate indices that provide a comprehensive overview of temperature and precipitation statistics focusing particularly on extreme aspects.

In the present work we study the spatial distributions and the time evolution of top 5 ETCCDI thermal climate indices over Southeast Europe in projected future climate up to the end of the 21 century. The indices are based on selected CMIP5 simulations of the projected future climate and are computed for all 4 RCP emission scenarios. The study reveals clearly expressed warming signal for all of the considered indices, which is also spatially dominating and statistically significant. The revealed patterns of climate change intensify with the increasing radiative forcing in the considered scenarios, which also agrees generally with the outcome of the prevailing number recent studies. Under RCP8.5, with its strongest radiative forcing at year 2100, annual regional averaged changes in temperature extremes (i.e. minimum and maximum temperature) of the multi-model mean are projected to be 4–8°C relative to the reference period 1961–1990. The 'warm days' index and especially the growing season length will increase with more than a month. Most drastic, however, seems the future for the 'cold nights' — the projected warming under RCP8.5 will lead to practically total disappearance of this index. Although the work, provided on annual basis, outlines some specifics of the spatial distribution and warming rate among the indices, there are not clear enough and rigor evidences for 'warming asymmetry' — systematic differences between the indices, based on the minimum temperature from the one hand and these, based on maximum temperature, from the other hand.

Solar Radiation Modelling for Bulgaria Based on Assimilated Surface Data

Hristo Chervenkov and Kiril Slavov

The downward surface shortwave radiation plays a crucial role in the global energy balance. Its transfer through the Earth's atmosphere and interaction with the land, air, and oceans are the drivers for the planetary radiation budget and, subsequently, the climate system. Continuous global energy issues, such as energy shortages, have increased the interest in energy-efficient buildings and solar energy systems. The accurate knowledge of solar radiation locally available at the Earth's surface is critical for precise performance evaluation and, ultimately, for optimal design of such systems. The most useful solar radiation data are global horizontal irradiance (GHI), but direct normal irradiance (DNI) or diffuse horizontal irradiance (DHI) are also important. Typically, not all three solar radiation components are available as measured data. A lack of DNI measurement data is quite often due to high cost and maintenance of the instruments. Solar radiation models are widely used in order to overcome this limitation, but only a few studies have been devoted to solar radiation data and modeling over the Balkan Peninsula. This has also to do with the lack of a dense network of ground stations in the area of the Eastern Mediterranean.

Main goal of the present article is to test the simulation capabilities of the solar radiation model DISC using assimilated data from in situ measurements as input and satellite retrieved estimations as reference. This study is a continuation of previous work, aiming to find reliable and consistent modelling tool for simulation of the missing solar radiation components and derived additional parameters. The single one source of all needed input parameters for DISC is the Bulgarian operative assimilation system ProData. As reference is used SARA2, which is surface radiation climate data record, based on the Meteosat satellites. It provides climatological data for 5 irradiance-related parameters including the considered in the present work GHI, DNI and sunshine duration (SDU). The numerical experiment is performed on hourly basis for the year 2015 over domain, which covers entirely Bulgaria with fine-spaced grid. The main conclusion is that the assimilated ground measurements of the GHI underestimates the satellite data. In contrast, the modelled with DISC DNI, as well as the derived from the DNI parameter SDU, are positively biased from the reference.

Finite Element Modeling of Effective Properties of Nanostructured Poroelastic Composites with Surface Effects

Danilchenko A.S., Nasedkin A.V., Nasedkina A.A.

Recently, there has been an increased interest in the problems of nanomechanics. Numerous studies have revealed a scale effect, which consists in changing the effective stiffness and other material moduli for nanoscale bodies in comparison with the corresponding values for bodies of macro-dimensions. A number of theories have been developed to explain the scale factor. One of such widely used theory is the model of surface elasticity. There are a number of reviews devoted to research on the surface theory of elasticity and its applications. In turn, among the theories of surface elasticity, the most popular is the Gurtin – Murdoch model. The use of this model actually leads to the fact that the boundaries of the nanosized body are covered with elastic membranes, the internal forces in which are determined by surface stresses. Elastic membranes can be placed on the interphase boundaries inside the body with nanoscale inclusions, which also allows to model imperfect interface boundaries with stress jumps.

This investigation concerns to the determination of the material properties of nanoscale two-phase poroelastic composites of an arbitrary anisotropy class with different connectivities between the phases. In order to take into account nanoscale level at the interface, the Gurtin – Murdoch model of surface elastic and porous stresses are used. This work is a continuation of the author’s researches. In the development of earlier investigations, the scale factor is associated with sizes of inclusions and the influence of the composite structure on the effective properties is studied.

Finite element packages ANSYS and ACELAN-COMPOS was used to simulate representative volumes and to calculate the effective material properties. This approach is based on the theory of effective moduli of composite mechanics, modeling of representative volumes and the finite element method. Here, the interface boundaries were covered by the shell elements in order to take the surface effects into account. For using the shell elements with suitable properties we apply an analogy between poroelastic and thermoelastic problems in coupled settings, and solve the poroelastic problems as corresponding thermoelastic problems with volume and shell elastic and thermal elements.

To create a representative volume of the composite, we use the special algorithms of the ACELAN-COMPOS package. This algorithm in a cubic volume generates the structure of the finite elements with material properties of two different phases and with different connectivities. The different algorithms support the coupling of main phase or the coupling of both phases.

For automated coating of interphase boundaries in the cubic representative volume the following algorithm was realized in APDL ANSYS program. At the beginning, as a result of the formation of the composite structure, the finite element mesh from

octanodal cubic elements was created, some of which had the material properties of the main poroelastic material, and the other part of the elements had the material properties of the material of second phase (inclusions or pores). Further, only the finite elements with main material properties were selected. The resulting elements on the outer boundaries were covered by four nodal target contact elements. Then, the contact elements, which were located on the external surfaces of the full representative volume, were removed, and the remaining contact elements were replaced by the four nodal membrane elastic elements. As a result, all the facets of the contact of poroelastic structural elements with inclusions or pores were coated by membrane finite elements.

The next step consisted in solving for obtained representative volume the static poroelastic problems in accordance the Bio model and filtration with the essential boundary conditions which were conventional for effective moduli method. Further, in the ANSYS postprocessor the averaged stresses were calculated, both on the volume finite elements and on the surface finite elements. Finally, the effective moduli of composite with surface effects were calculated from the corresponding formulas of the effective moduli method by using the estimated average characteristics.

In the results of computational experiments, the following features were observed. If we compare two similar bodies, one of which has usual dimensions and the other is a nanoscale body, then for the nanosized body due to the surface stresses the effective stiffness will be greater than for the body with usual sizes. Furthermore, for the porous body of the usual size the effective elastic stiffness decreases with increasing porosity. Meanwhile, the effective stiffness of nanocomposite porous body with the same porosity may either decrease or increase depending on the values of surface moduli, dimensions and number of pores. This effect is explained by the fact that the sizes of the surface pore with surface stresses depend not only on the overall porosity, but also on the configuration, size and number of pores. We can observe similar effects for the effective filtration permeability coefficients.

The work was done in the framework of the Ministry of Science and Higher Education of Russia project No. 9.1001.2017/4.6 in part of the analysis of algorithms for creating granular composite structures and in the framework of the RFBR project 19-58-18011 and NSFB in part of analyzing the effective properties of nanostructured porous poroelastic composites.

On the universal optimality of the 600-cell: the Levenshtein framework lifted

Peter Dragnev

The potential energy of a spherical code $C \subset \mathbb{S}^{n-1}$ with interaction potential h is defined as $E(C, n, h) := \sum_{x \neq y \in C} h(\langle x, y \rangle)$. In 2016, based on the Delsate-Yudin linear programming approach, we derived a universal lower bound (ULB) on energy for absolutely monotone potentials

$$E(C, n, h) \geq N^2 \sum_{i=1}^m \rho_i h(\alpha_i),$$

where the nodes $\{\alpha_i\}$ and weights $\{\rho_i\}$ depend only on the cardinality N and dimension n and not on the interacting potential. The nodes and weights are obtained from a quadrature rule framework introduced by Levenshtein in relation to maximal codes. The ULB is attained for all universally optimal codes discovered by Cohn and Kumar, except the 600-cell (a code with 120 points on \mathbb{S}^3).

In this talk we present a method for solving the linear program for polynomials of higher degree, essentially lifting the Levenshtein framework and obtaining a second level ULB. While there are numerous cases for which our method applies, we will emphasize the model examples of 24 points (24-cell) and 120 points (600-cell) on \mathbb{S}^3 . In particular, we provide a new proof that the 600-cell is universally optimal, and furthermore, we completely characterize the optimal linear programming polynomials of degree at most 17 by finding two new polynomials, which together with the Cohn-Kumar's polynomial form the vertices of the convex hull that consists of all optimal polynomials.

Joint work with P. Boyvalenkov - Bulgarian Academy of Sciences, D. Hardin and E. Saff - Vanderbilt University, and M. Stoyanova - Sofia University

New Ant Colony Optimization Including Weights

Stefka Fidanova, Krassimir Atanassov

A nature inspired methods and algorithms are widely used to solve NP-hard optimization problems. Examples are Genetic algorithm, evolutionary algorithms, bee colony optimization, bat algorithm, fire fly algorithm, particle swarm optimization, gray wolf algorithm and so on.

Ant Colony Optimization (ACO) is one of the most successful methods for solving discrete optimization problems. The idea for the method comes from real ants behavior, which manage to establish the shortest routes to feeding sources and back. The problem is represented by a graph called graph of the problem and the solutions are represented by path in a graph. Thus finding the optimal solutions is equivalent to finding the shorter path in a graph, taking in to account some constraints. The artificial ants start their walk in a graph from random node. They include new nodes in their partial solution applying probabilistic rule called transition probability. The probabilistic rule is a product of the quantity of the pheromone and heuristic information related to the problem. The ants in a nature mark their way back with a chemical substance called pheromone. Thus the most used path has more concentrated pheromone and is more desirable by other ants from the nest. Similar, in the algorithm a numerical information is related to the elements of the graph imitating the pheromone. The main rule is that the elements of the better solutions, according the fitness function, receive more pheromone than others. Thus they become more desirable in the next iteration. The random start is used for diversification of the search in the search space and the pheromone is a concentration of the search close to best so far solutions. Combination of this two rules helps to avoid local optimums. Sometimes some elements of the graph accumulates more pheromone than others and the ants explore same regions of the search space. In this paper we include weights related with the nodes of the graph. At the beginning the weight of the nodes is the same for all nodes. If some node is included in some solution, its weight decreases. In our algorithm the transition probability is a product of three elements: quantity of the pheromone; heuristic information and weight. As a results the regions with best so far solutions and unexplored regions in a search space are more desirable, than explored regions with worse solutions. This new element in the transition probability leads to enlarging diversification of the search and giving more chance to unexplored regions of the search space.

Our idea is tested on Multiple Knapsack Problem as a representative of subset problems. It is capital budgeting problem and a lot of real life and industrial problems can be defined as a knapsack problem.

Numerical determination of elastic material properties of closed cell aluminum foam

Ivan Georgiev, Roumen Iankov, Maria Datcheva

The aluminium foams are porous materials with open or closed cell structure. The aluminium metal foams are widely used in many industrial applications such as energy absorption structures, noise barrier structures, lightweight highly effective constructions and many other applications.

In present paper a 3D numerical homogenization technique is proposed for determination of elastic material properties of closed cell aluminium foams. The performed homogenization procedure employs micro-computed tomography (micro-CT) and instrumented indentation testing data (IIT).

The results from micro-CT observations are used to determinate the following characteristics of the aluminium foam considered as a porous material the volume fractions of the pores and the solid phases, the average size of the pores, the pore size distribution in a representative volume element (RVE). Using the micro-CT data, a 3D geometrical model of a RVE is created and this geometrical model is used to generate a finite element model. In order to apply the homogenization technique, periodic boundary conditions are imposed to the RVE finite element model. For simplicity, the pores are considered to have a spherical form as it is depicted in Fig. 1. The employed material model is the linear elastic model. The elastic properties of the solid phase (aluminium) are determined based on IIT data from testing of small volumes of the aluminium foam material. The obtained according to the homogenization procedure six boundary value problems with periodic boundary conditions are solved using the commercial finite element code ANSYS. The determined elastic characteristics are analysed against data from literature in order to reveal the applicability of the

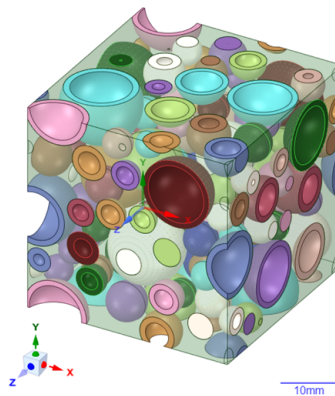


Figure 1: RVE with random particle distribution and spherical pores.

followed in this study homogenization procedure.

Acknowledgement

The first author gratefully acknowledges the financial support of the Bulgarian National Science Fund under Grant No. KP-06-H27-6 "Digital laboratory for multiscale modelling and characterization of porous materials: a multidisciplinary approach". We also acknowledge the provided access to the infrastructure of the Laboratory for 3D Digitalization and Microstructure Analysis and of the Laboratory for Nanos-structure Characterization, financially supported by the Science and Education for Smart Growth Operational Program (2014-2020) and the European Structural and Investment fund through Grants No BG05M2OP001-1.001-0003 and BG05M2OP001-1.001-0008-C01, respectively.

References

- [1] Baltov, A., Iankov, R., Datcheva, M.: A New Approach to Determine the Yield Loci of Heterogeneous Media. *J. Teor. Appl. Mech.* **4**, 13–19 (1996)
- [2] ANSYS, Inc. Theory Reference Manual. Release 2019.
- [3] Yang, Z. and Xiaofeng, P., MicroCT scanning analysis for inner structure of porous media. *Heat Trans. Asian Res.*, 36: 208-214 (2007)

Numerical methods for fractional diffusion-reaction problems based on operator splitting and BURA

K. Georgiev, S. Margenov

The interaction of the operator splitting methods and the applied discretization schemes to the solution of the related sub-processes has been actively studied during last decades (see, e.g., [1]). As a rule, the operators describing the sub-processes are supposed to be simpler than the whole spatial differential operator, providing attractive opportunities to utilize the best available solvers for the resulting sub-tasks. The principle novelty of this study is that the coupled problem involves fractional powers of elliptic operators.

We consider a system of time dependent fractional-in-space diffusion-reaction equations for the unknown functions $u_k(x, t)$ in the form

$$\begin{aligned} \frac{du_k(x, t)}{dt} &= \mathcal{L}_k^{\alpha_k} u_k(x, t) + \mathcal{R}_k(u_1, \dots, u_m) + f_k(x, t), \quad k = 1, \dots, m, \\ u_k(x, 0) &= u_{k,0}(x), \end{aligned} \quad (8)$$

$x \in \Omega \subset \mathbb{R}^d$, $t \in [0, T]$, $0 < \alpha_k < 1$. \mathcal{L}_k corresponds to the bilinear form

$$(v, w)_{\mathcal{L}_k} = \int_{\Omega} a_k(x) \nabla v(x) \cdot \nabla w(x) dx, \quad 0 < \underline{a}_k \leq a_i(x),$$

assuming homogeneous boundary conditions on $\partial\Omega$. The system (8) is coupled through the reaction operators $\mathcal{R}_i(u_1, \dots, u_m)$. We follow the definition of fractional power of the diffusion operator introduced by the spectral decomposition, i.e.,

$$\mathcal{L}^{\alpha} v(x) = \sum_{i=1}^{\infty} \lambda_i^{\alpha} c_i \phi_i(x), \quad \mathcal{L}^{-\alpha} v(x) = \sum_{i=1}^{\infty} \lambda_i^{-\alpha} c_i \phi_i(x), \quad c_i = \int_{\Omega} v(x) \phi_i(x) dx,$$

where $0 < \alpha < 1$, $\{\phi_i(x)\}_{i=1}^{\infty}$ are the orthonormal eigenfunctions of \mathcal{L} , and $0 < \lambda_1 \leq \lambda_2 \leq \dots$ are the related eigenvalues. Now, let us rewrite (8) in the form

$$\begin{aligned} \frac{d\mathbf{u}}{dt} &= (\mathcal{A} + \mathcal{B})\mathbf{u}, \quad t \in [0, T] \\ \mathbf{u}(0) &= \mathbf{u}_0, \end{aligned} \quad (9)$$

where \mathcal{A} and \mathcal{B} represent the fractional diffusion and the reaction plus source parts of (8) respectively, and $\mathbf{u} = (u_1, \dots, u_m)^T$, $\mathbf{u}_0 = (u_{1,0}, \dots, u_{m,0})^T$.

The operators in (9) have different nature. \mathcal{A} is non-local and fully decoupled with respect to the unknowns u_k . \mathcal{B} couples the system but could be treated as fully local in space. The operator splitting is one of the most powerful methods to solve such

problems. In this study, we analyze a composite algorithm which integrates the so called *sequential splitting*:

Step 1:

$$\begin{aligned}\frac{d\mathbf{u}_1^j}{dt}(t) &= \mathcal{A}\mathbf{u}_1^j(t), & (j-1)\tau < t \leq j\tau, \\ \mathbf{u}_1^j((j-1)\tau) &= \mathbf{u}_2^{j-1}((j-1)\tau),\end{aligned}$$

Step 2:

$$\begin{aligned}\frac{d\mathbf{u}_2^j}{dt}(t) &= \mathcal{B}\mathbf{u}_2^j(t), & (j-1)\tau < t \leq j\tau, \\ \mathbf{u}_2^j((j-1)\tau) &= \mathbf{u}_1^j(j\tau),\end{aligned}$$

and $j = 1, 2, \dots, J$, where $\tau = T/J$ is the uniform time step.

Backward Euler approximation of the time derivatives at Step 1 is combined with a properly chosen Runge-Kutta solution method at Step 2, thus ensuring a balanced order of accuracy with respect to τ . Finite differences or linear finite elements are used for discretization in space providing accuracy of order $O(h^{2\alpha_k})$. The next key question concerns the numerical solution of non-local linear systems with dense matrices $L_k^{\alpha_k} + q_k I$, arising at Step 2. The involved symmetric and positive definite sparse matrices L_k correspond to the diffusion operator \mathcal{L}_k , where $q_k > 0$ is a parameter depending on τ . The recently introduced BURA method [2] is utilized for this purpose. The method is based on best uniform rational approximation of the scalar function $1/(\xi^{-\alpha_k} + q_k)$, $\xi \in [0, 1]$. The most important advantage of BURA approach is that the non-local problem is reduced to a number of local systems with matrices like $L_k + t_k I$, $t_k > 0$. We assume that fast iterative solver (e.g. BoomerAMG) is used for these systems, thus obtaining a total computational complexity of optimal order for the presented composite numerical method.

Acknowledgments. This work is accomplished with the partial support by the Grant No BG05M2OP001-1.001-0003, financed by the Science and Education for Smart Growth Operational Program (2014-2020) and co-financed by the European Union through the European structural and Investment funds. The partial support through the Bulgarian NSF Grant DN 12/1 is also acknowledged.

References

- [1] I. Farago, *Splitting Methods and Their Application to the Abstract Cauchy Problems*, Springer LNCS, Vol 3401 (2005), 35-45
- [2] S. Harizanov, R. Lazarov., S. Margenov, P. Marinov, Numerical solution of fractional diffusion-reaction problems based on BURA, *Computers & Mathematics with Applications* (2019), <https://doi.org/10.1016/j.camwa.2019.07.002>

Reconstruction of Time-Dependent Implied Volatility by Market Observations for European Options in Jump–Diffusion Models

Slavi G. Georgiev, Lubin G. Vulkov

Model fitting in an accurate and robust way using real market data is one of the most fundamental problems in contemporary finance. As the models become more complicated than the classical Black–Scholes framework, their *calibration* is a challenging task. In particular, both empirical and theoretical analyses show that the constant volatility models are unable to explain the market price dynamics since they do not take into account heavy tails, volatility clustering or volatility smiles and skews. On the other hand, the underlying price in the *jump-diffusion* models is not continuous function of time and it allows to account large changes in price for infinitesimal time interval thus replicating the real market conditions. When we combine the possibility of price jumps with a *time-dependent volatility* model, we derive a powerful tool for pricing and hedging options in an accurate and meaningful manner.

Volatility, measuring the amount of randomness, is heavily used in risk and portfolio management since it is the only unobservable parameter from the financial markets. In general, it can be estimated from the quoted option prices. So, the reliable *reconstruction* of the volatility from observed market data is (still) of high interest, see e. g. [1].

The European call option premium $V = V(S, \tau := T - t; K, T)$ satisfies the following generalized forward PIDE

$$\frac{\partial V}{\partial \tau} = \frac{1}{2} \sigma^2(\tau) S^2 \frac{\partial^2 V}{\partial S^2} + (r(\tau) - \lambda \kappa) S \frac{\partial V}{\partial S} - (r(\tau) + \lambda) V + \lambda \int_0^\infty V(S\eta) f(\eta) d\eta, \quad (10)$$

where $S \in [0, +\infty)$ is underlying asset, T is the maturity, $\tau \in [0, T)$ is the remaining time to maturity, K is the strike price, $r(\tau)$ is the risk-free interest rate, $\sigma(\tau)$ is the volatility function, λ is the jump intensity and $f(\eta)$ is the probability density function of the jump amplitude η , $\kappa := \mathbb{E}[\eta - 1]$. We solve equation (10) imposing Dirichlet boundary conditions and the initial condition $V(S, 0) = \max(S - K, 0) \equiv (S - K)^+$. We consider two particular models of $f(\cdot)$: Merton's model and Kou's model.

In Merton's model, $f(\eta)$ is given by the lognormal density

$$f(\eta) = \frac{1}{\sqrt{2\pi}\sigma_\eta\eta} \exp\left(-\frac{(\ln\eta - \mu_\eta)^2}{2\sigma_\eta^2}\right), \quad \kappa = \exp\left(\mu_\eta + \frac{\sigma_\eta^2}{2}\right) - 1,$$

where μ_η and σ_η^2 determine the mean and the variance of the return jumps. In Kou's model, $f(\eta)$ is the following log-double-exponential density

$$f(\eta) = p\eta_1\eta^{-\eta_1-1}\mathbb{1}_{\{\eta \geq 1\}} + q\eta_2\eta^{\eta_2-1}\mathbb{1}_{\{\eta < 1\}}, \quad \kappa = \frac{p\eta_1}{\eta_1 - 1} + \frac{q\eta_2}{\eta_2 + 1} - 1,$$

where $\eta_1 > 1$, $\eta_2, p, q > 0$, $p + q = 1$. In case of presence of jumps, that is $\lambda > 0$, and for Merton's model, an explicit formula (in terms of an infinite sum) for $V(S, \tau)$ is derived only for the constant volatility case. For other models, and when $\sigma = \sigma(\tau)$, we have to resort to numerical algorithms for solving (10).

Suppose now that we have a set of market measurements $\{\omega_\beta^\alpha\}$, where ω_β^α is the quoted price of a call option with maturity T_α , $\alpha = 1, \dots, M_T$ and strike K_β , $\beta = 1, \dots, M_K$, assuming that $T_1 \leq \dots \leq T_{M_T}$. Using the available data, we determine the volatility function $\sigma(\tau)$ in a least-squares sense. More rigorously, we minimize the following mean-square error function

$$\Gamma_\alpha(\sigma) = \frac{1}{M_K} \sum_{\beta=1}^{M_K} [v_{K_\beta}(\sigma_\alpha(\tau_\alpha); S_0, T_\alpha) - \omega_\beta^\alpha]^2 \chi_\beta^\alpha, \quad \tau_\alpha \in (0, T_\alpha], \quad \alpha = 1, \dots, M_T.$$

where $v_{K_\beta}(\sigma_\alpha(\tau_\alpha); S_0, T_\alpha)$ is the numerical solution of (10) at $S = S_0$ with exercise price K_β and expiry time T_α . χ_β^α is an indicator function which shows whether ω_β^α is available or not. $\sigma_1(\tau_1)$ is a constant function and $\sigma_\alpha(\tau_\alpha)$ is a piecewise linear function for $\alpha > 1$. Since we minimize $\Gamma_\alpha(\sigma)$ in an iterative manner (over α), $\sigma_\alpha(\tau_\alpha)$ represents the calculated values up to the current iteration and the last linear part that depends on the current minimizer σ . We comment on the approach to solve numerically (10) and the special features and optimization techniques while minimizing the cost function $\Gamma_\alpha(\sigma)$. Then we present an *algorithm* to recover the time dependent volatility function. We supply numerical experiments with synthetic and real market data in case of jumps and no jumps, as well as minimizing the error function in case of 2D call option:

$$\Gamma_\alpha(\sigma) = \frac{1}{M_{K^1} M_{K^2}} \sum_{\beta_1=1}^{M_{K^1}} \sum_{\beta_2=1}^{M_{K^2}} [v_{K_{\beta_1}^1, K_{\beta_2}^2}(\sigma_\alpha(\tau_\alpha); S_0^1, S_0^2, T_\alpha) - \omega_{\beta_1, \beta_2}^\alpha]^2 \chi_{\beta_1, \beta_2}^\alpha,$$

$$\tau_\alpha \in (0, T_\alpha], \quad \alpha = 1, \dots, M_T.$$

Acknowledgments. The authors are supported by the Bulgarian National Science Fund under Project DN 12/4 “Advanced analytical and numerical methods for nonlinear differential equations with applications in finance and environmental pollution”, 2017. The first author is also partially supported by the National Science Fund at University of Ruse.

References

- [1] Georgiev S., L. Vulkov, Computational recovery of time-dependent volatility from integral observations in option pricing, J. Comp. Sci., DOI:10.1016/j.jocs.2019.101054, (2019).

On mKdV equations and 2-dimensional Toda field theories: algebraic structures and Hamiltonian properties

Gerdjikov V. S.

In 1981 A. V. Mikhailov [1] introduced the reduction group for soliton equations and as a result discovered the class of 2-dimensional Toda field theories (2d-TFT) related to the algebras $sl(n)$. Soon after that it was established that 2d-TFT can be related to each simple Lie algebra [2] and also to Kac-Moody algebras [3]. The Lax representations of 2d-TFT related to the simple Lie algebra \mathfrak{g} graded by its Coxeter automorphism C is [2]:

$$\begin{aligned} L\psi &\equiv i\frac{\partial\psi}{\partial x} + (U_0(x,t) - \lambda U_1(x,t))\psi = 0, & U_0 &= i\frac{\partial\phi}{\partial x}, & U_1 &= \sum_{\alpha \in A} e^{\phi_\alpha} E_\alpha \\ M\psi &\equiv i\frac{\partial\psi}{\partial t} + (V_0(x,t) - \lambda^{-1}V_1(x,t))\psi = 0, & V_0 &= -i\frac{\partial\phi}{\partial t}, & V_1 &= \sum_{\alpha \in A} e^{\phi_\alpha} E_{-\alpha}. \end{aligned} \tag{11}$$

Here the real-valued function $\phi(x,t) \in \mathfrak{h}$ and A is the set of admissible roots of \mathfrak{g} , see [2]. The Lax pair (11) possesses \mathbb{D}_h as Mikhailov reduction group where h is the Coxeter number of \mathfrak{g} , $C^h = 1$. The corresponding 2d-TFT take the form:

$$2\frac{\partial\phi}{\partial x\partial t} = \sum_{\alpha \in A} \alpha e^{2\phi_\alpha(x,t)}. \tag{12}$$

The seminal paper [3] establishes the close relation between \mathbb{Z}_h Mikhailov reductions and the Kac-Moody algebras [4]. Typical construction of a Kac-Moody algebra is based on a \mathbb{Z}_h -graded simple Lie algebra, where h is the Coxeter number of \mathfrak{g} . This means that \mathfrak{g} is split into direct sum of the commutative subalgebra $\mathfrak{g}^{(0)}$ and the linear subspaces $\mathfrak{g}^{(k)}$ which satisfy

$$CYC^{-1} = \omega^k Y \quad \text{for all } Y \in \mathfrak{g}^{(k)}; \quad [\mathfrak{g}^{(k)}, \mathfrak{g}^{(m)}] \in \mathfrak{g}^{(k+m)}, \quad k, m = 0, 1, \dots, h-1,$$

where $k+m$ should be understood modulo h . The Lax pairs analyzed in [3] are of the form:

$$\begin{aligned} \tilde{L}\tilde{\psi} &\equiv i\frac{\partial\tilde{\psi}}{\partial x} + (Q(x,t) - \lambda J)\tilde{\psi} = 0, & Q(x,t) &= \sum_{\alpha_s \in A} q_s(x,t)\tilde{E}_{\alpha_s} \in \mathfrak{g}^{(0)}, \\ \tilde{M}_{(m)}\tilde{\psi} &\equiv i\frac{\partial\tilde{\psi}}{\partial t} + \left(\sum_{k=0}^{m-1} \lambda^k V_s(x,t) - \lambda^m K \right) \tilde{\psi} = 0, & V_s(x,t) &\in \mathfrak{g}^{(s)}, \end{aligned} \tag{13}$$

where $m = ch + m_a$, $c \geq 0$ is an integer and m_a is an exponent of \mathfrak{g} . Besides J and K are constant matrices such that $J \in \mathfrak{g}^{(1)} \cap \mathfrak{h}$ and $K \in \mathfrak{g}^{(m_a)} \cap \mathfrak{h}$. For each admissible

value of m the compatibility condition of the Lax pair (13) gives rise to a system of integrable NLEE for the functions $q_s(x, t)$. If we put $m = 3$ then the corresponding system of NLEE will be natural generalization of the mKdV equation.

One can check that the operators L in (11) and \tilde{L} in (13) are gauge equivalent. That is why we can consider the 2-dimensional TFT (12) as the simplest negative flow of the hierarchy (13). Therefore the 2-dimensional TFT and the generalized mKdV equations belong to the same hierarchy and share the same Hamiltonian properties, integrals of motion etc.

The present paper extends our results in [5] and [6, 7]. We demonstrate that both the 2-dimensional TFT and the mKdV systems can be linearized using special generalized Fourier transforms [6, 7]. This allows one to derive their action-angle variables in terms of the scattering data. Besides we extend the Zakharov-Shabat dressing method [8, 9] and construct dressing factors $u(x, t, \lambda)$ for both classes of graded Lax pairs (11) and (13). This would allow us to derive the soliton solutions of both the 2d-TFT (12) and of the generalized mKdV equations.

Acknowledgements. I am grateful to professor D. Mladenov and to Drs S. Varbev and A. Stefanov for numerous useful discussions. This work is supported by the Bulgarian Science Foundation (grant NTS-Russia 02/101 from 23.10.2017).

References

- [1] Mikhailov, A. V. The reduction problem and the inverse scattering problem. *Physica D*, **3D**, n. 1/2, 73–117, 1981.
- [2] Mikhailov, A. V., Olshanetsky, M. A., Perelomov A. M. Two-Dimensional Generalized Toda Lattice, *Commun. Math. Phys.* **79**, 473-488 (1981).
- [3] Drinfel'd, V., Sokolov. V. V. Lie Algebras and equations of Korteweg - de Vries type. *Sov. J. Math.* **30**, 1975–2036 (1985).
- [4] V. Kac, " *Infinite Dimensional Lie Algebras*", (Cambridge University Press, Cambridge, 1995).
- [5] V. S. Gerdjikov, D. M. Mladenov, A. A. Stefanov, S. K. Varbev. Integrable equations and recursion operators related to the affine Lie algebras $A_r^{(1)}$. *J. Math. Phys.* **56**, 052702 (2015).
- [6] V. S. Gerdjikov, A. B. Yanovski. *Completeness of the eigenfunctions for the Caudrey–Beals–Coifman system*. *J. Math. Phys.* **35**, no. 7, 3687–3725 (1994).
- [7] V S Gerdjikov, A B Yanovski. CBC systems with Mikhailov reductions by Coxeter Automorphism. I. Spectral Theory of the Recursion Operators. *Studies in Applied Mathematics* **134** (2), 145–180 (2015). DOI: 10.1111/sapm.12065.
- [8] Zakharov, V. E., Shabat, A. B. A scheme for integrating nonlinear equations of mathematical physics by the method of the inverse scattering transform. I. *Funct. Anal. and Appl.* **8**, no. 3, 43–53 (1974); and II. *Funct. Anal. Appl.* **13**(3) 13-23, (1979).
- [9] A.V. Mikhailov, V.E. Zakharov, "On the integrability of classical spinor models in two-dimensional space-time", *Comm. Math. Phys.* **74**, 21-40 (1980).

Analysis of a Space-Fractional Diffusion Problem with a Piecewise Constant Diffusion Coefficient

Stanislav Harizanov, Svetozar Margenov, Nedyu Popivanov

The topic of space-fractional diffusion in homogeneous media, that is the fractional Laplacian, is addressed in a quite large number of publications. In this study we assume that the spectral diffusion of fractional power of the elliptic operator is used. In general, the regularity of the solution decreases with the value of the fractional power $\alpha \in (0, 1)$. One of the most studied cases is the 1-D problem with homogeneous Dirichlet boundary conditions and constant right hand side $f \equiv 1$. In this setting, there are very rapid estimates regarding the boundary layers of solutions.

Here, we consider a similar 1-D problem in non-homogeneous media with piecewise constant diffusion coefficient. We assume that the (spectral) fractional diffusion problem is defined via spectral decomposition of the related standard (local) elliptic operator. Let us consider the weak formulation of the homogeneous Dirichlet problem: find $u \in V$ such that

$$a(u, v) := \int_{\Omega} (p(\mathbf{x}) \nabla u(\mathbf{x}) \cdot \nabla v(\mathbf{x})) d\mathbf{x} = \int_{\Omega} f(\mathbf{x}) v(\mathbf{x}) d\mathbf{x}, \quad \forall v \in V,$$

where $f(\mathbf{x}) \in L_2(\Omega)$, $p(\mathbf{x}) > 0$ is uniformly bounded in Ω , and $V := \{v \in H^1(\Omega) : v(\mathbf{x}) = 0 \text{ on } \partial\Omega\}$. Then, the nonlocal operator \mathcal{L}^α , $0 < \alpha < 1$ is introduced through its spectral decomposition, i.e.

$$\mathcal{L}^\alpha u(\mathbf{x}) = \sum_{i=1}^{\infty} \lambda_i^\alpha c_i \psi_i(\mathbf{x}), \quad u(\mathbf{x}) = \sum_{i=1}^{\infty} c_i \psi_i(\mathbf{x}),$$

where $\{\psi_i(\mathbf{x})\}_{i=1}^{\infty}$ are the eigenfunctions of \mathcal{L} , orthonormal in L_2 -inner product (\cdot, \cdot) , and $\{\lambda_i\}_{i=1}^{\infty}$ are the corresponding positive real eigenvalues.

We consider the 1-D problem in $\Omega = [0, 1]$, $f(x) \equiv 1$, $\delta, \theta \in (0, 1)$ and

$$p(x) = \begin{cases} \delta, & 0 \leq x < \theta; \\ 1, & \theta < x \leq 1. \end{cases}$$

The coefficient jump introduces some additional irregularity of the fractional diffusion problem. One of the main goals of this talk is the analytical study of the spectrum. We show for example, that the structure of the spectrum substantially depends on the coordinate of the jump $\theta \in (0, 1)$. The second major contribution is the analysis of the interface layers of the solution, and its dependence on the fractional power α .

Acknowledgment: The partial support through the Bulgarian NSF Grant DN 12/1 is highly acknowledged.

System and Parameter Identification Methods for Ground Models in Mechanized Tunneling

Raoul Hölter, Elham Mahmoudi, Markus König, Chenyang Zhao, Maria Datcheva

The numerical simulations of the mechanized tunneling process have to include the complex interactions between the subsoil, the tunnel boring machine (TBM) and the existing or forthcoming surface structures. The consideration of these interactions requires an adequate representation of the material and geometric features of the subsoil that is a very challenging task. Moreover, an accurate prediction of the investigated tunneling system response (e.g. ground surface heave or settlement and construction deformations) in both the design and the construction execution phase can be realistic only if the complex system properties are reliably identified. Therefore, for realistic numerical simulations in mechanized tunneling it is required to develop an efficient procedure for system parameters identification, numerical model validation, and adoption of adequate soil models. Fundamental part of this procedure is the implementation of adequate methods for model sensitivity analysis and hybrid modelling techniques. This contribution presents a concept for tunneling model identification, validation and verification (Fig. 2) as well as a concept for an optimal measurement design (OED) for obtaining of the most promising sensor location in mechanised tunneling for reliable model parameter identification and validation (Fig. 3) .

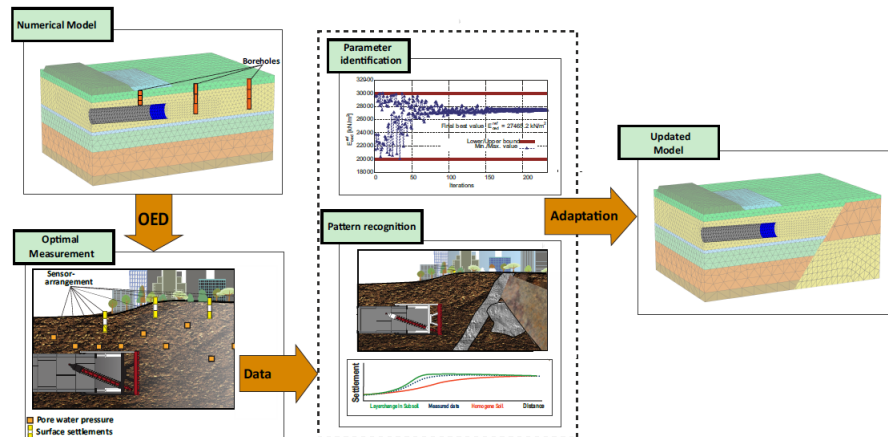


Figure 2: Overall concept of tunneling model identification and validation.

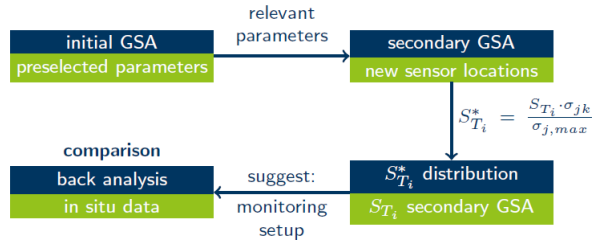


Figure 3: Flowchart of the employed OED approach.

Acknowledgement

The authors gratefully acknowledges the financial provided by the German Science Foundation (DFG) under the framework of subproject C2 in the Collaborative Research Center SFB 837. We also acknowledge the provided access to the infrastructure of the Laboratory for 3D Digitalization and Microstructure Analysis financially supported by the Science and Education for Smart Growth Operational Program (2014-2020) and the European Structural and Investment fund through Grants No BG05M2OP001-1.001-0003.

References

- [1] Hölter, R., Mahmoudi, E., Rose, S., König, M., Datcheva, M., Schanz, T.: Employment of the bootstrap method for optimal sensor location considering uncertainties in a coupled hydro-mechanical application. *Applied Soft Computing*. **75**, 298–309 (2019)
- [2] Zhao, C., Hölter, R., König, M., Lavasan, A. A.: A hybrid model for estimation of ground movements due to mechanized tunnel excavation. *Computer-Aided Civil and Infrastructure Engineering*. DOI: 10.1111/mice.1243, (2019)

Computing reliable solutions of chaotic dynamical systems using multiple-precision arithmetic

Radoslava Hristova, Ivan Hristov

Obtaining a mathematically reliable long-term solution of a chaotic dynamical system is a difficult task due to the sensitive dependence on the initial conditions. To achieve this goal we have to combine a class of numerical methods allowing arbitrary high order of accuracy with a multiple-precision floating point arithmetic. At least two classes of numerical methods work well towards this goal. They are Taylor series methods used in [1], and Gauss-Legendre methods used in [2]. In our work we choose Taylor series methods, because of their simplicity.

A comparison approach for verification the solution is used in [1]. The computed solutions for a sequence of numerical schemes (with different orders and different precisions) are compared globally (on the entire computational grid). If the solutions in the sequence differ less then some tolerance over a given interval, the solution is considered to be a mathematically reliable one on that interval. Such kind of comparison approach is widely accepted by the scientific community, although it is not fully rigour. It is important to mention that if we use the classical variable step size approach with estimating the local error, we have no verification for the solution at all. In contrast to the local error approach, the solution in [1] is with fixed step size and is verified globally.

In our work we improve the approach for verification in [1] by additional computation of the solution on globally refined grids [3]. Globally grid refinement is again a comparison approach but it gives a more rigour verification. We calculate the practical order of convergence from the solutions in three embedded and refined by two grids, and compare this order with the theoretical order of convergence. When the practical and theoretical orders differ say by less then 1% in almost all grid points in a given interval, we conclude that the effect of rounding errors can be neglected and also we can give a practical estimations of the errors in the grid points of that interval. Coincidence of practical and theoretical order of convergence is our criterion for a mathematically reliable solution.

We use as a model problem the classical Rossler system with the standard parameters and the GMP library for our multiple-precision floating point arithmetic.

References

- [1] Liao, Shijun. On the reliability of computed chaotic solutions of non-linear differential equations. *Tellus A: Dynamic Meteorology and Oceanography* 61.4 (2008): 550-564
- [2] Kehlet, Benjamin, and Anders Logg. Quantifying the computability of the Lorenz system. arXiv preprint arXiv:1306.2782 (2013).

- [3] Kalitkin, N. N., and P. V. Koryakin. Numerical Methods, Vol. 2: Methods of Mathematical Physics. (2013).

Incentivizing Research Using DLT-based Smart Contract Platforms

J. Jeliaskov, H. Kostadinov

Establishing trust between several parties without relying on a trusted intermediary is a common goal of modern distributed ledger technologies (DLT). Bitcoin's successors could typically be classified as either public/permissionless blockchains (such as Ethereum and EOS), enterprise/permissioned blockchains (such as MultiChain, and Hyperledger Fabric), or DLTs that are not based on blockchain (such as Corda and Tangle). The original application of DLT in Bitcoin to act as a trustless peer-to-peer digital cash system is extended in many directions in the recent years. Some of the directions in which DLTs are evolving are improvements of the processing speed, scalability, power consumptions, consensus mechanisms, and many security and integration features. The introduction of smart contracts and blockchain oracles in Ethereum created the first universal DLT-based smart contract platform. an environment suitable to support more complicated scenarios for various industries such as finance, supply chain, insurance, healthcare, government and many others. Smart contract platforms based on DLT are create trust medium that is decentralized and not only validate execution of smart contracts but in some cases (EOS, Corda) also support Ricardian contracts. Modern Smart Contract Platforms allow for secure and trustless automation of complex process that required involvement of legal entities or a party that is trusted by all involved partners. In this article we propose a system that could automate the receival of the prize for competition of a specific technical tasks. The technical parameters of the tasks are described in the provided data of the public smart contract. Regardless of the complexity of the task its solution(s) are computationally easy to verify. The process of verification and prize awarding is executed automatically by the dApp either when a confirmed solution to the task is provided or to the best submitted solution after specific period of time has passed. There are various possible configurations depending on the level of cooperation that is allowed and desired between participants. In some cases, the proposals for solution may be public, for other they may be kept secret until the final decision is taken, and for some even after the decision is done the secret of the best solution may be kept. In the latest case the Smart Contract Platform is the guarantee that the right decision is taken. Zero Knowledge Proof elements may be incorporated for the participants to be sure that the winning solution is really the best one. This information, although not disclosed, could also hint towards the optimal known solution.

Nonlinear waves in a generalized model of interacting high density populations

I. Jordanov, N. Vitanov, E. Nikolova

Reaction-diffusion equations have many applications for describing different kinds of processes in physics, chemistry, biology, economics and social sciences. In this study we extend the generalized reaction-diffusion model presented in [1-2], which describes spatio-temporal dynamics of interacting populations. In more detail, we generalize the model system of differential equations for the interaction of 3 populations in which the growth rates and competition coefficients of populations depend on the number of members of all populations. We assume that there nonlinearity in growth rates and interaction coefficients in the generalized model exist according to high density of their individuals. Analytical solution of the extended model is derived by applying the modified method of simplest equation [3-5] for obtaining exact traveling solutions of nonlinear reaction-diffusion PDEs from this class equations. Traveling wave solutions of these equations are of special interest as they describe the motion of wave fronts or the motion of boundary between two different states existing in this system. Numerical simulations of this solution demonstrate propagation of nonlinear waves in the considered extended model. The characteristics of the the obtained traveling wave solution are visualized and discussed.

Acknowledgments. This work contains results, which are supported by the UNWE project for scientific research with grant agreement No. NID NI – 21/2019

References

- [1] Z. I. Dimitrova, N. K. Vitanov, Influence of Adaptation on the Nonlinear Dynamics of a System of Competing Populations, *Physics Letters A* **272**, 368–380 (2000).
- [2] Z. I. Dimitrova, N. K. Vitanov, Dynamical Consequences of Adaptation of the Growth Rates in a System of Three Competing Populations, *Journal of Physics A: Mathematical and General* **34**, 7459–7453 (2001).
- [3] Nikolay K. Vitanov, Zlatinka I. Dimitrova, Holger Kantz. Modified method of simplest equation and its application to nonlinear PDEs. *Applied Mathematics and Computation* **216**, 2587–2595 (2010).
- [4] Nikolay K. Vitanov. Modified method of simplest equation: Powerful tool for obtaining exact and approximate traveling-wave solutions of nonlinear PDEs. *Communications in Nonlinear Science and Numerical Simulation* **16**, 1176–1185 (2011).
- [5] Nikolay K. Vitanov, Zlatinka I. Dimitrova, Kaloyan N. Vitanov. Modified method of simplest equation for obtaining exact analytical solutions of nonlinear partial

differential equations: further development of the methodology with applications.
Applied Mathematics and Computation **269**, 363–378 (2015).

Increasing the Resolution and Readability of Digital Images

D. Kamenov, S. Harizanov, S. Nikolova, D. Toneva

Digital image processing is a modern and extremely active scientific field that combines research techniques from mathematics and informatics. The obtained scientific results are applicable practically almost everywhere, e.g., in medicine, engineering, national security, photography, material sciences, production quality control, nondestructive testing, archeology, architecture and many others.

This talk is devoted to an important issue in medical X-ray and CT imaging, namely how to increase the image resolution and image readability without exposing the patient to higher radiation. This is an unsolved problem in the CT community where Radon techniques are used, as the resolution of the image depends on the number of the generated 2D radiographic projections, thus is proportional to the radiation dose. Alternatively to the most popular approach of using Machine Learning and Convolutional Neural Networks (CNN), here, we analyse a more theoretical approach, based on both Multi-resolution analysis (MRA) techniques and total variation (TV) energy minimization.

The change in the image resolution is obtained via the application of the so called *up-sampling operator* U and *down-sampling operator* D . The latter is the left inverse of the former, i.e., $DU = Id$, meaning that if we increase the resolution of an image and then decrease it, without performing any additional modifications in-between, we should derive the original image. We consider two different classes of operators U . The first class is based on B-spline subdivision and is the natural generalization of the simplest choice for U - the constant mapping, where a parent pixel is split into four children pixels, each of them inheriting the same gray-scale intensity as their predecessor. Increasing the degree of the B-spline, we increase the regularity of the high-resolution image. On one hand, this filters the noise image, but on the other - reduces the contrast along the image edges and introduces blurring effects. The second class is based on piece-wise linear edge-preservation [1] and incorporates structural image information into the up-sampling, thus avoids the blurring effects. All the considered operators U are compactly-supported and local. The corresponding operators D are again local, but also linear. The gray-scale intensity of the parent pixel is always a weighted average of gray-scale intensities of neighboring children pixels. When U is edge-preserving, all the weights are positive (convex combination), while in the case of B-splines some of the weights become negative, which creates additional numerical problems.

In case of edge-preserving up-sampling, the noise in the image is not reduced, but even enhanced within the process. In [1], a denoising filter, based on TV regularization is proposed for improving the image readability in the presence of additive Gaussian noise. The minimization problem is the following:

$$\hat{u} = \underset{u}{\operatorname{argmin}} \left\{ TV(u) + \frac{\lambda}{2} (\|f - D(h * u)\|_{L_2}^2 - \sigma^2) \right\}, \quad (14)$$

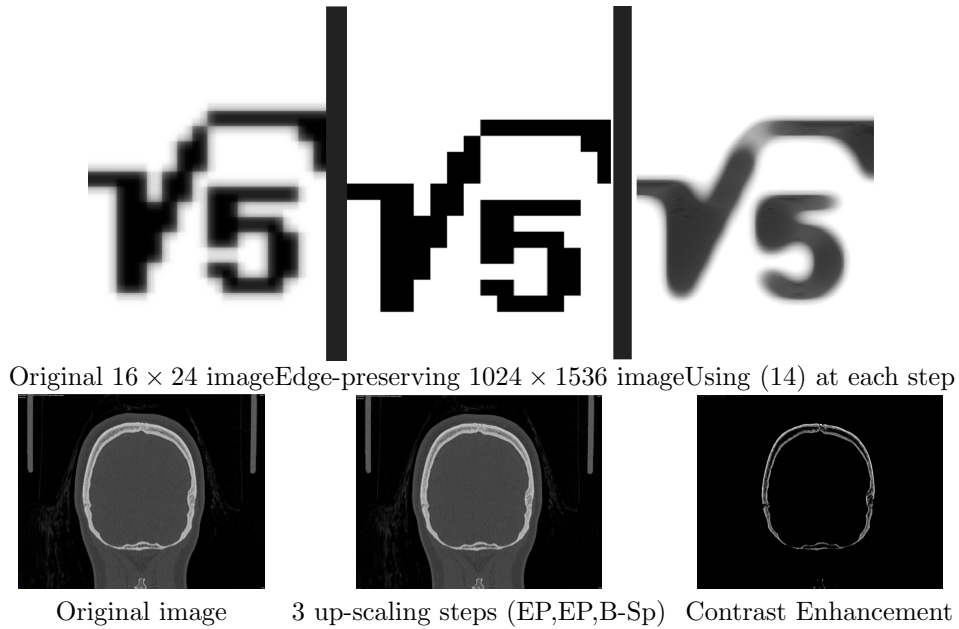


Figure 4: Numerical experiments

where $f = D(h * u) + n$ is the low resolution image, u is the unknown high-resolution image we want to reconstruct, n is a white noise with standard deviation σ , and λ is a regularization parameter (a degree of freedom for the algorithm).

In this talk we numerically compare the two classes of up-sampling operators U and study the effect of the additional image readability procedure (14). All algorithms are implemented in $C\#$. Some results are summarized in Fig. 4. We use both classical 2D gray-scale images from free online data-bases and medical images, generated by Toshiba Aquilion 64. The additional contrast enhancement was achieved via the standard open software gThumb.

Acknowledgment: The support through the Bulgarian NSF Grant DN 01/15 from 20.12.2016 is highly appreciated. D. Kamenov and S. Nikolova are also partially supported by the Small Educational-Research Community, funded by the BAS High School Institute under the governmental programme “Education in Science”.

References

- [1] S. Joshi, A. Marquina, S. Osher, I. Dinov, J. Van Horn, A. Toga, *Edge-enhanced image reconstruction using (TV) total variation and Bregman refinement*, International Conference on Scale Space and Variational Methods in Computer Vision, LNCS Volume 5567, pp. 389–400, Springer, Berlin, Heidelberg, 2009.

Numerical Study of an Initial Concentration Identification Problem in Porous Media

Juri D. Kandilarov, Lubin G. Vulkov

A numerical study for a mathematical model in the context of industrial or accidental pollution in soil with a liquid volatile organic pollutant is proposed. Mathematical models describing volatile organic compounds (VOCs) in the gas phase of the soil have been developed by [3]. The considered here model assumes that the rate-limited vaporization is described with first-order kinetics. Thus a linear system of 2D reaction diffusion-convection equations is presented. An inverse problem is formulated which to identify the liquid concentration of the volatile organic contaminant at initial time, since one can compute its concentration in gaseous phase at final time. The inverse problem is derived in [2] from a time-dependent pollution problem, modelling the flow vapor and mass-transfer of contaminant between the vapor and liquid phases, in unsaturated soils during vapor extraction. The existence and uniqueness of solution of the direct problem is proved.

The speed of the flow v is assumed to be small such that the volume fractions of liquid and gaseous phases θ_w and θ_a can be considered constant. The absorption is neglected, and we denote by C_a , respectively by C_w the concentration of the pollutant in the gaseous and in the liquid phases. The positive constants H , C^* stand respectively for the Henry constant and the saturation concentration in gas, and D is the effective diffusion coefficient.

A 2D mathematical model for the mass transfer between two phases reads as follows, see e.g. [2]:

$$\frac{\partial C_a}{\partial t} - \nabla(D\nabla C_a - C_a v) = HC_w - C_a \quad \text{in } Q_T \quad (15)$$

$$\frac{\partial C_w}{\partial t} = -\alpha(HC_w - C_a), \quad \alpha = -\frac{\theta_a}{\theta_w}, \quad \text{in } Q_T \quad (16)$$

$$C_a(x, t) = C^* \quad \text{on } \Gamma_1 \times (0, T), \quad (17)$$

$$D\nabla C_a \cdot \mathbf{n} = 0 \quad \text{on } \Gamma_2 \times (0, T), \quad (18)$$

$$C_a(x, 0) = C_a^0(x) \quad \text{in } \Omega, \quad (19)$$

$$C_w(x, 0) = C_w^0(x) \quad \text{in } \Omega. \quad (20)$$

The functions C_a^0 and C_w^0 are initial concentrations. From equations (2) and (6), the function C_w writes under the form:

$$C_w(x, t) = C_w^0(x) \exp(-\alpha H t) + \alpha H \int_0^t \exp(-\alpha H(t-s)) C_a(x, s) ds, \quad \forall (x, t) \text{ in } Q_T. \quad (21)$$

By inserting (7) in equation (1), we get for $u(x, t) = 1/H \exp(\alpha H t) C_a(x, t)$:

$$\frac{\partial u}{\partial t} - \nabla(D\nabla u - vu) + (1 - \alpha H)u = f(x) + \alpha H \int_0^t u(s) ds \quad \text{in } Q_T \quad (22)$$

where the function $f(x) = C_w^0(x)$.
 Let us define the following space:

$$W = \{\phi \in L^2(0, T; H^1(\Omega)); \frac{\partial \phi}{\partial t} \in L^2(0, T; L^2(\Omega))\}. \quad (23)$$

Following [1], we assume that:

(A1) D is positive and continuously time-differentiable function, such that

$$\forall x \in \bar{\Omega}, \forall t \in (0, T), \quad 0 < D_{min} \leq D(x, t) \leq D_{max} < +\infty,$$

(A2) $\nu \in C^1(\bar{\Omega})^2$; (A3) $u_0 \in H^1(\Omega)$; (A4) $f \in H^2(\Omega)$;

(A5) There exists a constant $\beta \geq 0$ such that $\nabla(v) + (1 - \alpha H) \geq \beta/2$ *a.e.* in (Ω) .

Then, there exists unique solution $u \in W$.

In this paper we solve numerically the inverse problem for identifying the solution $u(x, t)$ and the source term $f(x)$ at the final overdetermination $u(x, T) = h(x)$. We develop an iterative numerical algorithm based on the conjugate gradient method, see also [4]. For the numerical experiments we solve first the direct problem to have a final overdetermination condition, and then after small perturbation, we solve the inverse problem. Numerical experiments illustrate the efficiency of the algorithm.

Acknowledgements This work is supported by the Bulgarian National Science Fund under the Bilateral Project DNTS/Russia 02/12 "Development and investigation of finite-difference schemes of higher order of accuracy for solving applied problems of fluid and gas mechanics, and ecology" from 2018.

References

- [1] Aboulaich R., Achchab B., Darouchi A., Meskine D.: A study of a pollution problem in porous media during vapor extraction. *J. Math. Sci. Adv. Appl. Math.* **1**(3), 635-662 (2008).
- [2] Aboulaich R., Achchab B., Darouchi A.: Parameter identification by optimization method for a pollution problem in a porous media. *Acta Math. Scientica* **38B**(4), 1345-1360 (2018).
- [3] Armstrong J.E., Frind G.O., Mc Ckllan R.D.: Nonequilibrium mass transfer between the vapor, aqueous and solid phases in unsaturated soils during vapor extraction water. *Resources Research.* **30**(2), 355-368 (1994).
- [4] Samarskii A., Vabishchevich P.: *Numerical Methods for Solving Inverse Problems of Mathematical Physics*, Walter de Gruyter, Berlin. New York, (2007).

Studying the Social Impact of *#NAPLeaks* Networks Discussions: Responsive Fusion(s), Diffusion(s), Confusion(s)

Kristina G. Kapanova, Velislava Stoykova

Recently, Social Networks (SNs) are widely used as a media for sharing and discussing by presenting and commenting users' personal opinions on various subjects including important events which have wide social impacts and thus, they can be used to study public opinions and social attitudes. By using the mechanism of information spreading, sharing and linking, the SNs are reliable source to analyze fluctuations of public attitude toward a certain event or phenomenon, which can be studied by tracking the dynamics of its topicality, so to evaluate the impact of the event and its resulting social response.

In our talk, we are going to present the analysis of SNs discussions invoked by the massive leakage of personal data from the National Revenue Agency caused in July 2019. We use the techniques of Big Data Analytics mainly, the complex Neural Network Analysis and word embedding model, so to study the topicality of the hashtag *#NAPLeaks* networks discussions. By analyzing the topical dynamics and change over time (through studying the topical fusion(s) and diffusion(s)), we outline the structure and complexity of the social impact and related response caused by the event.

The received results (presented at the conclusion) reflect the importance of related terminology and legislation for adequate discussions topical interpretation of the event and a phenomenon of resulting social responsive confusion(s).

Quantum effects on dislocation motion in pure and hydrogen charged Fe from ring-polymer molecular dynamics

Ivaylo Katsarov, Nevena Ilieva, Ludmil Drenchev

Hydrogen has well known and devastating effects on the toughness of high strength steel. It is widely accepted that a detailed theory of hydrogen embrittlement is still lacking. Ultimately there must be decohesion for there to be cracking; on the other hand, the fracture is always accompanied by large amounts of plasticity and indeed it is thought that hydrogen has the effect of localizing plasticity, which may lead to failure by fracture at a lower stress than in the absence of hydrogen. A possible cause of hydrogen embrittlement in Fe is the softening of materials by hydrogen solute atoms arising from increased dislocation mobility and reduced flow stress when hydrogen atoms are introduced into the metal [1]. Understanding the effect of hydrogen on dislocations is essential for understanding how hydrogen reduces ductility in metals. The physics that lies behind enhanced dislocation motion due to hydrogen is not yet established. A comprehensive understanding of the softening mechanism requires a more detailed description of dislocation mobility in combination with the diffusion and trapping of H atoms.

Atomistic modelling of a hydrogen interstitial in α -iron poses enormous challenges. The time scale required to measure the dislocation motion and H diffusivity is usually not accessible in *ab initio* MD simulations. To make the matter even more complex, the small mass of the proton means that nuclear quantum effects (NQEs), including large zero-point energies (ZPE) and tunnelling, can play an important role at room temperature and below. In the standard MD implementations, the nuclei behave as classical particles, which for light nuclei such as hydrogen is often a very poor approximation as the effect of ZPE and quantum tunnelling are neglected. Apart from quantum H effects on dislocation mobility, quantum motion of atoms was recently proposed to explain a long-standing discrepancy between theoretically computed and experimentally measured low-temperature resistance (Peierls stress) to dislocation motion in iron and possibly other metals with high atomic masses [2]. This finding challenges the traditional notion that quantum effects are relatively unimportant in solids comprised of heavy atoms. The estimation of nuclear quantum effects on dislocation mobility requires extension of the reach of quantum atomistic simulations to length and time scales relevant for extended defects in materials.

The evaluation of NQEs can be achieved by using the imaginary time path integral formalism of quantum mechanics. The current state-of-the-art method to include NQEs in the calculation of properties of condensed phase systems is the *path integral molecular dynamics* (PIMD) [3]. PIMD generates the quantum-mechanical ensemble of a system of interacting particles by using MD in an extended phase space which allows quantum phase space averages to be calculated from classical trajectories, with only about an order of magnitude more computing time than would be required for standard MD. Since PIMD is just classical MD in an extended phase space, many

of the techniques developed to improve the scope and efficiency of the MD simulations can be applied, thus making feasible PIMD simulations with thousands of atoms and the use of *ab initio* electronic structure calculations to propagate the dynamics for small systems. The open-source code **i-PI** [4] contains a comprehensive array of PIMD techniques. **i-PI** is designed to be used together with an *ab initio* evaluation of the interactions between the atoms. The implementation is based on decoupling the evolution of the atomic positions from the problem of computing the inter-atomic forces. **i-PI** acts as a server and deals with the nuclear dynamics, whereas the calculation of the forces and the potential energy is delegated to one or more instances of an external code, acting as clients.

To extend the reach of quantum atomistic simulations to length and time scales relevant for extended defects in materials, we develop an external FORTRAN client code, using embedded atom model (EAM) potential [5, 6] to calculate the interatomic interactions in Fe-H system. In order to run massive parallel calculations we use socket internet mode for interfacing the EAM code to **i-PI**. Here we report quantum dynamic simulations of quantum effects on straight dislocation motion in pure and H charged α -iron (Fig. 1), aimed as initial steps in capturing the full range

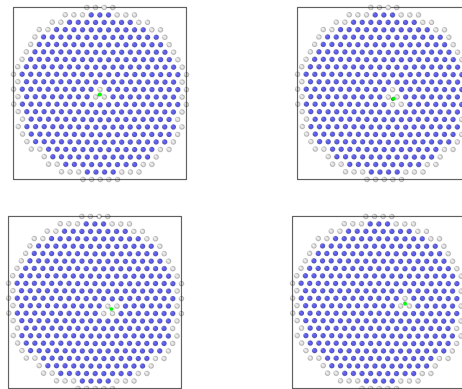


Figure 5: Snapshots of a moving $1/2$ $[111]$ screw dislocation in response to applied shear stress at $T = 100$ K.

of processes contributing to H-enhanced dislocation mobility in Fe.

Acknowledgements This research was supported in part by the Bulgarian Science Fund under Grant KP-06-N27/19/17.12.2018, the Bulgarian Ministry of Education and Science (contract D01–205/23.11.2018) under the National Research Program “Information and Communication Technologies for a Single Digital Market in Science, Education and Security (ICTinSES)”, approved by DCM # 577/17.08.2018, and the European Regional Development Fund, within the Operational Programme “Science and Education for Smart Growth 2014–2020” under the Project CoE “National center of mechatronics and clean technologies” BG05M20P001-1.001-0008-C01.

References

- [1] Robertson, I. and Birnbaum, H., Acta Metall. **34** (1986) 353.
- [2] Barvinschi, B., Proville, L., & Rodney, D., Model. Simul. Mater. Sci. Eng. **22** (2014) 2.
- [3] Craig, I. R. & Manolopoulos, D. E., J. Chem. Phys. **123** (2005) 34102.
- [4] Kapil et al., Comp. Phys. Comm. **236** (2018) 214.
- [5] Ackland, G. J. et al., J. Phys.: Condens. Matter **16** (2004) S2629.
- [6] Ramasubramaniam, A. et al., Phys. Rev. **B79** (2009) 174101.

Quantifying Important Genes in a Gene Regulatory Network with Applications to Network Compression

Eunji Kim, Ivan Ivanov, Edward R. Dougherty

It has been long recognized that canalizing genes possess broad regulatory power, and can enforce corrective actions on cellular processes for the purpose of biological robustness to maintain a constant phenotype despite genetic mutations or environmental perturbations. The notion of genes that can constrain a biological system to a specific behavior was originally proposed in [1]. Waddington suggested the existence of genes that can produce reliable developmental effects against genetic mutations or environmental changes during evolution [1], [2]. Lehner studied Waddingtons intuition and stated that canalizing genes are hub genes that provide robustness when faced with environmental, stochastic and genetic perturbations [3]. The term canalizing gene has been used in [4] to refer to genes that possess broad regulatory power, and their action sweeps across a wide swath of processes for which the full set of affected genes are not highly correlated under normal conditions. Such genes are crucial in a complex system so it can buffer itself from the effects of random alterations or operating errors. Canalizing genes are analogous to master switches that set in motion a cascade of regulatory events that have huge impacts on downstream genes for the sake of driving the system to a desired condition. Therefore, analyzing canalizational properties of the network and preserving canalizing genes are important to maintain homeostasis or to derive intervention strategies for beneficially altering cell dynamics. Probabilistic Boolean networks (PBNs) form a widely accepted mathematical model for cellular systems and gene regulatory networks [5]. One of their important applications is to design intervention strategies that beneficially alter cell dynamics through studying long-run network behavior. Because the dynamics of a PBN are represented by an ergodic and irreducible finite Markov chain, the model possesses a steady-state distribution (SSD) reflecting its long-run dynamics. However, even relatively small networks can pose serious difficulties in assessing the dynamics, considering that a Boolean network of n genes has 2^n states and the transition probability matrix has size $2^n \times 2^n$. Given the exponential dependence of the state space on the number of nodes, there is a need for network reduction mappings that produce models that are more tractable. The major focus of this talk is the preservation of the canalizing properties of genes in the original network under a wide class of compression mappings. For this purpose, we first introduce, [6], the important quantification of a gene Canalizing Power (CP) and then examine what happens to the network CP vector when genes are consecutively deleted. It is hypothesized that deleting a gene with the smallest canalizing power may help to preserve the canalizational properties of the original network under network reduction. In addition, we point out to an important observation related to this hypothesis; namely, that genes in some networks

retain their canalization properties after network compression, while there is a class of networks that do not possess this property. Naturally, this hypothesis leads to definitions of reducible and irreducible networks. Thus, one can formulate a related classification problem that aims to find relevant network features that can separate reducible from irreducible networks.

References

- [1] C. H. Waddington, Canalization of development and the inheritance of acquired characters, *Nature*, vol. 150, no. 3811, pp. 563–565, 1942.
- [2] A. Wagner, *Robustness and evolvability in living systems*. 2005.
- [3] B. Lehner, Genes Confer Similar Robustness to Environmental, Stochastic, and Genetic Perturbations in Yeast, *PLOS ONE*, vol. 5, no. 2, p. e9035, Feb. 2010.
- [4] D. C. Martins, U. M. Braga-Neto, R. F. Hashimoto, M. L. Bittner, and E. R. Dougherty, Intrinsically Multivariate Predictive Genes, *IEEE J. Sel. Top. Signal Process.*, vol. 2, no. 3, pp. 424–439, 2008.
- [5] I. Shmulevich, E. R. Dougherty, S. Kim, and W. Zhang, Probabilistic Boolean networks: a rule-based uncertainty model for gene regulatory networks, *Bioinformatics*, vol. 18, no. 2, pp. 261–274, Feb. 2002.
- [6] E. Kim, I. Ivanov, and E. R. Dougherty, Quantifying the notions of canalizing and master genes in a gene regulatory network: a Boolean network modeling perspective, *Bioinformatics*, vol. 35, no. 4, pp. 643–649, Jul. 2018.

Exponential difference scheme approximations for Richards' equation with piecewise constant and degenerate absolute permeability

Miglena N. Koleva, Sergey V. Polyakov, Lubin G. Vulkov

Richards' equation can be formulated for pressure function p , assuming that the z -axis points in the direction are opposite to the gravity vector $\mathbf{g} = (0, -g)$ [6]:

$$\frac{\partial(\rho\phi s)}{\partial t} + \operatorname{div}(\rho\mathbf{q}) = 0, \quad \mathbf{q} = -\mathbf{k} \frac{a(p)}{\mu} (\nabla p - \rho\mathbf{g}). \quad (24)$$

The fluid flow is driven by gravity and boundary conditions on $\Gamma = \Gamma_D \cup \Gamma_G$

$$p = p_D(x) \quad \text{on } \Gamma_D \quad \text{and} \quad \mathbf{q} \cdot \mathbf{n} = q_N(x) \quad \text{on } \Gamma_N. \quad (25)$$

Here $s(p_c)$ is the water saturation function of capillary pressure $p_c = p_{\text{atm}} - p$ and \mathbf{q} is Darcy velocity. The medium properties are described by porosity ϕ , absolute permeability tensor \mathbf{k} , and relative permeability function $a(s)$. The fluid properties are described by density ρ and viscosity μ .

The problem (24), (25) is completed by initial condition for the pressure p .

Very often the variably flow is calculated by the Richards' equation in volumetric water content $\theta = \theta(h)$, using typical empirical constitutive relation.

We consider a slightly modification of the classical one-dimensional Richards' equation of water content on time in porous medium [3]:

$$\frac{\partial u}{\partial t} = \frac{\partial}{\partial x} \left(k(x)a(u) \left(\frac{\partial u}{\partial x} + g \right) \right), \quad (26)$$

where $u = u(t, x)$ stands for the water content, $x \in \Omega = (0, L)$, $L > 0$, $t \in (0, T)$, $g \geq 0$ is the magnitude of gravity constant, $K(x, u) = k(x)a(u)$ stands for hydraulic conductivity function, $k(x)$ is absolute permeability function, $a(u)$ is an absolutely continuous Lipschitz function on \mathbb{R} . Function $k(x)$ is either piecewise constant [3]

$$k(x) = \begin{cases} k_1, & x \in [0, x^*], \quad k_1 > 0, \\ k_2, & x \in (x^*, L], \quad k_2 > 0, \end{cases} \quad (27)$$

or [1, 2]

$$k(x) \in C(\Omega), \quad k(0) = 0, \quad (28)$$

such that the equation (26) degenerate in the fluid melt.

To complete the problem, we impose the following initial and boundary conditions

$$u(x, 0) = u^0(x), \quad x \in \Omega, \quad u(0, t) = u_l(t), \quad u(L, t) = u_r(t), \quad t \in [0, T]. \quad (29)$$

Existence and uniqueness of a weak solution of (26), (27),(29) is discussed in [3]. Also, the authors construct explicit monotone method for solving (26), (27),(29), which require very small time step.

In this work, we develop second-order implicit exponential scheme for solving the non-linear parabolic problem (26)-(29). The discretization is based on backward Euler time approximation and quasilinearization of the obtained elliptic equation. For space discretization, we use the idea in [4, 5] to construct exponential finite difference schemes. The robustness of the proposed scheme in the case of piecewise constant and degenerate absolute permeability is illustrated by various numerical tests.

Acknowledgement. This work is supported by the bilateral Project "Development and investigation of finite-difference schemes of higher order of accuracy for solving applied problems of fluid and gas mechanics, and ecology" of Bulgarian National Science Fund under Project DNTS/Russia 02/12 and Russian Foundation for Basic Research under Project 18-51-18004-bolg_a.

References

- [1] Arbogast, T., Taicher, A.L.: A linear degenerate elliptic equation arising from two-phase mixtures, *SIAM J. Numer. Anal.* **54**(5) (2016) 3105–3122.
- [2] Arbogast, T., Taicher, A.L.: A cell-centered finite difference method for a degenerate elliptic equation arising from two-phase mixtures, *Computational Geosciences* **21**(4), 700–712 (2017).
- [3] Misiats, O., Lipnikov, K.: Second-order accurate finite volume scheme for Richards' equation, *J. Comput. Phys.* **239**, 125–137 (2013).
Water Resour. Res. **12**, 513–522 (1976).
- [4] Polyakov, S.V.: Exponential finite difference scheme with double integral transformation for solving convection-diffusion equation, *Math. Models Comput. Simul.* **5**(4), 338–340 (2013).
- [5] Polyakov, S.V., Karamzin, Yu. N., Kudryashova T.A., Tsybulin, I.V.: Exponential difference schemes for solving boundary-value problems for convection-diffusion type equations, *Math. Models Comput. Simul.* **9**(1), 71–82 (2017).
- [6] Svyatsky, D., Lipnikov, K.: Second-order accurate finite volume schemes with the discrete maximum principle for solving Richards' equation on unstructured meshes, *Advances in Water Resources* **104**, 114–126 (2017).

Image segmentation via Echo state network

Petia Koprinkova-Hristova, Ivan Georgiev

Echo state networks (ESN) belong to a novel and fast developing family of reservoir computing approaches [2, 3] whose primary aim was development of fast trainable recurrent neural network architectures (RNN) able to approximate highly nonlinear time series. Following different view point to dynamic reservoir structure and its properties, in [1] a novel approach for unsupervised clustering of static multidimensional data sets using ESN was proposed. Its core was to use the reservoir equilibrium states corresponding to each one multidimensional input data. As it was shown in [5], the fitting of the ESN reservoir dynamics to reflect the input data structure can be achieved by an approach for ESN reservoir tuning called Intrinsic Plasticity (IP) [6, 7]. The proposed first in [1] approach was successfully tested on numerous practical examples (see [4]), among which clustering and segmentation of multi-spectral images achieved interesting results.

In present work we tested modified version of that approach for segmentation of gray scale images. In order to enhance original image we exploit IP tuned ESN reservoir to extract multiple features from each pixel intensity value. Next we compare original features (image pixels intensity) vs. increased number of extracted via ESN features (reservoir equilibrium states for each pixel intensity) using kmeans clustering to divide image into several segments (clusters). Our results demonstrated that increased number of clusters in combination with increased number of pixels features reveals new details in the gray scale images.

Next we also tested individual extracted features vs. original pixels intensity. Clustering results based on single feature per pixel demonstrated that some of the reservoir equilibrium states yielded better segmentation of gray image in comparison with segmentation by its original pixels intensity.

These preliminary results are good basis for further development of hierarchical (deep) approach for gray images segmentation combining ESN and clustering approaches.

Acknowledgement

The partial support by the Bulgarian National Science Fund under Grant No. DN 01/15 from 20.12.2016. We also acknowledge the provided access to the infrastructure of the Laboratory for 3D Digitalization and Microstructure Analysis, financed by the Science and Education for Smart Growth Operational Program (2014-2020) and co-financed the European Structural and Investment fund through Grant No BG05M2OP001-1.001-0003.

References

- [1] Koprinkova-Hristova, P., Tontchev, N., Echo state networks for multidimensional data clustering, In: Villa, A.E.P., Duch, W., Érdi, P., Masulli, F., Palm, G.

- (eds.) Int. Conf. on Artificial Neural Networks 2012, LNCS vol. 7552, pp. 571–578. Springer, Heidelberg (2012)
- [2] Jaeger, H., Tutorial on training recurrent neural networks, covering BPPT, RTRL, EKF and the "echo state network" approach. GMD Report 159, German National Research Center for Information Technology (2002)
 - [3] Lukosevicius, M., Jaeger, H., Reservoir computing approaches to recurrent neural network training, *Computer Science Review*, vol. 3, pp. 127–149 (2009)
 - [4] Koprinkova-Hristova, P., Multidimensional data clustering and visualization via Echo state networks, In: Kountchev, R., Nakamatsu, K. (eds.) *New Approaches in Intelligent Image Analysis*, Intelligent Systems Reference Library vol. 108, pp. 93–122. Springer, Cham (2016)
 - [5] Koprinkova-Hristova, P., On effects of IP improvement of ESN reservoirs for reflecting of data structure. In: *Proc. of the International Joint Conference on Neural Networks (IJCNN) 2015*, IEEE, Killarney, Ireland, DOI: 10.1109/IJCNN.2015.7280703 (2015)
 - [6] Steil, J.J., Online reservoir adaptation by intrinsic plasticity for back-propagation-deceleration and echo state learning, *Neural Networks*, vol. 20, pp. 353–364 (2007)
 - [7] Schrauwen, B., Wandermann, M., Verstraeten, D., Steil, J.J., Stroobandt, D., Improving reservoirs using intrinsic plasticity, *Neurocomputing*, vol. 71, pp. 1159–1171 (2008)

Finite time blow up of the solutions to nonlinear dispersive equations with critical initial energy

N. Kutev, M. Dimova, N. Kolkovska

The aim of this paper is to investigate the finite time blow up of the solutions to the nonlinear Klein-Gordon equation

$$\begin{aligned} u_{tt} - u_{xx} + u &= f(u), & (t, x) &\in \mathbb{R} \times \mathbb{R}^n, \\ u(0, x) &= u_0(x), \quad u_t(0, x) = u_1(x), & x &\in \mathbb{R}^n, \\ u_0(x) &\in H^1(\mathbb{R}^n), \quad u_1(x) \in L^2(\mathbb{R}^n) \end{aligned} \quad (30)$$

and the double dispersive equation with linear restoring force

$$\begin{aligned} u_{tt} - u_{xx} - u_{ttxx} + u_{xxxx} + u + f(u)_{xx} &= 0, & (t, x) &\in \mathbb{R}^+ \times \mathbb{R}, \\ u(0, x) &= u_0(x), \quad u_t(0, x) = u_1(x), & x &\in \mathbb{R}, \\ u_0 &\in H^1(\mathbb{R}), \quad (-\Delta)^{-1/2}u_0 \in L^2(\mathbb{R}), \quad u_1 \in L^2(\mathbb{R}), \quad (-\Delta)^{-1/2}u_1 \in L^2(\mathbb{R}). \end{aligned} \quad (31)$$

Here $(-\Delta)^{-s}u = \mathcal{F}^{-1}(|\xi|^{-2s}\mathcal{F}(u))$ for $s > 0$, $\mathcal{F}(u)$, $\mathcal{F}^{-1}(u)$ are the Fourier transform and the inverse Fourier transform, respectively. The nonlinearity $f(u)$ in (30) and (31) has one of the following forms:

$$\begin{aligned} f(u) &= \sum_{k=1}^l a_k |u|^{p_k-1}u - \sum_{j=1}^s b_j |u|^{q_j-1}u, \\ f(u) &= a_1 |u|^{p_1} + \sum_{k=2}^l a_k |u|^{p_k-1}u - \sum_{j=1}^s b_j |u|^{q_j-1}u. \end{aligned} \quad (32)$$

Here the constants a_k , p_k ($k = 1, 2, \dots, l$) and b_j , q_j ($j = 1, 2, \dots, s$) fulfill the conditions

$$\begin{aligned} a_1 &> 0, \quad a_k \geq 0, \quad b_j \geq 0 \quad \text{for } k = 2, \dots, l, \quad j = 1, \dots, s, \\ 1 &< q_s < q_{s-1} < \dots < q_1 < p_1 < p_2 < \dots < p_l, \\ p_l &< \infty \quad \text{for } n = 1, 2; \quad p_l < \frac{n+2}{n-2} \quad \text{for } n \geq 3. \end{aligned}$$

A special case of (32) is the quadratic-cubic nonlinearity, $f(u) = u^2 + u^3$, which appears in mathematical models of dislocations of crystals [1], propagation of longitudinal strain waves in an isotropic cylindrical compressible elastic rod [2] and others. The global existence or finite time blow up of the solution to problems (30) and (31) is fully investigated for nonpositive energy $E(0) \leq 0$ and for subcritical energy $0 < E(0) < d$ by means of the potential well method [3].

In the present paper we focus on the case of critical initial energy, $E(0) = d$, which is not completely investigated in the literature. When the initial energy is critical, then the qualitative properties of the weak solutions to (30) and (31) substantially depend

on the sign of the Nehari functional $I(u_0)$ and the sign of the scalar product of the initial data u_0, u_1 , where

$$I(u) = \langle u, u \rangle + \|\nabla u\|_{L^2(\mathbb{R}^n)}^2 - \int_{\mathbb{R}^n} uf(u) dx.$$

Here $\langle u, v \rangle = (u, v)$ for problem (30), $\langle u, v \rangle = (u, v) + ((-\Delta)^{-1/2}u, (-\Delta)^{-1/2}v)$ for problem (31), and (u, v) is the standard scalar product in \mathbb{R}^n .

More precisely, for $E(0) = d$ the solutions to problems (30) and (31) are globally defined for every $t \geq 0$ when $I(u_0) \geq 0$ independently of the sign of $\langle u_0, u_1 \rangle$, while the solutions blow up in a finite time when $I(u_0) < 0$ and $\langle u_0, u_1 \rangle \geq 0$, see [1, 4] for the nonlinear Klein-Gordon equation, and e.g. [5] for double dispersive equation without linear restoring force. The case $E(0) = d$, $I(u_0) < 0$ and $\langle u_0, u_1 \rangle < 0$ is partially studied only to Klein-Gordon equation (30) in [1, 4].

Our main result is the proof of a necessary and sufficient condition for finite time of the solutions to problems (30) and (31) when $E(0) = d$ and $I(u_0) < 0$. We prescribe precise conditions on the initial data u_0 and u_1 , which guarantee global existence or finite time blow up of the corresponding solutions. In this way we give a complete description of the behaviour of the solutions to problems (30) and (31) when $E(0) = d$ and $I(u_0) < 0$.

Acknowledgments. The first author is partially supported by the National Scientific Program “Information and Communication Technologies for a Single Digital Market in Science, Education and Security (ICTinSES)”, contract No D01–205/23.11.2018, financed by the Ministry of Education and Science in Bulgaria, the second one is partially supported by the Bulgarian National Science Fund under grant and the DFNI 12/5 and the third author is partially supported by the Bulgarian National Science Fund under grant KII-06-H22/2.

References

- [1] K. Li, Q. Zhang, Existence and nonexistence of global solutions for the equation of dislocation of crystals, *J. Differential Equations* 146 (1998) 5–21.
- [2] A. Porubov, *Amplification of nonlinear strain waves in solids*, World Scientific, 2003.
- [3] L.E. Payne, D.H. Sattinger, Saddle points and instability of nonlinear hyperbolic equations, *Israel Journal of Mathematics* 22(3-4) (1975) 273–303.
- [4] J. Esquivel-Avila, Blow up and asymptotic behavior in a nondissipative nonlinear wave equation, *Appl. Anal.* 93(9) (2014) 1963–1978.
- [5] Y. Liu, R. Xu, Potential well method for Cauchy problem of generalized double dispersion equations, *J. Math. Anal. Appl.* 338(2) (2008) 1169–1187.

Axisymmetric oscillatory flow of Carreau fluid in tube

Nilolay Kutev, Sonia Tabakova, Stefan Radev

The Carreau fluid flow in an infinite circular tube, caused by an oscillatory pressure gradient, is studied theoretically. The problem is axisymmetric in space and periodic in time and reduces to a parabolic non-linear equation for the axial velocity. This equation has no analytical solution in the general case of different Womersley and Carreau numbers. In the present paper, it is proven that the velocity and its gradient, as well as their differences from the similar Newtonian solutions, are bounded by constants, which depend on the Carreau number and the other parameters of the viscosity model. Analogous bounds have been proven for the 2D channel flow in our previous works [1], [2]. The differences between the bounds of the 2D channel and axisymmetric tube flows are also discussed using numerical examples at different Carreau and Womersley numbers.

Acknowledgment: The author N.K. has been partially supported for this research by the Grant No BG05M2OP001-1.001-0003-C01, financed by the Science and Education for Smart Growth Operational Program (2018-2023).

References

- [1] N. Kutev, S. Tabakova and St. Radev, Velocity and shear rate estimates of some non-Newtonian oscillatory flows in tubes, *AIP Conference Proceedings* **1773**, 080002-1 – 080002-8 (2016)
- [2] S. Tabakova, N. Kutev and St. Radev, Oscillatory Carreau flows in straight channels, *Roy. Soc. Open Science* (2019, under review).

In silico study of the self-organisation process in mono-component solutions of antimicrobial peptides

T. Lazarova, P. Petkov, N. Ilieva, E. Lilkova, L. Litov

Antimicrobial peptides (AMPs) are essential components of innate immunity in most multicellular organisms and represent an ancient nonspecific host defense mechanism against infectious pathogens, that complements the highly specific cell-mediated immune response. They are known to also exhibit anticancer, antiinflammatory and immunomodulatory activity. In addition, despite the millions of years co-evolution, no signs can be seen of a wide-spread or even limited bacterial resistance against their action. All this makes natural AMPs a prime target for research and an ideal template for the design of sustainable antibiotic biologicals.

The mechanism of the AMPs bactericidal action is not yet well understood. Along these way, important components are the interaction of these small, generally cationic and amphiphilic peptides with the bacterial membrane but also their largely underestimated and not well studied solvation behaviour, prior to reaching the target membrane. In recent papers [1, 2], we discussed the process of peptide aggregation and its effect on the monomer's secondary structure in the case of one intrinsically disordered AMP (indolicidin) and one α -helical AMP, magainin 2. We could justify our hypothesis that most of the small linear AMPs in general do not exist in solution as isolated monomers but rather self-assemble in the solvent into aggregates that provide the critical local concentration of peptides in a fully functional form to exert their action on the lipid bilayer, also on the example of bombinin 2 — a peptide secreted by the skin of *European Bombina variegata* frog species [3].

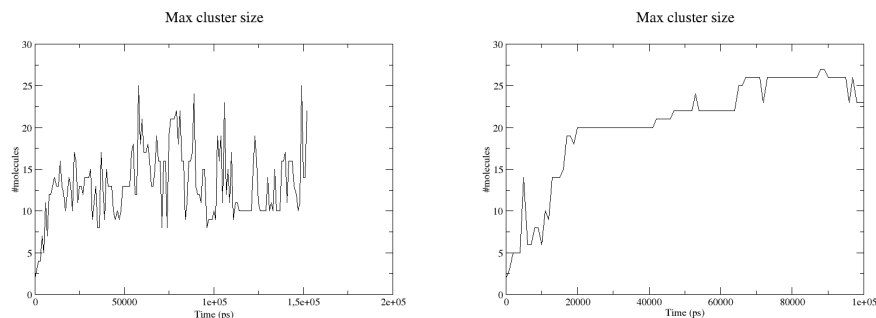


Figure 6: The largest-clusters size along the trajectory of the peptide p8 (left panel) and p15 (right panel).

Here we present the first results of a molecular-dynamics study on two newly identified peptides in the 1–3 kDa fraction of the mucus of the snail *Cornu aspersum* — the peptides with amino acid sequences LFGGHQGGGLVGGLWRK (17 amino acids long,

net charge +2, referred to as p8) and HAFDVAVGLLGGGGAGGGGLVGGGGLGGGA (32 amino acids long, net charge -1, referred to as p15). The researched sample substances have no homologies with any known experimental structure in the Protein Data Bank [4], so MD simulations were employed to also develop their 3D structural models. The simulated systems were composed out of 27 peptide monomers each, placed in a cubic simulation box filled with water, with a minimal distance to the box walls of 1.2 nm. All simulations were performed with the MD simulation package GROMACS 2016.8 [5]. The CHARMM 27 force field [6] was used for parameterisation of the peptides, in combination with the modified TIP3PS water model [7] for the solvent.

We observe that the smaller peptide, p8, exhibits fluctuations in the aggregation process, with the largest-cluster size varying between 10 and 25 monomers, while the peptide p15 (the largest one in the investigated fraction) shows stable increase in the largest-cluster size, till practically all monomers aggregate into a single formation, see Fig. 6. We discuss the possible reasons for the observed behavior, in line with the conclusions in [3]. We also analyze aggregation in a mixture of equal quantities of both peptides as a model system of a multi-component micelle-like aggregate with a hydrophobic core, composed of p15 monomers and a positively charged shell of p8 peptides. The latter will be used as a model system in the investigation of the AMP-membrane interaction.

Acknowledgements This research was supported in part by the Bulgarian Science Fund under Grant KP-06-OPR 03/10/2018, and the Bulgarian Ministry of Education and Science (Grant D01-217/30.11.2018) under the National Research Programme “Innovative Low-Toxic Bioactive Substances for Precision Medicine (BioActiveMed)” approved by DCM # 658/14.09.2018).

References

- [1] Marinova, R., Petkov, P., Ilieva, N., Lilkova, E., and Litov, L. Molecular Dynamics Study of the Solution Behaviour of Antimicrobial Peptide Indolicidin. *Stud. Comput. Intell.* 2019, 793, 257–265.
- [2] Petkov, P., Marinova, R., Kochev, V., Ilieva, N., Lilkova, E., Litov, L. Computational Study of Solution Behavior of Magainin 2 Monomers. *J. Biomol. Struct. Dyn.* 2019, 375, 1231–1240.
- [3] Petkov, P., Lilkova, E., Ilieva, N., Litov, L. Self-Association of Antimicrobial Peptides: A Molecular Dynamics Simulation Study on Bombinin. *Int. J. Mol. Sci.* 2019, 20, 5450.
- [4] Berman, H.M., Westbrook, J., Feng, Z., Gilliland, G., Bhat, T.N., Weissig, H., Shindyalov, I.N., Bourne, P.E. The Protein Data Bank. *Nucleic Acids Research*, 2000, 28, 235-242.
- [5] Abraham, M.J., Murtola, T., Schulz, R., Páll, S., Smith, J.C., Hess, B., Lindahl, E. GROMACS: High performance molecular simulations through multi-level parallelism from laptops to supercomputers. *SoftwareX* 2015, 1–2, 19–25.
- [6] Mackerell, A.D., Jr., Feig, M., Brooks, C.L., III. Extending the treatment of backbone energetics in protein force fields: Limitations of gas-phase quantum mechanics in reproducing protein conformational distributions in molecular dynamics simulations. *J. Comput. Chem.* 2004, 25, 1400–1415.
- [7] MacKerell, A.D., et al. All-Atom Empirical Potential for Molecular Modeling and Dynamics Studies of Proteins. *J. Phys. Chem. B* 1998, 102, 3586–3616.

Analysis of contaminant removal in constructed wetlands under step-feeding: A Monte Carlo based stochastic treatment accounting for uncertainty

Konstantinos Liolios, Georgios Skodras, Krassimir Georgiev,
Ivan Georgiev

Constructed wetlands (CW) are used as an ecological solution for the municipal wastewater treatment, especially in small settlements, in order to improve the groundwater quality [1]. Step-feeding (SF) is the phenomenon in which the wastewater is introduced to a CW at several points along the flow path in a gradational way, and not only at the beginning of its length. The purpose of this technique for the CWs operation is to increase the performance of these facilities. In the present study, this problem is analyzed by taking into account uncertainty for input parameters. A stochastic approach based on Monte Carlo simulation methods [2,3] is used.

The numerical simulation of CW operation is usually a deterministic one, based on the solution of the following system of Partial Differential Equations (PDE) [4,5]. The three-dimensional groundwater flow equation, providing as solution the hydraulic head h , is written, using tensorial notation ($i, j = 1, 2, 3$):

$$\frac{\partial}{\partial x_i} (K_{ij} \frac{\partial h}{\partial x_j}) + q_s = S_s \frac{\partial h}{\partial t} \quad (1)$$

where K_{ij} is a component of the hydraulic conductivity tensor; S_y is the specific yield of the porous materials; and q_s is the volumetric flow rate per unit area of aquifer. In the case of isolated source/sink points, e.g. injecting wells in step-feeding, the term q_s is expressed by using the Dirac Delta function concept [4].

The velocity field is computed through the Darcy relationship:

$$q_i = -K_{ij} \frac{\partial h}{\partial x_j} \quad (2)$$

The partial differential equation, which describes the fate and transport of a contaminant with adsorption in 3-D, transient groundwater flow systems, is:

$$\varepsilon R_d \frac{\partial C}{\partial t} = \frac{\partial}{\partial x_i} \left(\varepsilon D_{S_{ij}} \frac{\partial C}{\partial x_j} \right) - \frac{\partial}{\partial x_i} (q_i C) + q_s C_s + \sum_{n=1}^N R_n, \quad (3)$$

where ε is the porosity of the subsurface medium; R_d is the retardation factor; C is the dissolved concentration of solute; $D_{S_{ij}}$ is the solute hydrodynamic dispersion coefficient tensor; C_s is the concentration of the source or sink flux; and $\sum R_n$ is the chemical reaction term. The last parameter is given by the formula:

$$\sum R_n = -\lambda R_d C^\alpha, \quad (4)$$

where λ and α are removal coefficients. When $\alpha = 1$, then the usual linear reaction case of first-order decay is active.

For the determination of the above parameters of equations (1)-(4), usually detailed in-situ measurements are required. The numerical treatment of the above deterministic problem is usually realized in the praxis by using a mean-value estimate of the various coefficients.

A Monte Carlo simulation is applied, for the quantitative estimation of the various uncertainties; this simulation is simply a repeated process of generating deterministic solutions to a given problem [2, 3]. Each solution corresponds to a set of deterministic input values of the underlying random variables. A statistical analysis of these obtained simulated solutions is then performed. According to the computational methodology, first the above deterministic problem for each set of the random input variables is solved and then a statistical analysis is followed. In the present study, a numerical example concerning the removal of the pollutant of Biochemically Oxygen Demand (BOD) in a pilot-scale CW, operating under the step-feeding technique, is presented. For the sensitivity analysis of the model, the stochastic computational results are compared with available experimental ones.

References

- [1] Kadlec, R.H., Wallace, S.: Treatment Wetlands. CRC Press, Boca Raton (2009)
- [2] Kottegoda, N., Rosso, R.: Statistics, Probability and Reliability for Civil and Environmental Engineers. McGraw-Hill, London (2000)
- [3] Dimov, I.T.: Monte Carlo Methods for Applied Scientists. World Scientific Publishing Co. (2008)
- [4] Bear, J., Cheng, A.D.: Modelling Groundwater Flow and Contaminant Transport. Springer, Berlin (2010)
- [5] Zheng, C., Bennett G.D.: Applied Contaminant Transport Modelling. Wiley, NewYork (2002)

Live-graphing with LoRaWAN and Python

Rositsa Maksimova, Krassimir Kolev

The world of the Internet of Things is evolving at a rapid pace. The need to reduce power consumption, increase the reliability of devices and improve wireless communication between devices leads to the search for modern approaches to implement these tasks. LoRaWAN (Long Range Wide Area Network) is a good alternative in the process of long-term and large-scale communication, as well as in cases where it is necessary to collect information from hard to reach places. This concept has been implemented as part of the overall realization of this idea. The Things Network (TTN) products based on the LoRaWAN protocol are purchased to achieve the objectives. The data sent to the TTN server is accessed through the Message Queuing Telemetry Transport (MQTT) protocol, relying on the provided API by TTN, which allows sending and receiving messages to and from IoT devices. The requests in question are implemented through the `ttn` Python library which is imported in the overall web application development platform - the Python's Dash library. The purpose of this combination of software techniques is to provide an individual instance of a dashboard for live-graphing and managing of the data received from TTN server. In addition to the ability to actually monitor the data live, the ability to upload spreadsheets is also available, which can be accessed and reopened through the developed Dash web application. Such an ideology eliminates the need to use predefined dashboard templates, minimizes the dependence on paid and foreign platforms to provide a control panel for real-time monitoring of fetched data and provides code access and custom layout tools. TTN provides a suite of open tools and a global open network for building IoT applications with maximum security through reliable end-to-end encryption and the ability to scale into a shared Internet of Things that is spread across many countries around the world, where thousands of gateways are in operation, providing millions of people with coverage. TTN can be used to build a concept with fast installation, knowing the additional security and scalability features that can be added later, providing highly secure solutions. Application in TTN means everything that devices can communicate with on the Internet. Before you can communicate with devices, you must add an application to the network and register devices to it. There are numerous options for integrating applications with TTN, starting with working directly with the API, through a friendlier SDK or click-and-run Platform Integrations. Dash is a Python framework for building web applications. Based on Flask, Plotly.js and React.js, Dash is suitable for building data visualization applications with a highly customized User Interface (UI) in pure Python. It is especially suitable for anyone who works with data in Python. Dash apps are rendered in the web browser. Created applications can be deployed to servers and shared via URLs. Because Dash applications are viewed in the web browser, Dash is inherently cross-platform and mobile ready. Dash is an open-source library licensed under the MIT license and is developed by Plotly, which provides a platform for easily deploying Dash applications in an enterprise environment. All ideas in this abstract can be used to conduct personal and

scientific experiments in various scientific fields, due to the fact that all types of data fetched by a customized sensor hardware can be graphed and saved through different approaches. The goal of such a system is intended to be included in a Biotech hardware for example wastewater treatment equipment hardware with the possibility for a real-time control panel. The ability for remote access from each Internet connected node of the world would provide the freedom in the sense of IoT. The advantage of such a custom dashboard over other ready dashboards is the ability and flexibility of its source code. The fact that this dashboard can be adapted to different needs allows it to be used not only in the world of computer technology but also in interdisciplinary branches of science where various fundamental natural processes can be monitored live through the available sensors and LoRaWAN.

Two series which generalize certain sums expressed in terms of zeta values

Lubomir Markov

Let $\zeta(s)$ be the Riemann zeta function – i.e., the function initially defined for $\Re(s) > 1$ by the relation $\zeta(s) = \sum_{k=1}^{\infty} \frac{1}{k^s}$, and then extended to all complex $s \neq 1$ by analytic continuation (see [1]). An active area of recent research has been the study of zeta and associated functions that are themselves expressed in terms of zeta values. A substantial collection of such results may be found in the book by Srivastava and Choi [10], or in the research-expository article [9], the latter dealing especially with most recent developments. Historically, the first example of a series in terms of values of the Riemann zeta function was given by Euler [6]. In contemporary notation that series is

$$\zeta(3) = -\frac{4\pi^2}{7} \sum_{k=0}^{\infty} \frac{\zeta(2k)}{(2k+1)(2k+2)2^{2k}},$$

which was also rediscovered by Ewell [7]. The above sum converges more rapidly than $\sum_{k=1}^{\infty} \frac{1}{k^3}$ itself, and exemplifies the interest in such representations. In the present paper we introduce two series (believed to be new) that provide interesting generalizations of some results [10, Chapter 4] by Ewell, Zhang and Williams, and others, including a generalization of the above formula. Additionally, we investigate a set of sums also motivated by Euler's work, the simplest example of which is the representation

$$\sum_{k=1}^{\infty} \left\{ \sum_{m=1}^{k-1} \frac{1}{m^2} \right\} \frac{1}{k^3} = -\frac{11}{2} \zeta(5) + 3\zeta(2)\zeta(3).$$

As a side note we mention that rapidly convergent sums are valuable tools in analysis and analytic number theory. It was the fast convergence of the series

$$\zeta(3) = \frac{5}{2} \sum_{k=1}^{\infty} \frac{(-1)^{k-1}}{k^3 \binom{2k}{k}}$$

that was instrumental in Apéry's proof of the irrationality of $\zeta(3)$.

References

- [1] T.M. Apostol, *Introduction to Analytic Number Theory*, Springer Verlag, New York/Berlin/Heidelberg, 1976
- [2] R. Ayoub, Euler and the Zeta function, *Amer. Math. Monthly* **81** (1974), 1067-1086
- [3] D. Borwein, J. Borwein and R. Girgensohn, Explicit evaluation of Euler sums, *Proc. Edinburgh Math. Soc.* **38** (1995), 277-294
- [4] M.-P. Chen and H.M. Srivastava, Some families of series representations for the Riemann $\zeta(3)$, *Result. Math.* **33** (1998), 179-197
- [5] R. Choe, An elementary proof of $\sum_{n=1}^{\infty} \frac{1}{n^2} = \frac{\pi^2}{6}$, *Amer. Math. Monthly* **94** (1987), 662-663
- [6] L. Euler, Exercitationes analyticae, *Novi Comment. Acad. Sci. Imp. Petropol.* **17** (1772), 173-204
- [7] J. Ewell, A new series representation for $\zeta(3)$, *Amer. Math. Monthly* **97** (1990), 219-220
- [8] H.M. Srivastava, Some simple algorithms for the evaluations and representations of the Riemann Zeta Function at positive integer arguments, *J. Math. Anal. Appl.* **246** (2000), 331-351
- [9] H.M. Srivastava, Some properties and results involving the zeta and associated functions, *Funct. Anal. Approx. Comput.* **7** (2015), 89-133
- [10] H.M. Srivastava and J. Choi, *Series Associated with the Zeta and Related Functions*, Kluwer Academic Publishers, Dordrecht/Boston/London, 2001

Simulation of Diffusion Process in Bimetallic Nanofilms

Vladimir Myasnichenko, Rossen Mikhov, Leoneed Kirilov,
Nikolay Sdobnyakov, Denis Sokolov, Stefka Fidanova

As it is known, atom ordering in the process of forming nanoalloys is one of the factors defining the structure and properties of the materials. Knowing the mechanism of this process helps to obtain materials with preset properties. At present this kind of problem is extensively studied — Li et al. (2018). An example is welding due to the mutual diffusion at the atomic level of the surfaces of parts to be welded (diffusion welding) — Korznikova et al. (2019). Surface diffusion plays a crucial role in the formation of the shape and morphology of growing nanoparticles and nanofilms. Bulk heterodiffusion occurs at uneven (irregular) concentrations of several metals, in the presence of free energy in the system. Atoms of each sort tend to be evenly distributed in volume and form mixed bonds.

In this paper, we propose an approach for modelling diffusion processes in nanoalloys by vacancy mechanism. The approach is based on computing the probability for a transition of each atom belonging to the first three coordination spheres. The potential energy of the system is computed by Gupta (tight binding) potential (1981). The model uses the hybrid Monte Carlo method developed earlier by the authors Myasnichenko et al. (2019) that is appropriately modified to solve the diffusion problem. The efficiency of the approach is demonstrated by solving some test examples with a different number of vacancies in the crystal lattice and different temperature.

Acknowledgments: The reported study was partially funded by RFBR, project number 20-37-70007 and National Scientific Program “Information and Communication Technologies for a Single Digital Market in Science, Education and Security (ICTinSES)”, Ministry of Education and Science — Bulgaria and the Bulgarian NSF under the grant DFNI-DN 12/5.

References

- [1] X.-Y. Li, B. Zhu, R. Qi and Y. Gao B., Real-time simulation of nonequilibrium nanocrystal transformations. *Advanced Theory and Simulation*. Vol. 2 (1) pp. 1800127-1-1800127-8. WILEY-VCH Verlag GmbH & Co. KGaA, Weinheim, 2018.
- [2] E.A. Korznikova, E.A. Sharapov, A.R. Khalikov and S.V. Dmitriev, Simulation of the binary alloy ordering kinetics during diffusion bonding. *Materials, Technologies, Design — MaTeD*, vol. 1 (1) pp. 58-64, 2019.
- [3] R.P. Gupta, Lattice relaxation at a metal surface. *Physical Review B*. Vol. 23 (1) pp. 6265-6270, 1981
- [4] V. Myasnichenko, L. Kirilov, R. Mikhov, S. Fidanova and N. Sdobnyakov, Simulated annealing method for metal nanoparticle structures optimization. *Advanced*

Computing in Industrial Mathematics. BGSIAM 2017. Studies in Computational Intelligence; Ed. by K. Georgiev, M. Todorov, I. Georgiev. Vol. 793 pp. 277-289, 2019.

Chaotic behaviour in a generalized model of three interacting economic sectors

Elena V. Nikolova, Denislav Z. Serbezov

In this study we extend a basic model, proposed in [1], which describes dynamical interactions between decision-making components in the public sector and the private sector. We add a new ordinary differential equation to the basic system, which describes dynamics of non-governmental organizations (NGOs) sector and we choose investments in the three sectors to be the common economic variable indicator for the extended system. For our convenience we reduce the number of system parameters and analyze dynamical properties of the equilibrium points of the three-dimensional system for selected values of its parameters. On the basis of this analysis we identify two equilibrium points of the system which evolution corresponds to development of chaos of Shilnikov kind [2]. We find that a such chaos in the three-sector interaction system occurs only for the case, in which the private sector investments dominates on the progress of the public and NGOs investments. We illustrate numerically the development of a chaotic system attractor with increasing the value of an appropriate control parameter.

References

- [1] D. Dendrinos. The dynamics of cities: Ecological determinism, dualism and chaos, Routledge, London, 1992.
- [2] L. P. Shilnikov. A case of the existence of a denumerable set of periodic motions, *Sov. Math. Dokl.*, **6** (1965), 163–166.

Sensitivity Study of a Large-Scale Air Pollution Model by Using Latin Hypercube Sampling

Tzvetan Ostromsky, Venelin Todorov, Ivan Dimov, Stoyan Apostolov, Yuri Dimitrov, Zahari Zlatev

In this paper a systematic procedure for multidimensional sensitivity analysis of a case study in the area of air pollution modeling has been done. The Unified Danish Eulerian Model (UNI-DEM) [2] is used in our investigation as one of the most advanced large-scale mathematical models that describes adequately all physical and chemical processes [3]. Sensitivity study of the output of UNI-DEM according to emission levels and chemical reaction rates is performed. Sensitivity Analysis decomposes the uncertainty in inference to uncertainty in inputs to identify which inputs are relevant for the prediction and then investigate how their uncertainty can be reduced in order to improve the accuracy of the prediction.

We discuss a systematic approach for sensitivity analysis studies in the area of air pollution modelling. Different parts of the large amount of output data, produced by the model, were used in various practical applications, where the reliability of this data should be properly estimated. Another reason to choose this model as a case study here is its sophisticated chemical scheme, where all relevant chemical processes in the atmosphere are accurately represented. We study the sensitivity of concentration variations of some of the most dangerous air pollutants with respect to the anthropogenic emissions levels and with respect to some chemical reactions rates. A comprehensive experimental study of Monte Carlo algorithm based on randomized latin hypercube sampling for multidimensional numerical integration has been done. Samplings with different seeds [1] has been analyzed. We use a division of the distribution of each variable into equiprobable intervals. The values obtained for each variable are paired randomly. A comparison with standard Monte Carlo approach is also given. This has been made for the first time for sensitivity analysis of UNI-DEM. The algorithms have been successfully applied to compute global Sobol sensitivity measures corresponding to the six chemical reactions rates and four different groups of pollutants.

Acknowledgement. This work is supported by the Bulgarian National Science Fund under Young Scientists Project KP-06-PM32/4-2019 and by the Project DN 12/5-2017.

References

- [1] McKay, M.D.; Beckman, R.J.; Conover, W.J., A Comparison of Three Methods for Selecting Values of Input Variables in the Analysis of Output from a Computer Code, *Technometrics*. American Statistical Association. 21 (2): pp. 239–245, 1979.
- [2] Z. Zlatev, I. Dimov, *Computational and Numerical Challenges in Environmental Modelling*, Elsevier, Amsterdam, 2006.

- [3] Z. Zlatev, I. Dimov, K. Georgiev, Three-dimensional version of the Danish Eulerian Model, *Zeitschrift für Angewandte Mathematik und Mechanik*, 76, S4, pp.473-476, 1996.

Semantic Technologies in a Decision Support System

Marcin Paprzycki

The aim of our work is to design a decision support system based on ontological representation of domain(s) and semantic technologies. Specifically, we consider the case when Grid / Cloud user describes his/her requirements regarding a “resource” as a semantic expression (based on domain capturing ontology), while the instances of (the same) ontology represent available resources.

The goal is to help the user to find the best option with respect to his/her requirements, while remembering that user’s knowledge may be “limited.” In this context, we discuss multiple approaches based on semantic data processing, which involve different “forms” of user interaction with the system.

Characterization of porous materials by homogenization models based on a generalized mixture rule

Ludmila Parashkevova

Objectives:

In the present study a new variant of the generalized mixture rule for porous media is presented. The homogenization procedure applied takes into account the phenomenological ground of the Generalized Mixture Rule (GMR), see [1], [2] and the mathematical structure of equations of Giodrano's method of homogenization of a composite with ellipsoidal inclusions, [3]. Analytical expressions for the elastic moduli has been derived for a material, which contains close spherical / cylindrical randomly distributed pores in wide interval of porosity.

According to the GMR a given modulus of the two-phase composite is related to the moduli of the constituents through a power equation: $M_c^J = (1 - c)M_m^J + cM_i^J$, where J is a model parameter. For a porous composite the elastic Young's, bulk and shear moduli are equal to zero and the above relation is much simpler. The parameter J expresses the combined influence of a few microstructure features like shape, volume fraction of inclusions and interactions between phases. In practice, the specific manufacturing conditions also affects the value of this exponent. Relationships of power law type have demonstrated remarkable abilities at fitting experimental data obtained from a wide variety of porous materials, [2]. If one choses balk and shear moduli, they will depend on porosity as follows:

$$K_c = K_m(1 - c)^{\alpha_K}, \quad G_c = G_m(1 - c)^{\alpha_G}, \quad (5)$$

where the index m is set for the matrix. In the new model GMR-1 the parameters α_K , α_G have been linked with Mori-Tanaka model supposing that both models demonstrate similar behavior at low pore volume fraction. Applying expansions in Maclaurin's series it is possible to get the exponents α_K , α_G as particular expressions, which depend only on the matrix Poisson's ratio.

$$\alpha_K^{(1)} = 3(1 - \nu_m)/2(1 - 2\nu_m), \quad \alpha_G^{(1)} = 15(1 - \nu_m)/(7 - 5\nu_m). \quad (6)$$

For deriving the corresponding model parameters for the variants GMR-2 and GMR-3 of the presented approach, α_G has been linked to the upper bound for composite shear modulus of McCoy- Silnutzer, [4] and the difference of quantities $(\alpha_K - \alpha_G)$ have been estimated by means of composite Poisson's ratio.

$$\begin{aligned} \alpha_K^{(2)} &= 3/(1 - 2\nu_m) + 15(1 - \nu_m)/(7 - 5\nu_m), \\ \alpha_G^{(2)} &= \alpha_G^{(1)} = 15(1 - \nu_m)/(7 - 5\nu_m), \quad \alpha_K^{(2)} - \alpha_G^{(2)} > 0; \end{aligned} \quad (7)$$

$$\begin{aligned} \alpha_K^{(3)} &= \alpha_K^{(1)} = 3(1 - \nu_m)/2(1 - 2\nu_m), \\ \alpha_G^{(3)} &= 3/2(1 + \nu_m) + 3(1 - \nu_m)/2(1 - 2\nu_m), \quad \alpha_K^{(3)} - \alpha_G^{(3)} < 0. \end{aligned} \quad (8)$$

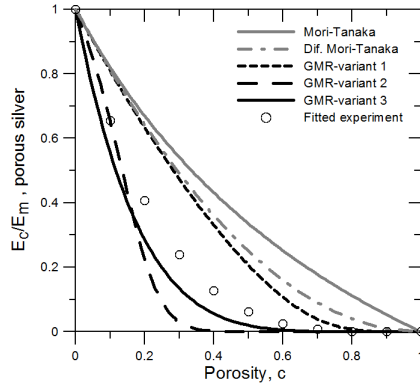


Figure 7: Dependence of the relative Young's modulus on porosity, $\nu_m = 0.4$. Models predictions and experiment, [2]

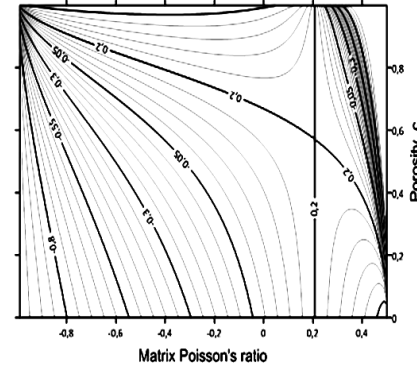


Figure 8: Plain isolines of Poisson's ratio relation $\nu_c = \nu_c(\nu_m, c)$, corresponding to the model GMR-1.

Results:

The presented homogenization models are aimed to elastic properties characterization of porous composites, (Fig.7, Fig.8). New explicit formulae are developed on the base of the phenomenological mixture rule, [1] combined with Mori-Takaka formulae and the upper bound of McCoy - Selnutzer, [4]. Comparing several suggested models a special attention has been paid to the predictions of Poisson's ratio as a material characteristic related to the brittle/ductile post elastic material behavior. The model GMR-3 showed a better predictive capacity in comparisons with experimental data obtained from porous media with matrix Poisson's ratio varying in the interval $0.094 \leq \nu_m \leq 0.43$.

The overall properties are incorporated into newly defined variants of a yield condition. The numerical simulations provided herein reveals the particular role of Poisson's ratio for correct prediction of the elastic-plastic behavior of composite materials with closed pores.

Acknowledgements: This research is carrying out in the frame of KMM-VIN, European Virtual Institute on Knowledge-based Multifunctional Materials AISBL. The support from BG FSI through the grant No *KII-06-27/6-2018* is gratefully acknowledged.

References

- [1] Ji, S., Qi Gu, J Mater Sci, **41**, 1757–1768 (2006)
- [2] Yu, Ch., Ji, Sh., Li, Qi, J. of Rock Mechanics and Geotech. Eng., **8**, 35–49 (2016)
- [3] Giordano, S., Eur J Mech A-Solid, **22**, 885–902 (2003)
- [4] Milton, G. W., J Mech Phys Sol, **30**,3, 177–191 (1982)

Comparison analysis of graph-Laplacian-based methods for image segmentation

Marek Pecha, Stanislav Harizanov

In this talk we experimentally compare two different methods for image segmentation based on graph Laplacian matrices: spectral clustering and energy minimization.

1 Spectral clustering

The spectral clustering [2] is generally a collection of techniques, which exploit underlying properties of the spectrum and eigenvectors related to similarity matrices; eigenpairs of the Laplacian matrices are typically incorporated into clustering process. Employing the spectral properties may significantly improve the performance in the sense of model quality attained utilizing the standard clustering techniques, e.g., the k-means like algorithms. We can include the hidden properties of samples, e.g., pixels or voxels in case of segmentation-based object categorization, geometries or topologies of objects situated in an image scene into the processing of CT-scans for example.

An integral part of the spectral clustering is based on graph theory. Relations between samples are modelled using the similarity graph, where samples are represented as vertices and relation among them as edges; a weight of edge corresponds to a strength of the relation. Commonly, the strength is determined using the Gaussian radial basis function. Regarding spectral clustering, we commonly distinguish two types of the Laplacian matrices, namely the unnormalized and normalized graph Laplacians typically denoted as L , L_{sym} , respectively, and defined as follow:

$$L = D - W, \quad (9)$$

$$L_{sym} = D^{-\frac{1}{2}} L D^{-\frac{1}{2}} = I - D^{-\frac{1}{2}} W D^{-\frac{1}{2}}, \quad (10)$$

where W is an adjacency matrix arising from similarity graph and D is degree matrix such that $D := \text{diag}(d)$, where $d = [\text{deg}(v_1), \text{deg}(v_2), \dots, \text{deg}(v_m)]^T$. The multiplicity of zero eigenvalue is equal to the number of connected components and associated eigenvectors are characteristic vectors of these components. Practically, the multiplicity of zero eigenvalues is detected using Bartlett's test for homogeneity of variances. After determining the number of zero eigenvalues, we construct the matrix $X \in \mathbb{R}^{m \times k}$ that contains the eigenvectors as columns. By this approach, we remap samples $x_i \in \mathbb{R}^n \mapsto x_i \in \mathbb{R}^k$. Afterwards, the samples in new representation are clustered employing standard clustering techniques, e.g., k -means or k -means++ [1].

2 Energy minimization

An alternative approach should be semi-supervised image segmentation that again involves the graph Laplacian matrix L based on the minimization of the following quadratic function

$$\operatorname{argmin}_{v_U \in \{0,1\}^{n_1}} \frac{1}{2} \langle Lv_U, v_U \rangle - \langle q, v_U \rangle \quad \text{subject to} \quad \|v_U\|_0 = N_1. \quad (\mathcal{P}_0),$$

where U is the set of unlabeled pixels in the image, $q = W_{UL}v_L$ is a dense element-wise non-negative vector that incorporates the weight information between unlabelled and labelled pixels, and the additional constraint $\|v_U\|_0 = N_1$ allows for volume preservation of the solid phase. The problem (\mathcal{P}_0) is ill-posed, as we look for a solution only in the vertices of the n_1 -dimensional unit cube and ℓ_0 is a pseudo-norm, thus non-convex. Solution always exists but it may not be unique. However, when N_1 is correctly chosen (i.e., has the physical meaning of the actual volume of the scanned object) and the image noise level is moderate, uniqueness can be achieved. To solve the optimization problem, we solve a sequence of relaxed and generalized versions of the problem

$$\operatorname{argmin}_{\mathbf{0} \leq v_U \leq \mathbf{1}} \frac{1}{2} \langle Qv_U, v_U \rangle - \langle q, v_U \rangle - \langle s, v_U \rangle \quad \text{s. t.} \quad \|v_U\|_1 = N_1, \quad (\mathcal{P}_1(s))$$

which are well-posed, and the binary image s corresponds to the current potential minimizer of (\mathcal{P}_0) (see [3] for more detail). An efficient numerical solver for $(\mathcal{P}_1(s))$ is based on change of basis in the spatial domain and decoupling the pixels information via $v'_U = Q^{1/2}v_U$, $q' = Q^{-1/2}q$, $e' = Q^{-1/2}\mathbf{1}$, $s' = Q^{-1/2}s$. For the computation of the action of the operator $Q^{-1/2}$, univariate best uniform rational approximations of \sqrt{t} in the unit interval are used. Unlike the spectral clustering, here we do not need to know a priori the full spectrum of the operator, but just an interval that covers it (i.e., to estimate from below the lowest eigenvector and to estimate from above the largest eigenvector).

Acknowledgments: M. Pecha acknowledges the support of the grant programme “Support for Science and Research in the Moravia- Silesia Region 2017” (RRC/10/2017), financed from the budget of the Moravian-Silesian Region. S. Harizanov acknowledges the support by grant KP-06-N27/6 from the Bulgarian NSF.

References

- [1] J. Macqueen, *Some methods for classification and analysis of multivariate observations*, In 5-th Berkeley Symposium on Math. Statistics and Probability, pp. 281–297, 1967.
- [2] Ulrike von Luxburg, *A tutorial on spectral clustering*, Statistics and Computing, 17(4) 395–416, 2007.
- [3] S. Harizanov, I. Georgiev, *Fast Algorithm for Optimal Graph-Laplacian Based 3D Image Segmentation*, In AIP Conf. Proc., volume 1773, pp. 110006, 2016.

Information theory with new vision on hierachy and evolution in dynamic systems

Iliyan Petrov

Introduction. Dynamics and volatility in social systems and world markets generate increased volumes of data about evolution and interactions in their structures. Often, existing research methods cannot provide effective treatment and assessment of multilevel information. Scientific analysis needs improved theory concepts and innovative, but reliable methods and models to produce justified forecasts, policies and programs.

Existing indicators for concentration and entropy are specific "type of measures" reflecting the status of system's structure. Although traditionally called "indices", they are not classical ratios of two values. Another important feature is their definition on two levels (two stages). At the first level, basic information (input data) about relative weights s_i of system's individual elements is modeled, as a rule, by some non-linear basic transfer function $f(s_i)$. The second level is universal as approach for any basic function - it summarizes results from first level's - the output data for all elements of the system. Depending on concept we obtain indication for entropy $EN(s_i) = \text{Sum}_{i=1}^N \varepsilon\nu(s_i)$ or for concentration $IE(s_i) = \text{Sum}_{i=1}^N \iota\varepsilon(s_i)$ (where greek letters $\varepsilon\nu$ stand for $\varepsilon\nu\tau\rho\rho\pi\iota\alpha$ [entropia] and $\iota\varepsilon$ for $\iota\varepsilon\rho\alpha\rho\chi\iota\alpha$ [ierarhia]).

Concentration reflect accumulation of resources among limited number of elements in different systems. In Hirschman-Herfindal index (HHI) the basic function is a rather simplistic quadratic expression with monotonically increasing exponential profile $\iota\varepsilon(s_i) = s_i^2$. HHI is used mainly in economics (markets, industry sectors, competition interactions, etc.) - exclusively for systems with few elements.

Entropy reflects variety and higher values of $\text{Sum}_{i=1}^N \varepsilon(s_i) \geq 1$ reflect system status with large number of elements and small relative weights $s_i \leq 0.2$. Traditionally they are preferred in areas like telecommunication and computer technologies, biology, etc. Information theory introduced logarithmic techniques for modeling input data in the basic function of Shannon-Wiener Index (SWI): $\varepsilon(s_i) = -s_i \log_2(s_i)$. SWI has concave profile with one maximum at $s_i = 0.37$, creating ambiguity in interpretation for elements bellow and above maximum.

Practically, existing concentration or entropy indicators are based on unbalanced models which are non-applicable to systems with both a small or high number of elements.

New vision for hierarchy and concentration in Information Theory. In its classical approach Information Theory explores entropy (diversity) mainly with SWI model, which is suitable only for systems with high diversity. To enlarge areas and improve quality of research we propose new concept: assessment of hierarchy with a model called Multiset Concentration Indicator (MCI). MCI is flexible and allows to define not just one, but sets of monotonically increasing functions with logistical profiles (S-curves) suitable for different applications.

$$MCI_{\iota\varepsilon}(s_i) = \frac{s_i}{1 + \left(\frac{\sum_{j=1}^J \log_{R_j}(s_i)}{J} \right)^n}$$

where: s_i - relative weights of system elements; R_j -

referral weights ; J - number of referral weights; n - interaction intensity.

Research and Experiments. The flexibility of MCI allows to derive assymetric S-curves and to select a "golden section" with following values: $J = 2; R_1 = 0.25, R_2 = 0.001; n = 2$. From conceptual and instrumental point of view MCI model is very close to Shannon-Wiener approach and adds logical development in information theory in 3 major innovative aspects: - MCI assesses hierarchy/concentration, instead of entropy/diversity;

- MCI can transform flexibly input-output data with appropriate referral weights;
- MCI basic function corresponds to the definition for an index - it is a ratio (i.e. comparison) of one value (variable) to another value (constant value "1" + logarithmic expression).

A) Theory and concepts. For better systematic description of structural evolution we introduce the notion of Phased-Structure States (PhSS) and define classification frames for the following basic types of PHSS: a) fully and near-to-symmetric; b) maximum asymmetric; and c) average. PhSS concept is universal and can be applied both for entropy and hierarchy: for hierarchy full symmetry/equality of relative weights for given number of elements means minimum concentration, while for entropy - maximum diversity.

B) Methodology. New classification system with clear and logical distinction between:

- a) concentrated PhSS $MCISum > 0.5$ (monopoly, concentrated- classic-enlarged oligopolies);
- b) non-concentrated structures PhSS $MCISum < 0.5$ (polipoly- multiply-hiperpoly).

B) Applied research. For improving analysis of structural interactions we develop a family of new indexes for market, industrial and social systems: structure/market competitive force, structure/market power for individual and cluster entities, type of structure, forming with MCI-PhSS a comprehensive Structure assessment and classification system (SACS).

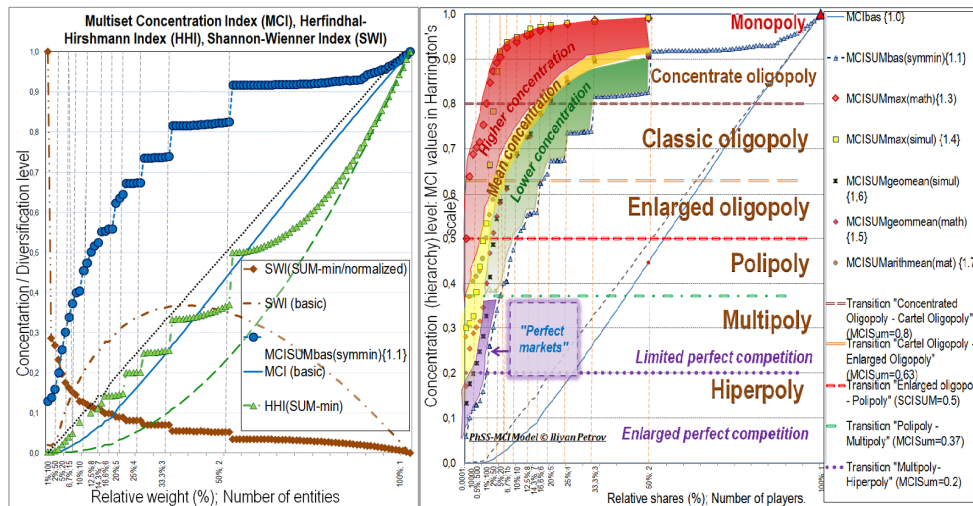


Figure 1: MCI, SWI, HHI

Figure 2: MCI-PhSS classification system

D) Implementation in practice. Pilot testing was applied successfully for analyzing the evolution of word energy markets (oil, gas, coil). Future development and implementation areas include banking, insurance, information technologies, bio- and social systems, etc.

Conclusions MCI-PhSS model adds significant and original improvement in information theory. It is flexible and suitable for wide range of areas with open systems, dynamic redistribution of resources requiring optimization of decision making and effective management.

Some sufficient conditions for the well-posedness of a clamped Timoshenko beam type system

Svilen I. Popov, Vassil M. Vassilev

We consider a clamped Timoshenko beam type system consisting of four partial differential equations, whose coefficients are supposed to be sufficiently smooth functions in respect to the spatial variable. The system is based on a well-known physical model, describing the transverse vibration of a double-wall carbon nanotube regarded as a system of two separate nested nanotubes interacting via van der Waals forces. In a previous paper, we have already established the well-posedness of this system subjected to cantilever boundary conditions without taking into account the elastic medium, surrounding the outer nanotube. In the current paper, we provide sufficient conditions for the well-posedness of the problem accounting for the elastic medium. We prove that the system operator subject to additional assumptions is maximal monotone in an appropriate Sobolev space. Hence, by virtue of the classical Hille-Yosida generation theorem, our problem is solvable and its solutions are all stable.

Acknowledgements

This work was partially supported by the Bulgarian Ministry of Education and Science under the National Research Programme "Young scientists and postdoctoral students" approved by DCM No. 577/17.08.2018 and via contract No. H 22/2 with Bulgarian National Science Fund.

Parameterized Solutions to a Class of Interval Parametric Linear Systems

Evgenija D. Popova

The reliability analysis of many engineering problems, e.g., models of electrical circuits, finite element models in structural mechanics, etc., require solving linear systems of equations involving interval-valued parameters. Sharp interval enclosure of the unknowns in these systems is the goal of many research articles in the interval and the engineering literature. Here we present a recent approach deriving parameterized solutions, which are linear functions of the interval model parameters.

Consider systems of linear algebraic equations having affine-linear uncertainty structure

$$A(p)x = a(p), \quad p \in \mathbf{p} \in \mathbb{IR}^K, \quad (11)$$

where $A(p) := A_0 + \sum_{k=1}^K p_k A_k$, $a(p) := a_0 + \sum_{k=1}^K p_k a_k$, $A_k \in \mathbb{R}^{n \times n}$, $a_k \in \mathbb{R}^n$, $k = 0, \dots, K$ and the parameters $p = (p_1, \dots, p_K)^\top$ are considered to be uncertain and varying within given non-degenerate intervals $\mathbf{p} = (\mathbf{p}_1, \dots, \mathbf{p}_K)^\top$. The united parametric solution set of the system (11), which is considered most often, is $\Sigma_{\text{uni}}^p = \Sigma_{\text{uni}}(A(p), a(p), \mathbf{p}) := \{x \in \mathbb{R}^n \mid (\exists p \in \mathbf{p})(A(p)x = a(p))\}$. Interval methods traditionally find numerical vector $\mathbf{x} \supseteq \Sigma_{\text{uni}}^p$. It was discussed in [1] that each parametric linear system (11) has an equivalent representation by rank one numerical matrices

$$(A_0 + LD_{g(p_{\pi'})}R)x = a_0 + LD_{g(p_{\pi'})}t + Fp_{\pi''}, \quad p \in \mathbf{p} \quad (12)$$

where π' are the indices of the parameters that appear in both the matrix and the right-hand side of (11), while π'' involves the indices of the parameters that appear only in $a(p)$. Representation (12) implies a more general regularity condition (13) for the parametric matrix and a numerical methodology yielding sharper interval solution enclosures for systems having rank one uncertainty structure, cf. [1]. The latter systems are typical for the above mentioned domain-specific problems.

Basing on (12) and the numerical method in [1], we present two parameterized solutions to the system (11). Denote by \check{p}, \hat{p} the midpoint and the radius of an interval \mathbf{p} . Let the matrix $A(\check{p})$ be nonsingular. Denote $C = A^{-1}(\check{p})$ and $\check{x} = Ca(\check{p})$. If

$$\varrho \left(|(RCL)D_{g(\check{p}_{\pi'} - p_{\pi'})}| \right) < 1, \quad (13)$$

(i) [2] there exists an united parameterized solution of the system (11)

$$x(p) = \check{x} - (CF)(\check{p}_{\pi''} - p_{\pi''}) + (CLD_{|y-t|})g(\check{p}_{\pi'} - p_{\pi'}), \quad p \in \mathbf{p}, \quad (14)$$

where $\mathbf{y} \supseteq \Sigma_{\text{uni}}((15))$ is computable by weaker methods, cf.[1];

$$(I - RCLD_{g(\check{p}_{\pi'} - p_{\pi'})})y = R\check{x} - RCF(\check{p}_{\pi''} - p_{\pi''}) - RCLD_{g(\check{p}_{\pi'} - p_{\pi'})}t, \quad p \in \mathbf{p} \quad (15)$$

(ii) [3] there exists an united parameterized solution of the system (11)

$$x(p, r) = \check{x} - (CF)(\check{p}_{\pi''} - p_{\pi''}) + (CLD_{\check{y}-t})g(\check{p}_{\pi'} - p_{\pi'}) + r, \quad p \in \mathbf{p}, r \in [-\hat{r}, \hat{r}], \quad (16)$$

where $\check{y} = R\check{x}$, $\mathbf{y} \supseteq \Sigma_{\text{uni}}((15))$ and $\hat{r} = |CL|D_{|\mathbf{y}-\check{y}|}g(\hat{p}_{\pi'})$;

(iii) with the same \mathbf{y} used in (14), (16), interval evaluation $x(\mathbf{p})$ of $x(p)$ (14) is equal to the interval evaluation $x(\mathbf{p}, \mathbf{r})$ of $x(p, r)$ (16), and to the interval vector \mathbf{x} obtained by [1, Theorem 4.1]; and $x(\mathbf{p}) = x(\mathbf{p}, \mathbf{r}) = \mathbf{x} \supseteq \Sigma_{\text{uni}}^p$.

We discuss some properties of the parameterized solutions (14) and (16), and their application for

1. bounding derived variables $z = f(p, x)$, cf. [2],
2. proving that the extreme points in Σ_{uni}^p are attained at particular endpoints of the parameter intervals \mathbf{p} .

Numerical examples of finite element models of truss structures involving interval uncertainty of some bar properties illustrate the applications.

References

- [1] Popova, E.D.: Rank one interval enclosure of the parametric united solution set, BIT Numer. Math. **59**(2), 503–521 (2019) <https://doi.org/10.1007/s10543-018-0739-4>
- [2] Popova, E.D.: New parameterized solution with application to bounding secondary variables in FE models of structures, arXiv:1812.07300 (2018) <https://arxiv.org/pdf/1812.07300>
- [3] Popova, E.D.: On a class of parameterized solutions to interval parametric linear systems, arXiv:1906.00613 (2019) <https://arxiv.org/pdf/1906.00613>

Dimension reduction in epidemiological models for vector-borne diseases

Peter Rashkov

The motivation for the research reported at this conference comes from epidemiological modeling and, in particular, the spread of vector-borne diseases (such as yellow fever, dengue, malaria, chikungunya). Such diseases are called *emerging diseases* because their potential spread from tropical climate zones into temperate climate zones is facilitated by travel and trade patterns in today's world. Of particular importance to the Balkan and Eastern Mediterranean areas are the *Aedes albopictus* mosquitoes, transported from East Asia, which are able to carry and transmit the dengue virus.

To study the interaction between the human host and the mosquito vector, we use the classical framework of epidemiological models described by systems of nonlinear ODEs. We employ the susceptible-infected-susceptible (SIS) or the susceptible-infected-removed (SIR) model for the host and the susceptible-infected (SI) model for the vector population.

The law of mass action is assumed to model random encounters between vector and host. The total host population is assumed to be constant over time $N = S + I + R$. The compartments of the model are formed by susceptibles S , infected I and recovered R . The total vector population is assumed to be constant over time $M = U + V$ where U and V denote the susceptible and infected vectors. For the SIS model, the ODEs are

$$\begin{aligned}
 S' &= -\frac{\beta}{M}(N - I)V + \mu I \\
 I' &= \frac{\beta}{M}(N - I)V - \mu I \\
 U' &= -\frac{\vartheta}{N}(M - V)I + \nu V \\
 V' &= \frac{\vartheta}{N}(M - V)I - \nu V,
 \end{aligned}
 \tag{17}$$

The model (17) can be reduced to an equivalent two-dimensional model. For the SIR model, the ODEs are

$$\begin{aligned}
 S' &= -\frac{\beta}{M}SV + \mu(N - S) \\
 I' &= \frac{\beta}{M}SV - (\gamma + \mu)I \\
 R' &= \gamma I - \mu R \\
 U' &= -\frac{\vartheta}{N}UI + \nu(M - U) \\
 V' &= \frac{\vartheta}{N}UI - \nu V.
 \end{aligned}
 \tag{18}$$

The model (18) can be reduced to an equivalent three-dimensional model. When the vector's dynamics occurs at a faster scale than the host's dynamics during the epidemic, we use a time-scale argument to reduce the model's dimension further. Often this is implemented as a quasi steady-state assumption (QSSA) where the fast varying variable is set at equilibrium and its corresponding ODE is replaced by an algebraic equation.

Singular perturbation theory appears to be a useful tool to perform this derivation in a rigorous manner. We obtain an asymptotic expansion for the fast variable in the small parameter that represents the ratio of the two time scales for the dynamics of the host and vector. The derivation is achieved by means of an invariant manifold equation [1]. In the case of SIS model for the host, the QSSA assumption is equivalent to an algebraic equation, a hyperbolic relationship modelling a saturated incidence rate, and is similar to the Holling type II functional response from ecology and the Michaelis-Menten kinetics from biochemistry.

For multi-strain diseases such as dengue the algebraic equation is more complicated [2], but we are still able to approximate the invariant manifold using the asymptotic expansion. Numerical examples show this gives a better approximation of the fast variable dynamics compared to the QSSA approximation.

The ultimate goal of this analysis of dimension reduction is to validate how much complexity of the full model could be retained within the reduced model which would facilitate the solution of optimal control problems related to various measures taken to reduce the disease burden. Such measures include but are not limited to insecticides, repellents or campaigns for release of genetically-engineered mosquitoes in affected areas.

Acknowledgements This work has been partially supported by the National Scientific Programme *Information and Communication Technologies for a Single Digital Market in Science, Education and Security (IKT v NOS)*, contract No DOI-205/23.11.2018, financed by the Ministry of Education and Science of Bulgaria.

References

- [1] P. Rashkov, E. Venturino, M. Aguiar, N. Stollenwerk, B. W. Kooi. On the role of vector modeling in a minimalistic epidemic model. *Mathematical Biosciences and Engineering*, 2019, 16(5): 4314-4338.
- [2] P. Rashkov, B. W. Kooi. Complexity of host-vector dynamics in a two-strain dengue model (in preparation).

Comparison Between Different Permeability Field Approximations in MLMC Applications

N. Shegunov, O. Iliev, P. Armyanov

Monte Carlo methods are well know class of computational methods, that rely on repeated random sampling to obtain numerical results. This simple idea is widely used in many industry models, where it is difficult to impose some kind of physical limitations. However, a major drawback of this approach is its slow convergence rate, thus impaling a serous computational effort. An idea, based around sampling from different levels, not only from the true solution, and combining cheap raw fast samples with fine expensive computations, has been gaining popularity in recent years in order to overcome this limitation - namely Multilevel Monte Carlo. This approach is practically useful for applications involving Porous Medium Flows. The work of [1, 2, 4] show some promising results. A significant speed up in comparison with classical Monte Carlo is achieved. In general, the algorithm can be broken into three main parts: generating a correlated random field that represents some porosity material; solving formulated PDE, using established numerical method; quantifying the uncertainty, using Multilevel Monte Carlo. Choosing the algorithm for the permeability generation is a research topic on its own. One idea is to use Cholesky Decomposition. However, in this paper we follow the approach from previous papers [2, 3] and use Circulant Embedding algorithm, witch in its core is Fourier transform [5]. For the deterministic part we use standard cell centered finite volume. Finally, the levels of MLMC are chosen in accordance with the grid size. For the model equation we use Laplace equation. This particular selection of levels implies that some kind of approximation of the random field has to be used for representation on the coarser levels. This work investigates different approaches of doing so: how the approximation changes the number of samples on the different levels; the total computational time; how the expected value changes. The parallel implementation of the algorithm, is done using DUNE C++ library [6]. The authors gratefully acknowledge the Gauss Centre for Supercomputing e.V. (www.gauss-centre.eu) for funding this project by providing computing time on the GCS Supercomputer SuperMUC at Leibniz Supercomputing Centre (www.lrz.de).

References

- [1] Cliffe, K.A., Giles, M.B., Scheichl R., Teckentrup A.L.: *Multilevel Monte Carlo Methods and Applications to Elliptic PDEs with Random Coefficients*. Computing and Visualization in Science **14**(1) (pp. 3–15). Springer(2011)
- [2] Mohring, J., Milk, R., Ngo, A., Klein, O., Iliev, O., Ohlberger, M. and Bastian, P.: *Uncertainty Quantification for Porous Media Flow Using Multilevel Monte Carlo*. In International Conference on Large-Scale Scientific Computing (pp. 145–152). Springer(2015)
- [3] Iliev O., Mohring J., Shegunov N.: *Renormalization Based MLMC Method for Scalar Elliptic SPDE*. In: International Conference on Large-Scale Scientific Computing (pp. 145–152). Springer(2017)
- [4] Blaheta, R., Béréš, M., Domesoá, S.: *A study of stochastic FEM method for porous media flow problem*. In: Bris, R., Dao, P. (eds.) Applied Mathematics in Engineering and Reliability (pp. 281–289). 2016

- [5] Graham, G., Kuo F.Y., Nuyens, D., Scheichl, R., Sloan, I.H. *Quasi-Monte Carlo methods for elliptic PDEs with random coefficients and applications*. Journal of Computational Physics (230) (pp. 3668–3694). Elsevier(2011)
- [6] Bastian, P., Blatt, M., Dedner, A., Engwer, C., Kloeckner, R., Ohlberger, M., Sander, O.: *A Generic Grid Interface for Parallel and Adaptive Scientific Computing. Part I: Abstract Framework*. Computing 82(2-3) (pp. 103–119). (2008)

Performance analysis of a Parallel Hierarchical Semi-Separable compression solver in shared and distributed memory environment for BEM discretization of Flow around Airfoils

D. Slavchev, S. Margenov

We study the performance of a hierarchical solver for systems of linear algebraic equations arising from boundary elements (BEM) discretization of a 2D laminar flow around airfoils. The Structured Matrix Package (STRUMPACK) and its implementation of a Hierarchical Semi-Separable compression is utilized. We analyze the parallel scalability of the method. The achieved numerical accuracy and the related solution times and parallel speed-up are compared with the reference results obtained by the Gaussian Elimination solver from the Math Kernel Library (MKL).

The \mathcal{H} -matrices (\mathcal{H} stands for hierarchical) are introduced by Hackbusch in [1]. Their approximation properties are well suited in the case of matrices arising from numerical solution of integral equations by mesh methods like the Boundary Element Method. The Hierarchically Semi-Separable (HSS) matrices are a derivative concept (i.e. every HSS matrix is \mathcal{H} -matrix, but not vice versa) of dense matrices, whose off-diagonal blocks are rank-deficient in some sense [2]. The HSS structure allows for fast algebraic operations (matrix-vector multiplication, matrix factorization, etc) that provide promising efficiency when solving systems of linear equations with a certain classes of dense matrices.

In the spirit of this study, the $n \times n$ matrix is called *compressible* if it could effectively be approximated by a matrix in a compressed HSS form. If this is the case, solving the thus obtained approximate problem has computational complexity of order $O(r^2n)$, where r is the maximum rank of the off-diagonal blocks of the compressed matrix. Typically r is much smaller than n . For certain problems (like BEM matrices) r or grows as $O(\ln n)$, and the resulting method has *nearly optimal* complexity $O(n \ln n)$.

We examine the parallel implementation of the hierarchically semi-separable compression solver developed within the STRUMPACK project [3]. STRUMPACK uses the following three step method to solve the system of linear algebraic equations:

1. HSS compression: Uses random sampling to calculate the HSS approximation. of the original dense matrix. Has $O(r^2n)$ complexity.
2. ULV-like factorization: Factorizes and solves $O(n - r)$ unknowns. Has $O(r^2n)$ complexity
3. Solution: Uses Gaussian to solve the remaining system of linear equation in two passes - forward elimination and backward substitution. Has $O(rn)$ complexity.

The examined test problem is based on applying boundary element method for numerical simulation of laminar flow around airfoils [4]. In this particular case we consider the laminar flow around five airfoils. After solving the arising system of linear equations we obtain the values of the γ function for each boundary element on the airfoils. From there we can also compute the velocity field around the airfoils as well as the streamlines.

Our previous tests have shown good sequential scalability [4] compared to the traditional Gaussian elimination solver from MKL. The focus of this study is the parallel performance in both, distributed and shared memory environment.

The presented numerical tests are run on 2 servers Fujitsu Primergy RX 2540 M4 with the following configuration:

- CPU 2x Intel Xeon Gold 5118 2.30GHz 24 cores
- 128 GB RAM

Acknowledgments.

The partial support by the Bulgarian NSF Grant DN 12/1 is acknowledged. This first author is also partially supported by the National Scientific Program "Information and Communication Technologies for a Single Digital Market in Science, Education and Security (ICTinSES)", financed by the Ministry of Education and Science.

We acknowledge the provided access to the e-infrastructure of the Centre for Advanced Computing and Data Processing, with the financial support by the Grant No BG05M2OP001-1.001-0003, financed by the Science and Education for Smart Growth Operational Program (2014-2020) and co-financed by the European Union through the European structural and Investment funds.

References

- [1] W. Hackbusch. A sparse matrix arithmetic based on H-matrices. part I: Introduction to H-matrices. *Computing*, 62(2):89–108, Apr 1999.
- [2] P. G. Martinsson. A fast randomized algorithm for computing a hierarchically semiseparable representation of a matrix. *SIAM J. Matrix Anal. Appl.*, 32(4):1251–1274, 2011.
- [3] François-Henry Rouet, Xiaoye S. Li, Pieter Ghysels, and Artem Napov. A distributed-memory package for dense hierarchically semi-separable matrix computations using randomization. *ACM Trans. Math. Softw.*, 42(4):27:1–27:35, June 2016.
- [4] D. Slavchev and S. Margenov. *Performance Analysis of Intel Xeon Phi MICs and Intel Xeon CPUs for Solving Dense Systems of Linear Algebraic Equations: Case Study of Boundary Element Method for Flow Around Airfoils*, pages 369–381. Springer International Publishing, Cham, 2019.

Nanomaterials for hydrogen production and storage

Tony Spassov

Hydrogen sorption and storage in amorphous and nanocrystalline materials is still an intriguing issue. The present lecture gives an overview on the development of this subject during the last years in the Faculty of chemistry and pharmacy. Amorphous and nanostructured alloys and composites on the base of magnesium, zirconium and titanium are synthesized by rapid quenching from the melt and by ball-milling. Through alloying and variation of the preparation conditions materials with different microstructure were synthesized. Their morphology, structure and microstructure have been characterized by x-ray and electron diffraction, and electron microscopy. The thermal behavior of the metastable and unstable materials as well as the thermodynamics and kinetics of their phase transformations during annealing were studied by differential scanning calorimetry and differential thermal analysis. The hydrogen absorption/desorption and hydriding/dehydriding thermodynamics and kinetics of the materials have been studied applying high pressure DSC, Sieverts type volumetric and electrochemical methods. Conclusions have been made on the structure-hydriding properties relationship and on the approaches to optimize the alloys microstructure with respect to achieve their improved hydrogen storage performance.

Effects of satellite data assimilation on air quality parameters simulated by the Bulgarian Chemical Weather Forecast System (BgCWFS)

Dimiter Syrakov, Emilia Georgieva, Maria Prodanova, Maria Dimitrova, Damyant Barantiev

Satellite derived air pollution data are nowadays increasingly used in combination with comprehensive chemical transport models for better description of the atmospheric composition and for improved forecast of pollutants concentrations at ground level [1, 2].

The off-line version of the Bulgarian Chemical Weather forecast system (BgCWFS) [3, 4] was recently updated for assimilation of satellite retrieved aerosol optical depth (AOD) and columnar values of NO₂ and SO₂. The AOD is a measure of the column-integrated extinction of radiation and is approximately proportional to the aerosol mass concentration. The main challenges in modifying the system were related to methods for AOD calculation in the model, to methods for assimilation and simulations in the five nested domains of the system, and to methods for testing the performance of the simulations. As AOD is not routinely calculated in BgCWFS, different approaches were tested for its estimation using data provided by GOME-2 instrument on board of MetOp satellites [5]. The assimilation is taking place in the first 3 domains (Europe, Balkan Peninsula and Bulgaria with resolution 81, 27 and 9 km, respectively) at the hour of satellite overpass over Bulgaria (around 09:00). A rather simple procedure is applied for the assimilation, based on a correction factor between model estimated and satellite derived parameters. The gridded values of the correction factor are then used to correct the initial (first-guess) profile concentrations of different pollutants and finally estimate particulate matter concentrations at ground level.

Simulations in the five nested domains were carried out for the month of August 2017 using two configurations of BgCWFS - without satellite data (base case run, M₀) and with assimilation of satellite data (M_s). The output of the two runs is analysed in terms of spatial distribution of AOD, and particulate matter (PM₁₀ and PM_{2.5}) over Bulgaria (domain 3 with 9 km resolution). Comparison of AOD at a few AERONET locations in the Balkan region (ground-based observations with sun photometers) provides some quantitative information on model performance. The AOD estimated by M_s is compared also to results from the operational global model at the Copernicus Atmosphere Monitoring Service - European Centre for Medium-Range Weather Forecasts (CAMS-ECMWF) that assimilates satellite data with a more advanced approach (4D Var).

On Figure 9 the effect of satellite data assimilation is demonstrated for AOD in domains Balkan Peninsula and Bulgaria (27 and 9 km resolution).

More detailed analysis and comparisons to the observations are in progress.

Acknowledgement

This study was carried out in the frame of the project “Satellite Information Downscaled to Urban Air Quality in Bulgaria (SIDUAQ)”, funded by the Government of Bulgaria through the ESA Contract №4000124150/18/NL/SC under the PECS (Plan for European Cooperating States). The view expressed herein can in no way be taken to reflect the official opinion of the European Space Agency.

References

- [1] Benedetti A., J.-J. Morcrette, O. Boucher, et al (2009) *J. Geophys. Res.*, 114, D13205, <https://doi.org/10.1029/2008JD011115>
- [2] Park R. S., Song C. H., Han K. M., et al (2011) *Atmos. Chem. Phys.*, 11, 12275–12296, <https://doi.org/10.5194/acp-11-12275-2011>
- [3] Syrakov, D., Prodanova, M., Slavov, K., et al (2013) *ECOLOGY & SAFETY*, Volume 7, Part 1, ISSN: 1313–2563, 325–334
- [4] Syrakov, D., Prodanova, M., Etropolska, I., et al. (2014) I. Lirkov et al. (Eds.): *LSSC 2013*, LNCS 8353, pp. 413–420, Springer-Verlag Berlin Heidelberg <https://doi.org/10.1007/978-3-662-43880-055>
- [5] Syrakov D., Prodanova M., Georgieva E. et al (2019) *Bulgarian Journal of Meteorology and Hydrology* (accepted for publication)

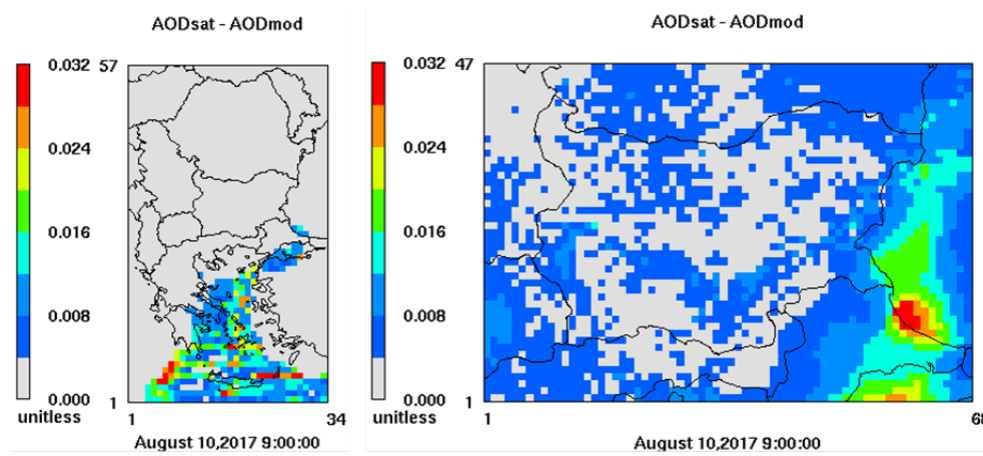


Figure 9: Difference in simulated AOD ($M_s - M_0$)

Extreme Learning Distributed Adaptive Neuro-Fuzzy Architecture for Chaotic Time Series Prediction

M. Terziyska, Zh. Terziyski, Y. Todorov, K. Kolev

Artificial neural networks (ANN) and fuzzy logic systems are commonly used soft computing techniques. Separately and in combination, these techniques are known as universal approximators. The fusion of both combines the learning power of artificial neural networks and the explicit knowledge representation of fuzzy inference systems. The resulting neuro-fuzzy structures are widely used to solve various problems in science, technology, business, education, medical diagnostics, etc. One of the most popular neuro-fuzzy architectures is the Adaptive Neuro-Fuzzy Inference System (ANFIS). This structure is a kind of artificial neural network that is based on the Takagi-Sugeno fuzzy inference system. In more details, the ANFIS has five layers and defines two sets of parameters namely premise parameters and consequent parameters. Researchers have used it mainly for modeling, prediction and control problems. The main drawback of ANFIS is that it is computationally intensive and generates complex models for even relatively simple problems. This is due to the large number of generated fuzzy rules and the huge number of parameters (premise and consequent parameters) that must be determined during the learning procedure. Therefore, to overcome this drawback, there are basically two ways - by reducing computational complexity and by developing fast learning algorithms.

In this paper, an Extreme Learning Distributed Adaptive Neuro-Fuzzy Architecture (EL-DANFA) is presented. This structure obtains both a reduced computational efforts and a fast learning algorithm. On the one hand, Distributed Adaptive Neuro-Fuzzy Architecture (DANFA) model is modification of ANFIS structure. Thus, DANFA has the advantages of ANFIS such as the ability to capture the nonlinear structure of a process and adaptation capability. In the same time, DANFA has reduced number of the fuzzy rules and respectively a smaller number of parameters for learning. The main idea of the designed DANFA structure is to distribute the input space through different fuzzy neural structures. From the other hand, Extreme Learning Machine (ELM) is applied as DANFA's learning technique. The main advantages of ELM is that, it produces faster computational time in simultaneously reaching the smallest training error and smallest norm of output weights. Introduction of ELM in DANFA model leads to increase in generalization accuracy and reduction of complexity in learning algorithm. The potentials of the proposed ELDANFA structure are evaluated in simulation experiments with two common benchmark chaotic systems — Mackey-Glass and Rossler.

Quasi-Monte Carlo methods based on low discrepancy sequences for sensitivity analysis in air pollution modeling

Venelin Todorov, Ivan Dimov, Tzvetan Ostromsky, Stoyan Apostolov, Yuri Dimitrov, Zahari Zlatev

An important issue when large-scale mathematical models are used to support decision makers is their reliability. Sensitivity analysis of model outputs to variation or natural uncertainties of model inputs is very significant for improving the reliability of these models. A comprehensive experimental study of quasi-Monte Carlo algorithm based on van der Corput sequence for computation of multidimensional numerical integration has been done. The van der Corput sequence [1] is often used to generate a "subrandom" sequence of points which have a better covering property than pseudorandom points. A comparison with the standard Monte Carlo approach is given. This is done for the first time for multidimensional sensitivity analysis. The van der Corput sequence generates a sequence of points in $[0,1]$ which never repeats with elements strictly less than 1. The algorithms have been successfully applied to compute global Sobol sensitivity measures corresponding to the influence of several input parameters (six chemical reactions rates and four different groups of pollutants) on the concentrations of important air pollutants.

The Unified Danish Eulerian Model (UNI-DEM) [2] is in the focus of our investigation as one of the most advanced large-scale mathematical models that describes adequately all physical and chemical processes. One of the most attractive features of UNI-DEM is its advanced chemical scheme — the Condensed CBM IV [3], which consider a large number of chemical species and numerous reactions between them, of which the ozone is one of the most important pollutants for its central role in many practical applications of the results. The calculations are done in a large spatial domain, which covers completely the European region and the Mediterranean, for certain time period. Studies of relationships between input parameters and model outputs is very useful for determining the reliability of the model. The influence of emission levels over three important air pollutants (ammonia, ozone, and ammonium sulphate and ammonium nitrate) over big European cities with different geographical locations is considered. Variance-based methods are most often used for providing sensitivity analysis. Sobol variance-based approach for global sensitivity analysis has been applied to compute the corresponding sensitivity measures.

References

- [1] Johannes van der Corput, Verteilungsfunktionen I & II, *Nederl. Akad. Wetensch. Proc.*, Volume 38, pp. 813-820, 1058-1066, 1935.
- [2] Z. Zlatev, I. Dimov, *Computational and Numerical Challenges in Environmental Modelling*, Elsevier, Amsterdam, 2006.
- [3] Z. Zlatev, *Computer treatment of large air pollution models*, KLUWER Academic Publishers, Dordrecht-Boston-London, 1995.

Genetic Algorithm Selection Operator Based on Recursion and Brute-Force

Petar Tomov, Iliyan Zankinski, Todor Balabanov

Introduction Genetic algorithms are global optimization meta-heuristics inspired by the ideas in the neutral evolution. Optimization process is organized in three common operations - selection, crossover and mutation. Crossover and mutation are responsible for proposition of new solutions into the population when selection is responsible for better choice of parents. During last five decades many selection operators are proposed in the literature - Proportional Selection, Tournament Selection, Rank-Based Selection, Boltzmann Selection, Soft Brood Selection, Disruptive Selection, Nonlinear Ranking Selection and Competitive Selection. This research proposes new selection operator based on recursive generations creation. At each level of recursion all individuals in the population are mate between each other (brute-force) and only the best individual goes up in the recursion levels.

Recursion and Brute-Force The population in the genetic algorithm is organized as a hierarchical structure. At the lowest level of the tree structure sub-population consists of randomly generated individuals. In each sub-population each individual mates with each other. Only the best produced individual is promoted for the upper level of the recursive structure. In this way each upper sub-population is established by the best individual promoted from the bottom levels. As benchmark Rastrigin and Griewank functions are taken. All experiments are done in 10K dimensional real numbers space.

Conclusions This study proposes genetic algorithms selection operator based on recursive trace and brute-force on each level. The experiments clearly shows that the proposed operator is very promising when it is applied in high-dimensional solutions spaces. Because of the high CPU consumption the proposed operator is suitable only in hybrid implementations for example in initial genetic algorithm population initialization. As further research it will be interesting brute-force part of the proposition to be replaced with something much more efficient.

Acknowledgments This work was supported by private funding of Velbazhd Software LLC.

Inuitionistic Fuzzy Anova Approach to the Management of Movie Sales Revenue

Velichka Traneva, Stoyan Tranev

The movie ticket sales are an important factor to increase the revenue of the movie exhibition industry. Since ticket price changes are infrequent, the management of sales is the most important strategic tool together with movie screening decisions. Movie theaters are still responsible for the premier release of movies and are the source of the first inflow of revenues that distributors receive before the movie is released on television and into video stores. The movie theater managers are interested in maximizing their revenues generated from movie ticket sales.

The paper analyzes a unique data set from a Cinema City Bulgaria multiplex, part of Cineworld PLC Group (one of the leading cinema groups in Europe) to address these issues and provide a better understanding of strategic behavior of movie theaters. The data set contains information on the amount of tickets sold for a month for two premiere films “Heights” (2D, 2017) and “Avengers” (3D, 2019).

Analysis of variance (ANOVA) is an important method in exploratory and confirmatory data analysis. The simplest type of ANOVA is one-way ANOVA for comparison among means of several populations. The central point in classical ANOVA is a test about the significance of the difference among population means, which allows us to conclude whether or not the differences among the means of several populations are too deviated to be attributed to the sampling error [5, 6].

In this article, for the first time we extend one-way ANOVA to a case where observed data are intuitionistic fuzzy observations (IFANOVA) rather than real numbers and we apply the method to analyze the dependence of the movie sales of the two premieres “Heights” and “Avengers” on ticket price and day of the week. The proposed approach employs the apparatus of intuitionistic fuzzy sets (IFSs) and index matrices (IMs). IFSs is first defined by Atanassov (IFSs, [1]) as an extension of the concept of fuzzy sets defined by Zadeh [7]. The concept of IMs is introduced in [2]. The emergent of FANOVA is due to the fact that the imprecise data sometimes occur in the real world, in two cases. The first case is due to technical conditions of measurements where the response variable cannot be measured exactly. The second case happens when the response variable will be given in terms of linguistic forms, such as linguistic report which are not numeric [6].

The outlined approach for IFANOVA, assisting the decision-making process, can be extended to n -dimensional and can be researched to other types of fuzzy or intuitionistic fuzzy multi-dimensional data in IMs [3].

Acknowledgements

The first author is supported by the Bulgarian National Scientific program “ICT in science, education and security” and the second author - by the “Asen Zlatarov” University project under Ref. No. NIX-423/2019 “Innovative methods for extracting knowledge management”.

References

- [1] Atanassov, K.: Intuitionistic fuzzy sets. In Proceedings of VII ITKR's Session, Sofia, (1983) (in Bulgarian)

- [2] Atanassov, K.: Generalized index matrices. *Comptes rendus de l'Academie Bulgare des Sciences* **40**(11), 15–18 (1987)
- [3] Atanassov, K., n-Dimensional extended index matrices Part 1. *Advanced Studies in Contemporary Mathematics*, **28** (2), 245–259 (2018)
- [4] Doane, D., Seward, L.: *Applied statistics in business and economics*. McGraw-Hill Education, New York, USA (2016)
- [5] Gil, M.A., Montenegro, M., González-Rodríguez, G., Colubi, A., and Casals, M.R.: Bootstrap Approach to the Multi-sample Test of Means with Imprecise Data, *Computer Statistics and Data Analysis*, **51**, 148–162 (2006)
- [6] Nourbakhsh, M.R., Parchami, A., Mashinchi, M.: Analysis of variance based on fuzzy observations. *Int. J. Syst. Sci.*, **44** (4), 714-726 (2011)
- [7] Zadeh, L.: Fuzzy Sets. *Information and Control* **8**(3), 338–353 (1965)

Interpolation of data in \mathbb{R}^3 using quartic triangular Bézier surfaces

Krassimira Vlachkova, Krum Radev

Interpolation of data points in \mathbb{R}^3 by smooth surface is an important problem in Computer Aided Geometric Design with applications in various areas such as medicine, architecture, archeology, computer graphics, scientific visualization, etc. The problem can be formulated as follows: Given a set of points $(x_i, y_i, z_i) \in \mathbb{R}^3$, $i = 1, \dots, n$, find a bivariate function $F(x, y)$ defined in a certain domain containing points $V_i = (x_i, y_i)$, such that F possesses continuous partial derivatives $\partial F/\partial x$, $\partial F/\partial y$, and $F(x_i, y_i) = z_i$.

A standard approach to solve the problem consists of two steps [2]:

1. Construct a triangulation $T = T(V_1, \dots, V_N)$;
2. For every triangle in T construct a surface which interpolates the data in the three vertices.

Shirman and Séquin [4] construct a smooth surface consisting of quartic triangular Bézier surfaces (TBS). First, they construct a smooth cubic curve network defined on the edges of T . Then for every triangle in T they apply procedure called *splitting* and a method proposed by Chiyokura [1] to determine the inner Bézier control points that are close to the edges of T .

Nielson [3] propose a method called *minimum norm network* (MNN) which computes a smooth interpolation cubic curve network defined on the edges of T so as to satisfy an extremal property. MNN is extended to a smooth interpolation surface using an appropriate *blending* method. Nielson's interpolant is a rational function on every triangle in T .

We present a new algorithm for interpolation of data in \mathbb{R}^3 which is computationally simple and produces visually pleasant smooth surfaces. The algorithm first computes the MNN and then constructs a smooth interpolation surface which consists of quartic TBS and is based on splitting. The choice of the inner Bézier control points allows to avoid bending, twisting, and tilting which appear in surfaces constructed by Shirman and Séquin's method [4], see Fig. 11.

We have created a program packages for implementation, 3D visualization and comparison of Shirman and Séquin's algorithm and the new algorithm. We have chosen `Plotly` [5] and `Three.js` [6] graphics libraries as our main implementation and visualization tools. We performed a large number of experiments using data of increasing complexity and analysed the results with respect to different criteria.

Example 1. The data are $(-1/2, -\sqrt{3}/6, 0)$, $(1/2, -\sqrt{3}/6, 0)$, $(0, \sqrt{3}/3, 0)$, $(0, 0, -1/2)$. The triangulation and the corresponding MNN are shown in Fig. 10. The Shirman and Séquin's surface and the new surface are shown in Fig. 11.

Acknowledgments. The first author was supported in part by Sofia University Science Fund Grant No. 80-10-59/2019, and by European Regional Development Fund and the Operational Program "Science and Education for Smart Growth" under Contract №BG05M2OP001-1.001-0004 (2018-2023).

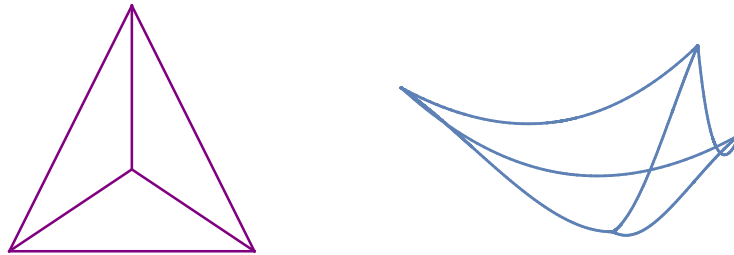


Figure 10: The triangulation and the corresponding MNN for the data in Example 1.

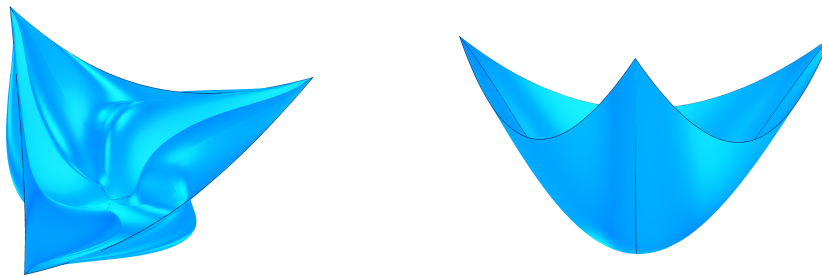


Figure 11: The interpolation surfaces obtained for the data in Example 1: (left) Shirman and Séquin's surface [4]; (right) The surface generated by our algorithm

References

- [1] H. Chiyokura. Localized surface interpolation method for irregular meshes, in: Kunii, T. (Ed.), *Advanced Computer Graphics*, Proceedings of Computer Graphics Tokyo'86, Springer, Tokyo. pp. 3-19. 1986.
- [2] S. Mann, C. Loop, M. Lounsbery, D. Meyers, J. Painter, T. DeRose, K. Sloan. A survey of parametric scattered data fitting using triangular interpolants, in: Hagen, H. (Ed.), *Curve and Surface Design*. SIAM, Philadelphia, pp. 145-172, 1992.
- [3] G. M. Nielson. A method for interpolating scattered data based upon a minimum norm network. *Mathematics of Computation*, 40(161):253–271, 1983.
- [4] L. Shirman, C. Séquin. Local surface interpolation with Bézier patches. *Comput. Aided Geom. Des.*, 4:279–295,1987
- [5] Plotly.js, <https://plot.ly/javascript>
- [6] Three.js, <https://threejs.org>

Probability distributions connected to the flows of substance in a channel of a network

Roumen Borisov, Nikolay K. Vitanov, Zlatinka I. Dimitrova

We study the flow of substance in a channel of a network. The substance can be of different kind (for an example, chemical components in a technological systems, or migrants in a migration channel). The channel consists of nodes of the network and edges that connect these nodes and form ways for motion of substance. The new point with respect to previous studies [1] - [6] is that studied channel can have an arbitrary number of arms and each arm can contain finite or infinite number of nodes. We discuss first the case of a channel that has arms containing infinite number of nodes. For stationary regime of motion of substance in such a channel we obtain probability distributions of substance in any of the arms of the channel and in entire channel. Next we discuss a mathematical model of flow of substance in a channel that has finite number of arms and in addition each arm has finite number of nodes. We consider again the stationary regime of flow of substance in detail in and obtain a class of probability distributions for the substance in the nodes of the channel. Finally we discuss some applications of the discussed model.

As an illustration of the new results obtained in the study we write below the form of stationary distribution of substance in nodes of a channel with N arms where each arm can contain infinite number of node. This distribution is denoted as $y_{q,i}^{*a,b} = x_{q,i}^{*a,b} / x_q^{*a,b}$ where $x_{q,i}^{*a,b}$ is the amount of the substance in the i -th node of the q -th arm of the channel. $x_q^{*a,b}$ is the amount of the substance in all of the cells of the q -th arm of the channel. The distribution is

$$\begin{aligned}
 y_{q,0}^{*a,b} &= \frac{1}{1 + \sum_{i=1}^{\infty} \frac{\prod_{j=0}^{i-1} \left[\alpha_{q,i-j-1}^{a,b} + (i-j-1)\beta_{q,i-j-1}^{a,b} \right]}{\prod_{j=0}^{i-1} \left[\alpha_{q,i-j}^{a,b} + (i-j)\beta_{q,i-j}^{a,b} + \gamma_{q,i-j}^{*a,b} \right]}} \\
 y_{q,i}^{*a,b} &= \frac{\frac{\prod_{j=0}^{i-1} \left[\alpha_{q,i-j-1}^{a,b} + (i-j-1)\beta_{q,i-j-1}^{a,b} \right]}{\prod_{j=0}^{i-1} \left[\alpha_{q,i-j}^{a,b} + (i-j)\beta_{q,i-j}^{a,b} + \gamma_{q,i-j}^{*a,b} \right]}}{1 + \sum_{i=1}^{\infty} \frac{\prod_{j=0}^{i-1} \left[\alpha_{q,i-j-1}^{a,b} + (i-j-1)\beta_{q,i-j-1}^{a,b} \right]}{\prod_{j=0}^{i-1} \left[\alpha_{q,i-j}^{a,b} + (i-j)\beta_{q,i-j}^{a,b} + \gamma_{q,i-j}^{*a,b} \right]}} \\
 & \qquad \qquad \qquad i = 1, 2, \dots \tag{19}
 \end{aligned}$$

Above a and b denote the parent arm and the parent node for the q -th arm of the channel, $\alpha_{q,i}^{a,b}$ and $\beta_{q,i}^{a,b}$ are parameters for properties of the transfer of substance between the nodes of the channel and $\gamma_{q,i}^{a,b}$ is a parameter reflecting the possible loss of substance in the i -th node of the q -th arm of the channel. The obtained distribution is not discussed up to now and contains as particular cases many famous long-time discrete probability distributions.

References

- [1] Vitanov N. K., Vitanov K. N. Box model of migration channels. *Mathematical Social Sciences* **80**, 108 – 114, (2016).
- [2] Vitanov, N. K., Vitanov, K.N.: On the motion of substance in a channel of network and human migration. *Physica A*, **490** , 1277 – 1290, (2018)
- [3] Vitanov, N. K., Vitanov, K. N.: Discrete-time model for a motion of substance in a channel of a network with application to channels of human migration. *Physica A* **509**, 635 – 650, (2018).
- [4] Vitanov, N. K., Vitanov, K. N., Ivanova, T.: Box model of migration in channels of migration networks. p.p. 203 - 215 in K. Georgiev et al. (Eds.) *Advanced Computing in Industrial Mathematics, Studies in Computational Intelligence No. 728*, Springer, Cham, (2018).
- [5] Vitanov, N. K., Borisov, R.: A model of a motion of substance in a channel of a network. *Journal of Theoretical and Applied Mechanics* **48**, 74 – 84, (2018).
- [6] Borisov, R., Vitanov, N. K.: Human migration: Model of a migration channel with a secondary and a tertiary arm. *AIP Conference Proceedings*, **2075**, 150001, (2019)

Part B

List of participants

A.Alexandrov

Institute of Information and
Communication Technologies
Bulgarian Academy of Sciences
Akad. G. Bonchev, Str., Bl. 2
Sofia, Bulgaria
akalexandrov@iit.bas.bg

Vera Angelova

Institute of Information and
Communication Technologies
Bulgarian Academy of Sciences
Akad. G. Bonchev, Str., Bl. 2
1113 Sofia, Bulgaria
vangelova@iit.bas.bg

Krassimir Angelow

Institute of Mathematics and Informatics
Bulgarian Academy of Sciences
Acad. G. Bonchev Str., Bl. 8
1113 Sofia, Bulgaria

Krassimir Atanassov

Institute of Biophysics and
Biomedical Engineering
Bulgarian Academy of Sciences
Acad. G. Bonchev str., bl.105
1113 Sofia, Bulgaria
krat@bas.bg

Todor Balabanov

Institute of Information and
Communication Technologies
Bulgarian Academy of Sciences
acad. G. Bontchev Str., block 2
1113 Sofia, Bulgaria
todorb@iinf.bas.bg

Milen K. Borisov

Institute of Mathematics and Informatics,
Bulgarian Academy of Sciences
Acad. Georgi Bonchev Str., Block 8
1113 Sofia, Bulgaria
milen.kb@math.bas.bg

Hristo Chervenkov

National Institute of
Meteorology and Hydrology
Bulgarian Academy of Sciences
Tsarigradsko Shose blvd. 66
1784 Sofia, Bulgaria
hristo.tchervenkov@meteo.bg

Maria Datcheva

Institute of Mechanics
Bulgarian Academy of Sciences
Acad. G. Bonchev Str., Bl. 4
1113 Sofia, Bulgaria
datcheva@imbm.bas.bg

Ivan Dimov

Institute of Information and
Communication Technologies,
Bulgarian Academy of Sciences
Acad. G. Bonchev Str., bl. 25A
1113 Sofia, Bulgaria
ivdimov@bas.bg

Milena Dimova

University of National and World Economy
Student Town
1700 Sofia, Bulgaria
mkoleva@math.bas.bg

Peter Dragnev

Purdue University Fort Wayne, Indiana,
USA

Stefka Fidanova

Institute of Information and
Communication Technologies
Bulgarian Academy of Sciences
Acad. G. Bontchev str., bl. 25A
1113 Sofia, Bulgaria
stefka@parallel.bas.bg

Ivan Georgiev

Institute of Information and
Communication Technologies
Bulgarian Academy of Sciences
Acad. G. Bonchev Str., bl. 2
and
Institute of Mathematics and Informatics
Bulgarian Academy of Sciences
Acad. G. Bonchev str., bl. 8
1113 Sofia, Bulgaria

Krassimir Georgiev

Institute of Information and
Communication Technologies
Bulgarian Academy of Sciences
Acad. G. Bontchev str., bl. 25A
1113 Sofia, Bulgaria
georgiev@parallel.bas.bg

Slavi Georgiev

Angel Kanchev University of Ruse
8 Studentska Str.
7017 Ruse, Bulgaria
georgiev.slavi.94@gmail.com

Vladimir Gerdjikov

Institute of Mathematics and Informatics
Bulgarian Academy of Sciences
Acad. G. Bonchev str., bl. 8
1113 Sofia, Bulgaria
vgerdjikov@math.bas.bg

Stanislav Harizanov

Institute of Information and
Communication Technologies
Bulgarian Academy of Sciences
Acad. G. Bonchev Str., bl. 25A
1113 Sofia, Bulgaria
sharizanov@parallel.bas.bg
and
Institute of Mathematics and Informatics
Bulgarian Academy of Sciences
Acad. G. Bonchev str., bl. 8
1113 Sofia, Bulgaria

Nevena Ilieva

Institute of Information and
Communication Technologies
Bulgarian Academy of Sciences
Acad. G. Bonchev Str, Block 25A
1113 Sofia, Bulgaria
nevena.ilieva@parallel.bas.bg
and
Institute of Mathematics and Informatics
Bulgarian Academy of Sciences
Acad. G. Bonchev str., bl. 8
1113 Sofia, Bulgaria

Ivan Ivanov

Texas A&M University, USA

David Kamenov

PMPG "St. Kliment Ohridski"
Montana, Bulgaria
deivid.kamenov@abv.bg

Juri Kandilarov

Ruse University
8 Studentska Str.
7017 Ruse, Bulgaria
ukandilarov@uni-ruse.bg

Kristina Kapanova

Institute of Information and
Communication Technologies
Bulgarian Academy of Sciences
Acad. G. Bonchev Str., bl. 25A
1113 Sofia, Bulgaria
kapanova@parallel.bas.bg

Leoneed Kirilov

Institute of Information and
Communication Technologies
Bulgarian Academy of Sciences
Acad. G. Bontchev str., bl. 2
1113 Sofia, Bulgaria
lkirilov@iinf.bas.bg

Natalia Kolkovska

Institute of Mathematics and Informatics
Bulgarian Academy of Sciences
Acad. G. Bonchev Str., Bl. 8
1113 Sofia, Bulgaria

Miglena Koleva

Ruse University
6 Studentska St
7017 Ruse, Bulgaria
mkoleva@uni-ruse.bg

Petia Koprinkova-Hristova

Institute of Information and
Communication Technologies
Bulgarian Academy of Sciences
Acad. G. Bontchev str., bl. 25-A
1113 Sofia, Bulgaria
pkoprinkova@bas.bg

Hristo Kostadinov

Institute of Mathematics and Informatics
Bulgarian Academy of Sciences
Acad. G. Bonchev str., bl. 8
1113 Sofia, Bulgaria

Elena Lilkova

Institute of Information and
Communication Technologies
Bulgarian Academy of Sciences
25A, Acad. G. Bonchev Str. , Block 25A
1113 Sofia, Bulgaria
elilkova@parallel.bas.bg

Svetozar Margenov

Institute of Information and
Communication Technologies
Bulgarian Academy of Sciences
Acad. G. Bonchev Str., bl. 25A
1113 Sofia, Bulgaria
margenov@parallel.bas.bg

Lubomir Markov

Department of Mathematics and CS
Barry University
11300 N.E. Second Avenue
Miami Shores, FL 33161, USA
lmarkov@barry.edu

Svetoslav Markov

Institute of Mathematics and Informatics,
Bulgarian Academy of Sciences
Acad. Georgi Bonchev Str., Block 8
1113 Sofia, Bulgaria
smarkov@bio.bas.bg

V. Monov

Institute of Information and
Communication Technologies
Bulgarian Academy of Sciences
Acad. G. Bontchev Str., Bl. 2
1113 Sofia, Bulgaria
vmonov@iit.bas.bg

Vladimir Myasnichenko

Tver State University
Tver, Russia
viplabs@yandex.ru

Elena V. Nikolova

Institute of Mechanics
Bulgarian Academy of Sciences
Acad. G. Bonchev Str., Bl. 4
1113 Sofia, Bulgaria
elena@imbm.bas.bg

Silviya Nikolova

Department of Anthropology
and Anatomy
Institute of Experimental Morphology,
Pathology and Anthropology
with Museum
Bulgarian Academy of Sciences
Acad. G. Bonchev Str., bl. 25
1113 Sofia, Bulgaria
sil_nikolova@abv.bg

Tzvetan Ostromsky

Institute of Information and
Communication Technologies,
Bulgarian Academy of Sciences
Acad. G. Bonchev Str., bl. 25A
1113 Sofia, Bulgaria
ceco@parallel.bas.bg

Marcin Paprzycki

Systems Research Institute, Polish Academy
of Sciences
paprzyck@ibspan.waw.pl

Ludmila Parashkevova

Institute of Mechanics
Bulgarian Academy of Sciences
Acad. G. Bontchev str., bl. 4
1113 Sofia, Bulgaria
lusy@imbm.bas.bg

Marek Pecha

Institute of Geonics of the CAS
708 00 Ostrava-Poruba
Czech Republic
marek.pecha@ugn.cas.cz

Nedyu Popivanov

Institute of Information and
Communication Technologies
Bulgarian Academy of Sciences and
Sofia University "St. Kliment Ohridski"
nedyu@parallel.bas.bg

Svilen I. Popov

Institute of Mechanics
Bulgarian Academy of Sciences
Acad. G. Bonchev Str., Bl. 4
1113 Sofia, Bulgaria

Evgenija D. Popova

Institute of Mathematics and Informatics
Bulgarian Academy of Sciences
Acad. G. Bonchev str., block 8
1113 Sofia, Bulgaria
epopova@math.bas.bg

Stefan Radev

Institute of Mechanics
Bulgarian Academy of Sciences
Acad. G. Bontchev str., bl. 4
1113 Sofia, Bulgaria
stradev@imbm.bas.bg

Nikolay Sdobnyakov

Tver State University
Tver, Russia

Nikolay Shegunov

Faculty of Mathematics and Informatics
Sofia University "St. Kl. Ohridski"
Blvd. James Bourchier 5
1164 Sofia, Bulgaria
nshegunov@fmi.uni-sofia.bg

Dimitar Slavchev

Institute of Information and
Communication Technologies,
Bulgarian Academy of Sciences
Acad. G. Bonchev Str., bl. 25A
1113 Sofia, Bulgaria
dimitargslavchev@parallel.bas.bg

Tony Spassov

Sofia University "St. Kliment Ohridski",
Bulgaria
TSpassov@chem.uni-sofia.bg

Dimitar Syrakov

National Institute of Meteorology and Hy-
drology
Sofia, Bulgaria
dimitar.syrakov@meteo.bg

Sonia Tabakova

Institute of Mechanics
Bulgarian Academy of Sciences
Acad. G. Bontchev str., bl. 4
1113 Sofia, Bulgaria
stabakova@gmail.com

Venelin Todorov

Institute of Information and
Communication Technologies
Bulgarian Academy of Sciences
Acad. G. Bonchev Str., bl. 25A
1113 Sofia, Bulgaria

Diana Toneva

Department of Anthropology
and Anatomy
Institute of Experimental Morphology,
Pathology and Anthropology
with Museum
Bulgarian Academy of Sciences
Acad. G. Bonchev Str., bl. 25
1113 Sofia, Bulgaria

Stoyan Tranev

"Prof. Asen Zlatarov" University
"Prof. Yakimov" Blvd 1
8000 Burgas, Bulgaria

Velichka Traneva

"Prof. Asen Zlatarov" University
"Prof. Yakimov" Blvd 1
8000 Burgas, Bulgaria

Vassil M. Vassilev

Institute of Mechanics
Bulgarian Academy of Sciences
Acad. G. Bonchev Str., Bl. 4
1113 Sofia, Bulgaria

Nikolay K. Vitanov

Institute of Mechanics
Bulgarian Academy of Sciences,
Acad. G. Bonchev Str., Bl. 4
1113 Sofia, Bulgaria
vitanov@imbm.bas.bg

Krassimira Vlachkova

Faculty of Mathematics and Informatics
Sofia University "St. Kl. Ohridski"
Blvd. James Bourchier 5
1164 Sofia, Bulgaria
krassivl@fmi.uni-sofia.bg

Lubin Vulkov

Ruse University
6 Studentska St
7017 Ruse, Bulgaria
lvulkov@uni-ruse.bg